DETERMINATION OF IMMUNOMODULATORY EFFECTS OF SARS-COV-2 STRUCTURAL, NONSTRUCTURAL, AND ACCESSORY PROTEINS ON MACROPHAGE-LIKE CELLS IN THE CONTEXT OF TYPE I IFN ANTAGONISM AND INFLAMMASOME ACTIVATION

A THESIS SUBMITTED TO
THE GRADUATE SCHOOL OF NATURAL AND APPLIED SCIENCES
OF
MIDDLE EAST TECHNICAL UNIVERSITY

BY

YAĞMUR AYDIN

IN PARTIAL FULFILLMENT OF THE REQUIREMENTS
FOR
THE DEGREE OF MASTER OF SCIENCE
IN
BIOLOGY

FEBRUARY 2022

Approval of the thesis:

DETERMINATION OF IMMUNOMODULATORY EFFECTS OF SARS-COV-2 STRUCTURAL, NONSTRUCTURAL, AND ACCESSORY PROTEINS ON MACROPHAGE-LIKE CELLS IN THE CONTEXT OF TYPE I IFN ANTAGONISM AND INFLAMMASOME ACTIVATION

submitted by **YAĞMUR AYDIN** in partial fulfillment of the requirements for the degree of **Master of Science** i**n Biology, Middle East Technical University** by,

Prof. Dr. Halil Kalıpçılar
Dean, Graduate School of **Natural and Applied Sciences** _____

Prof. Dr. Ayşegül Gözen
Head of the Department, **Biology** _____

Prof. Dr. Mayda Gürsel
Supervisor, **Biology Dept., METU** _____

Examining Committee Members:

Prof. Dr. Haluk Barbaros Oral
Department of Immunology, Uludağ University _____

Prof. Dr. Mayda Gürsel
Biological Sciences, METU _____

Assoc. Prof. Dr. Banu Bayyurt Kocabaş
Biological Sciences, METU _____

Date: 02.02.2022

I hereby declare that all information in this document has been obtained and presented in accordance with academic rules and ethical conduct. I also declare that, as required by these rules and conduct, I have fully cited and referenced all material and results that are not original to this work.

Name Last name : Aydın, Yağmur

Signature :

ABSTRACT

DETERMINATION OF IMMUNOMODULATORY EFFECTS OF SARS-COV-2 STRUCTURAL, NONSTRUCTURAL, AND ACCESSORY PROTEINS ON MACROPHAGE-LIKE CELLS IN THE CONTEXT OF TYPE I IFN ANTAGONISM AND INFLAMMASOME ACTIVATION

Aydın, Yağmur
Master of Science, Biology
Supervisor : Prof. Dr. Mayda Gürsel

February 2022, 110 pages

Infection with SARS-CoV-2 inhibits early type I interferon response but activates inflammasome signaling and pro-inflammatory cytokine production. The virus accomplishes these opposing effects by manipulating the host cell immunity through a multitude of encoded viral proteins of structural, non-structural, or accessory origin.

In this thesis, to investigate the immunomodulatory effects of SARS-CoV-2 encoded proteins on type I IFN antagonism and inflammasome activation, five SARS-CoV-2 structural, nonstructural, or accessory protein-expressing stable THP1-Dual cell lines (NSP9, NSP10, ORF3a, ORF8 or N) and a MOCK control was generated using a 3rd generation lentiviral gene transduction approach. The cell lines were then exposed to virus-mimetic pattern recognition ligands or to recombinant IFN-β. Their type I IFN as well as type I IFN-dependent ISG15 responses were assessed, respectively. Our findings indicate that ORF3a and ORF8 accessory proteins significantly antagonized type I IFN production and ORF3a downregulated ISG15 production. NSP9 and N were found to antagonize type I

IFN production only when compared to WT, but not to mock, suggestive of a minor impact.

To measure the impact of SARS-CoV-2-related protein expression on inflammasome activation, and pyroptosis, NLRP3, NLRC4, AIM2, or non-canonical inflammasomes were stimulated via corresponding activating ligands. Our results confirmed that ORF3a accessory protein significantly over-activated NLRP3 and NLRC4 inflammasome-mediated IL-1β production and lactate dehydrogenase enzyme release, indicative of pyroptotic cell death.

NPS9 expression in the cell line possibly blocked cell membrane trafficking in response to nigericin, thereby preventing nigericin-mediated cell death. Furthermore, N structural protein hindered pyroptosis but induced pyroptosis-independent cell death after non-canonical and NLRC4 inflammasome activation, suggesting that Nucleocapsid interfered with gasdermin-D-mediated pore formation, but triggered a pyroptosis-independent cell death mechanism.

Keywords: SARS-COV-2, Antiviral Immunity, Type I IFN Antagonism, Inflammasome

ÖZ

SARS-COV-2 YAPISAL, YAPISAL OLMAYAN VE AKSESUAR PROTEİNLERİN TİP I IFN ANTAGONİZM VE ENFLAMAZOM AKTİVASYONU BAĞLAMINDA MAKROFAJ BENZERİ HÜCRELER ÜZERİNDEKİ İMMÜNOMODÜLATÖR ETKİLERİNİN BELİRLENMESİ

Aydın, Yağmur
Yüksek Lisans, Biyoloji
Tez Yöneticisi: Prof. Dr. Mayda Gürsel

Şubat 2022, 110 sayfa

SARS-CoV-2 ile enfeksiyon, erken tip I interferon yanıtını inhibe ederken, enflamatuar sinyalleşmeyi ve proenflamatuar sitokin üretimini aktive eder. Virüs, bu zıt etkileri, yapısal, yapısal olmayan veya aksesuar kaynaklı kodlanmış viral proteinler yoluyla konakçı hücre bağışıklığını manipüle ederek gerçekleştirir.

Bu tezde, SARS-CoV-2 kodlu proteinlerin tip I IFN antagonizmi ve enflamazom aktivasyonu üzerindeki immünomudülatör etkilerini araştırmak için, SARS-CoV-2 yapısal, yapısal olmayan veya yardımcı proteini stabil bir şekilde ekspres eden THP1-Dual hücre hatları (NSP9, NSP10, ORF3a, ORF8 veya N) ve bir MOCK kontrolü, 3.nesil lentiviral gen transdüksiyon yaklaşımı kullanılarak üretildi. Hücre hatları daha sonra virus-mimetik model tanıma ligandlarına veya recombinant IFN-β'ya maruz bırakıldı. Sırasıyla tip I IFN ve tip I IFN'ye bağımlı ISG15 yanıtları değerlendirildi. Bulgularımız, ORF3a ve ORF8 aksesuar proteinlerinin tip I IFN üretimini önemli ölçüde antagonize ettiğini ve ORF3a'nın ISG15 üretimini aşağı yönde düzenlediğini göstermektedir. NSP9 ve N'nin yalnızca WT ile karşılaştırıldığında tip I IFN üretimini küçük bir etkiyle antagonize ettiği bulundu.

SARS-CoV-2 ile ilişkili protein ekspresyonunun enflamazom aktivasyonu üzerindeki etkisini ve piroptozu ölçmek için, NLRP3, NLRC4, AIM2 veya kanonik olmayan enflamazomlara karşılık gelen ve onları aktive edici ligandlar aracılığıyla uyarıldı. Sonuçlarımız ORF3a yardımcı proteinin, NLRP3 ve NLRC4 enflamazom aracılı IL-1β üretimini ve piroptotik hücre ölümünün göstergesi olan laktat dehidrojenaz enzim salınımını önemli ölçüde aşırı aktivite ettiğini doğruladı.

Hücre hattındaki NSP9 ekspresyonu, muhtemelen nigerisine yanıt olarak hücre zarı kaçakçılığını bloke etti ve böylece nigerisin aracılı hücre ölümünü önledi. Ayrıca, N yapısal proteini piroptozu engelledi ancak kanonik olmayan ve NLRC4 enflamazom aktivasyonundan sonra piroptozdan bağımsız hücre ölümünü indükledi. Bu da Nükleokapsidin Gasdermin-D aracılı gözenek oluşumuna müdahale ettiğini, ancak piroptozdan bağımsız hücre ölüm mekanizmasını tetiklediğini düşündürdü.

Anahtar Kelimeler: SARS-COV-2, Antiviral Bağışıklık, Tip I IFN Antagonizmi, Enflamazom

To my nephew Ada

ACKNOWLEDGMENTS

First of all, I would like to start by expressing my heartfelt gratitude and thanks to my supervisor, Prof. Mayda Gürsel. It was always a privilege to be a student in her lab and to benefit from her vast scientific knowledge and experience. Her endless support, courage, and interest in research of the new and unknown will be my academic guidance throughout my life. No words will be enough to dedicate my respect and admiration to her.

I also want to thank my thesis examining committee: Prof. Haluk Barbaros Oral and Assoc. Prof. Banu Bayyurt Kocabaş for sparing time to evaluate this thesis and their valuable comments.

I would also like to thank all my lab members for being my second family. Başak Kayaoğlu, Naz Yılmaz and İlayda Baydemir were always kind, helpful, friendly and supportive for the any type of problem I've faced. I am very glad that they spare time to share their scientific knowledge with me. Also, I have learned so many things while doing PID studies. I want to thank Dr. İsmail Cem Yılmaz for his support, help, and teachings during the vaccine project which I honestly believe couldn't go on without him. I would like to express my special thanks to Emre Mert İpekoğlu and Emre Dünüroğlu for their help and scientific comments on my studies. I also want to thank my lab partners Hatice Asena Şanlı, Büşranur Geçkin, Neşe Güvençli and Öykü Yağmur Başar for their contribution and friendship.

Of course, I also want to thank Prof. Ihsan Gürsel for his endless help and instructions during my both undergraduate and graduate years. MG lab and Gürsel family will always have a special place in my heart.

I'm very thankful that my beloved partner Ömer Atalay was always nearby my side whenever I need his love, support, and friendship. I hope a clear, good future

awaits us. I also thank my best friends Bader Bilgin, Sedat Mert, and Utku Yurtsever for their continuous support, help, and sharing countless funny moments over the 9 years. I hope that our friendship, breakfasts, and coffee talks will last forever.

Lastly, I want to express my eternal gratitude and love to my mom, dad, older brother, and older sister. They always support and believe in me throughout my life.

Lastly, this thesis study was supported by ODTÜBAP-Coordination Unit.

TABLE OF CONTENTS

LIST OF TABLES

TABLES

LIST OF FIGURES

FIGURES

LIST OF ABBREVIATIONS

ABBREVIATIONS

AIM	Absent in melanoma 2
AGE	Agarose gel electrophoresis
ALR	AIM2-like receptor
ALP	Alkaline phosphatase
ACE2	Angiotensin-converting enzyme 2
ASC	Apoptosis associated speck-like protein containing a CARD
AID	Autoinflammatory disease
bp	base pairs
BCR	B-cell receptor
BSA	Bovine serum albumin
CARD	Caspase activation and recruitment domain
cDC	Conventional dendritic cell
COV	Coronavirus
COVID-19	Coronavirus disease 2019
CLR	C-type lectin receptor
CMV	Cytomegalovirus
DAMP	Danger/damage associated molecular pattern
DC	Dendritic cells
DNA	Deoxyribonucleic acid
dsDNA	Double-stranded RNA
ELISA	Enzyme-linked immunosorbent assay
EDTA	Ethylenediaminetetraacetic acid
FBS	Fetal bovine serum
GSDMD	Gasdermin-D
GFP	Green fluorescent protein
HEPES	4-(2-hydroxyethyl1) -1-piperazineethane sulfonic acid

HSC	Hematopoietic stem cells
HSV-1	Herpes simplex virus 1
HRP	Horseradish peroxidase
IFN	Interferon
ISG	Interferon stimulated gene
IRF	Interferon-regulatory factor
IL	Interleukin
LGP2	Laboratory of genetics and physiology 2
LDH	Lactate dehydrogenase
LRR	Leucine-rich repeat
LPS	Lipopolysaccharides
MHC	Major histocompatibility complex
MDA-5	Melanoma differentiation associated protein 5
MERS	Middle east respiratory syndrome
MAVS	Mitochondrial anti-viral signaling protein
MAPK	Mitogen-activated protein kinase
MX	Myxovirus
NK	Natural killer
NSP	Non-structural protein
NF-κB	Nuclear factor- kappa B
NOD	Nucleotide-binding oligomerization domain
NLR	Nucleotide-binding oligomerization domain like receptors
ODN	Oligodeoxynucleotide
ORF	Open reading frame
PLP	Papain-like proteases
PNPP	Para-nitrophenyl pyro-phosphate
PAMP	Pathogen-associated molecular pattern
PRR	Pattern recognition receptor
PGN	Peptidoglycan
PMA	Phorbol 1-myristate 13-acetate

PBS	Phosphate buffered saline
PE	Phycoerythrin
pDC	Plasmacytoid dendritic cell
Poly I:C	Polyriboinosinic-cytidylic acid
PFD	Pore-forming domain
PI	Propidium iodine
PYD	Pyrin
ROS	Reactive-oxygen species
RBD	Receptor-binding domain
R848	Resiquimod
RIG-I	Retinoic acid-inducible gene-I
RLR	Retinoic acid-inducible gene-I like receptor
RNA	Ribonucleic acid
RPMI	Rosewell Park Memorial Institute
SEAP	Secreted embryonic alkaline phosphatase
SARS	Severe acute respiratory syndrome
STAT	Signal transducer and activator of transcription
SDS-PAGE	Sodium dodecyl sulfate - polyacrylamide gel
TBK	TANK-binding kinase
TCR	T-cell receptor
TMPRSS	TM protease serine 2
TLR	Toll-like receptor
PPP	Triphosphate
VSV-G	Vesicular stomatitis virus glycoprotein
WT	Wild-type

CHAPTER 1

INTRODUCTION

1.1 Immune system

The immune system is a well-organized defense mechanism that opposes intruding pathogens such as bacteria, viruses, fungi, and other infectious organisms. It is armed with various effector molecules and cells that constantly promote the clearance of dead cells, cellular debris, and foreign molecules. The immune system is divided into two categories: innate and adaptive immunity. While the innate arm of the immune system is generally considered as “frontline defense” due to its rapid action, adaptive immunity is relatively slower, antigen-specific and it generates long-lived immunological memory (Netea et al., 2019). Collectively, the two arms of the immune system work in an interactive relationship to pursue homeostasis. To produce the cellular components of the immune system, hematopoietic pluripotent stem cells (HSCs) undergo a process known as “hematopoiesis”. HSCs proliferate and differentiate into two distinct lineages: common lymphoid progenitors and common myeloid progenitors. While T-cells, B-cells, and Natural Killer (NK) cells differentiate from common lymphoid progenitors; erythrocytes, megakaryocytes, and other various innate immune cells are derived from common myeloid progenitors (Kovtonyuk et al., 2016). Antigen-specificity of adaptive immunity is based upon B- and T- lymphocytes which express their unique antigen-binding receptors: B-cell Receptors (BCR) and T-cell Receptors (TCR), respectively. Although B-cell receptors can directly bind to antigens, T-cell receptors bind to peptides that are represented on major histocompatibility complex (MHC) molecules (Minervina et al., 2019). Furthermore, adaptive immunity depends on clonal selection which is a process of generating a cell population that can

eliminate the same antigen. These antigen-specific responses are tightly regulated by crosstalk with one of the innate immune components, Dendritic Cells (DCs) which also originate in the bone marrow and are diversified as conventional DCs (cDCs) or plasmacytoid DCs (pDCs). cDCs and pDCs are found in the nonlymphoid, lymphoid tissues, and circulation. Especially, pDCs are well-known as the major type-I interferon-producing cells (Wu & Liu, 2007).

1.2 Innate Immunity

Innate immune defense is an evolutionarily conserved system that has been shared between plants, invertebrates, and mammals. All the mammalian tissues and physical barriers such as skin or mucosal surfaces like the respiratory tract are protected by innate immune cells. These cells diverge from the common myeloid progenitors into cells such as monocytes, macrophages, mast cells, and granulocytes which include neutrophils, basophils, and eosinophils (Iwasaki & Akashi, 2007). The innate immune system evolved a unique pathogen sensing mechanism that relies on pattern recognition receptors (PRRs) to sense and respond to a broad range of intruders that share common molecular surface and endogenous motifs, known as pathogen-associated molecular patterns (PAMPs) and damage-associated molecular patterns (DAMPs) (Schaefer, 2014).

1.2.1 PRRs and RNA sensing mechanisms

Innate immune cells express receptors that are important for discriminating non-infectious self and infectious non-self through pattern recognition receptors (PRRs). Germline-encoded PRRs are conserved and are divided into five families based on their protein domain homology: Toll-like receptors (TLRs), a retinoic acid-inducible gene I (RIG-I) -like receptors (RLRs), nucleotide oligomerization domain (NOD)-like receptors (NLRs), C-type lectin receptors (CLRs) and absent in melanoma-2 (AIM2)-like receptors (ALRs), as listed in Table 1.1 (D. Li & Wu,

2021). PRRs can be located on cellular and endosomal membranes, present in the cytosol, or can be found extracellularly, in secreted form (P. Zhang et al., 2015). Intracellular signaling pathways activated by these PRRs govern inflammatory genes and cascades that allow pathogens to be discarded.

RLRs are specialized in sensing RNA molecules in the cytosol, and these receptors consist of three distinct members: RIG-I, melanoma-differentiation-associated protein 5 (MDA-5), and laboratory of genetics and physiology 2 (LGP2) (Rehwinkel & Gack, 2020). The two major members of the RLRs, RIG-I, and MDA-5, detect immunostimulatory dsRNAs in the cytosol and interact with the adaptor protein MAVS (mitochondrial antiviral signaling protein). MAVS governs interaction with different proteins to form a protein complex, then catalyzes the activation of nuclear kappa B kinase (NF-kB) and serine-threonine-protein kinase 1 (TBK1). While NF-kB transcription factor facilitates the production of pro-inflammatory cytokines, TBK1 phosphorylates the transcription factors interferon regulatory factors 3 and 7 (IRF3 and IRF7) to direct their nuclear localization to the nucleus and activation of type I interferons production (Brisse & Ly, 2019). RNA molecules that are comprised of a triphosphate (PPP) group at their 5' end and short RNAs potently activate RIG-I (Hornung et al., 2006). On the other hand, longer RNA molecules such as poly(I:C), a synthetic RNA molecule, can activate the MDA-5-mediated signaling pathway (Pichlmair et al., 2009).

The toll-like receptors (TLRs), one of the most studied PRRs, are either localized on the plasma membrane or reside intracellularly on endosomal and lysosomal membranes. To date, 10 humans and 12 murine TLRs have been identified, each responsible for recognizing a specific self- or non-self-antigen. While TLR1, TLR2, TLR4, TLR5, and TLR6 are located on the plasma membrane; TLR3, TLR7, TLR8, and TLR9 are found on the endosomal membrane. In addition to cytosolic sensors, endosomal TLRs are also important in recognition of nucleic acids derived from viruses and bacteria. For example, TLR7/TLR8 in humans recognizes single-stranded RNA from RNA viruses and synthetic analog compounds such as R848 (Takeuchi & Akira, 2010).

Another important cytosolic sensor mechanism is mediated through the NOD-like receptor (NLRs) family. NLR members are composed of N-terminal protein attachment domain, a central nucleotide-binding domain NATCH, and a C-terminal leucine-rich repeat (LRR) domain. NLRs differ from each other with respect to their N-terminus, their caspase-recruitment and activation (CARD) or pyrin (PYD) domains (Kanneganti, 2010). NOD1 and NOD2 are important in sensing cytosolic bacterial motifs such as peptidoglycans. Upon activation of NOD1 and NOD2, they oligomerize and activate NF-kB and mitogen-activated protein kinase (MAPK) signaling pathways (Keestra-Gounder & Tsolis, 2017). Other NLRs that respond to a variety of PAMPs/DAMPs form multi-protein complexes called "inflammasomes" upon activation (shown in Figure 1.1). There are different types of inflammasomes some of which were investigated in this thesis in relation to their activity in the presence of various SARS-CoV-2 derived proteins.

Table 1.1. PRRs in innate immunity (Adapted from (Li & Wu, 2021)

Items	PRR	Domains	Cellular distribution	PAMP	Sources	Signaling pathways
Toll-like receptors (TLRs)	TLR1 (TLR1–TLR2)	LRR domain–transmembrane domain–TIR domain (extracellular to intracellular)	Mo, DC, Ma, Eo, Ba	Triacyl lipopeptide	Bacteria	Most TLRs: MyD88-dependent pathways; TLR3: TRIF-dependent pathways; TLR4: MyD88-dependent pathways and TRIF-dependent pathways
	TLR2 (TLR1–TLR2, TLR2–TLR6)		Mo, DC, Ma, Eo, Ba	Lipoteichoic acid	Bacteria	
				Arabinomannan	Mycobacterium	
				Peptidoglycan	Bacteria	
				Zymosan	Fungi	
				Lipoprotein	Mycoplasma	
				Pore protein	Neisseria	
	TLR3		Mφ, DC, IEC	dsRNA	Virus	
	TLR4 (MD-2/CD14)		Mφ, DC, Ma, Eo	Lipopolysaccharides	Bacteria	
				Heat-shock proteins	Host	
	TLR5		IEC	Flagellin	Bacteria	
	TLR6 (TLR2–TLR6)		Mo, DC, Ma, Eo, Ba	Lipoteichoic acid	Bacteria	
				Peptidoglycan	Bacteria	
	TLR7		pDC, Mφ, Eo	ssRNA	Virus	
				Imidazoquinoline	Artificially synthesized	
	TLR8		Mφ, N	ssRNA	Virus	
	TLR9		pDC, Eo, Ba	Non-methylated CpG DNA	Bacteria, Virus	
	TLR10 (human)		pDC, Eo, Ba	dsRNA	Virus	
	TLR11 (mouse)		Mφ, DC	Profilin and related proteins	*Toxoplasma gondii*	
	TLR12 (mouse)		DC	Profilin and related proteins	*Toxoplasma gondii*	
	TLR13 (mouse)		Unknown	23s ribosomal RNA	Bacteria	
Nucleotide-binding oligomerization domain-like receptors (NLRs)	NOD1	LRR domain–NBD–effector domains	IEC, cytosol of Mφ	iE-DAP	Gram negative bacteria	RIP2-TAK1-NF-κB pathways
	NOD2			MDP	Gram-negative bacteria, Gram-positive bacteria	
RIG-I-like receptors (RLRs)	RIG-I	(RD)-CTD-DexD/H helicase domain–CARD	Cytosol	5′-triphosphorylated RNA, short-chain dsRNA	Virus	MAVS-TRAF6-NF-κB/TBK1 pathways
	MDA5			poly IC, long-chain dsRNA	Virus	
	LGP2			dsRNA	Virus	
C-type lectin receptors (CLRs)	Dectin-1	CTLD–ITAM	DC, Mφ	β-Glucan	Fungus	Tyrosine kinase-dependent and non-tyrosine kinase-dependent pathways
	Dectin-2			α-Mannan	Fungus	
Absent in melanoma-2-like receptors (ALRs)	ALRs	HIN-200-PYD	Cytosol	dsDNA	Bacteria	Inflammasome–pyroptosis

LRR leucine-rich repeat, *TIR* Toll/IL-1R domain, *NBD* nucleotide-binding domain, *RD* repressor domain, *CTD* C-terminal domain, *CARD* caspase activation and recruitment domain, *CTLD* C-type lectin-like domains, *ITAM* immunoreceptor tyrosine-based activation motif, *PYD* pyrin domain, *Mo* monocyte, *DC* dendritic cell, *Ma* mastocyte, *Eo* eosinophils, *Ba* basophils, *pDC* plasmacytoid dendritic cell, *IEC* intestinal epithelial cell, *N* neutrophil, *dsRNA* double-stranded RNA, *ssRNA* single-stranded RNA, *iE-DAP* γ-D-glu-meso-diaminopimelic acid, *MDP* muramyl dipeptide, *MyD88* myeloid differentiation factor 88, *TRIF* TIR domain-containing adaptor protein-inducing interferon β, *RIP2* receptor-interacting serine–threonine protein 2, *TAK1* transforming growth factor-β-activated kinase 1, *NF-κB* nuclear factor κB, *MAVS* mitochondrial antiviral signaling protein, *TRAF6* tumor necrosis factor receptor-associated factor, *TBK1* TANK-binding kinase 1

1.2.2 Canonical and Non-canonical Inflammasome

Multiple PAMPs and DAMPs, including bacterial toxins, bacterial flagella, gram-negative bacteria outer membrane component lipopolysaccharides (LPS), cytosolic double-stranded DNA, uric acid crystals, trigger inflammasome activation through a variety of NLR family members. Inflammasomes are formed following interaction of pyrin (PYD) and caspase recruitment domains (CARD) of specific proteins. These multiprotein complexes recruit the evolutionarily conserved enzyme pro-caspase-1 through the adaptor molecule ASC (apoptosis-associated speck-like protein containing a CARD), and subsequently generate the inflammatory cytokines IL-1β and IL-18 (Kesavardhana & Kanneganti, 2017). Caspase-1 is one of the major inflammatory caspases in humans along with caspase-4, -5, and -12. When newly synthesized pro-caspase-1 is locally concentrated in the inflammasome, it homodimerizes resulting in autocleavage to its active form. Bioactive caspase-1 promotes the activation of pro-IL-1β and pro-IL-18 into their mature forms (IL-1β and IL-18). Moreover, caspase-11 in murine studies display inflammasome-mediated inflammatory cell death regardless of ASC and caspase-1 in response to intracellular LPS. Instead of caspase-11, human cells react to the same DAMP via caspase-4 and -5. Caspase-1-independent sensing of cytosolic LPS activates the non-canonical inflammasome signaling pathway (Sanders et al., 2015). Furthermore, the production of pro-caspases, pro-IL-1β, and pro-IL-18 requires a priming step that depends on transcriptional activation of NF-kB. This can be initiated through other PAMPs such as the TLR-mediated sensing or through activation via phorbol-12-myristate 13-acetate (PMA) (Gong et al., 2010; Gritsenko et al., 2020). As a consequence of caspase-1 activation (or -4, -5, -11, -12 depending on pathway and species), a pore forming protein GSDMD (gasdermin-D) is freed from its C-terminal repressor, and the N-terminal pore-forming domain (PFD) becomes active. PFD is translocated to plasma and mitochondrial membranes, bind to acidic lipid molecules and, then inserted into the lipid bilayer to form large pores (X. Chen et al., 2016). Through these pores, active

caspases, inflammatory cytokines IL-1β and IL-18, ASC protein, and other cellular inflammatory content leaks to the extracellular environment. Hence, these sequential events lead to an inflammatory form of cell death, known as pyroptosis. Released IL-1β and IL-18 (known as IL-1R and IL-18R, respectively) further contribute to inflammation through activation of the transcription factor NF-kB in target cells (Gay et al., 2014).

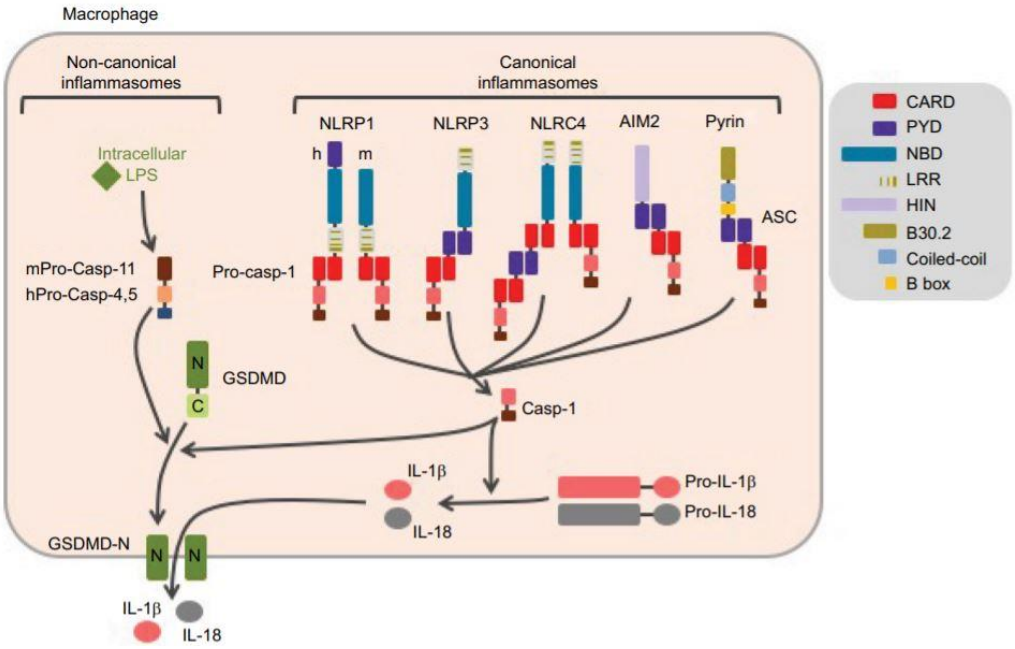

Figure 1.1. Non-canonical and canonical inflammasome activation summary figure in macrophages (Adapted from (Groslambert & Py, 2018))

1.2.2.1 The NLRP3 (NACHT, leucine-rich repeat, and PYD containing protein 3) Inflammasome

Multiple stimuli including bacterial/viral toxins (from RNA viruses; i.e. Influenza virus and vesicular stomatitis virus (VSV)), viroporin proteins from severe acute respiratory syndrome coronavirus (SARS-CoV), and uric acid crystals activate downstream signaling events through the NLRP3 inflammasome (I. Y. Chen et al., 2019; da Costa et al., 2019; Vanaja et al., 2015; Yamasaki et al., 2009). Four specific mechanisms lead to NLRP3 activation: the generation of reactive oxygen

species (ROS) derived from mitochondria, potassium (K^+) efflux, particulate-crystalline ligands such as silica that disrupts endo/lysosomal membranes, and pathogen associated RNA or RNA cleavage products produced by RNase L (Chakrabarti et al., 2015; Rathinam et al., 2012). These stimuli cause dissociation of chaperons from NLRP3, leading to recruitment of adaptor ASC through PYD domain interactions between these two proteins. The adaptor ASC then recruits pro-caspase-1 through its CARD domain. As a result of caspase-1 activation, biologically active IL-1β and IL-18 are released from the cell by pyroptosis. Although this inflammatory response helps the clearance of pathogens, over-activation of the inflammasome can lead to immune pathology. For example, NLRP3-associated autoinflammatory disease (NLRP3-AID) is a condition in which the patients present with complications such as fever, joint and musculoskeletal inflammation through hyperactivation of the NLRP3 inflammasome (Louvrier et al., 2020). Figure 1.2 and Figure 1.3 briefly describe the working principle of the NLRP3 inflammasome.

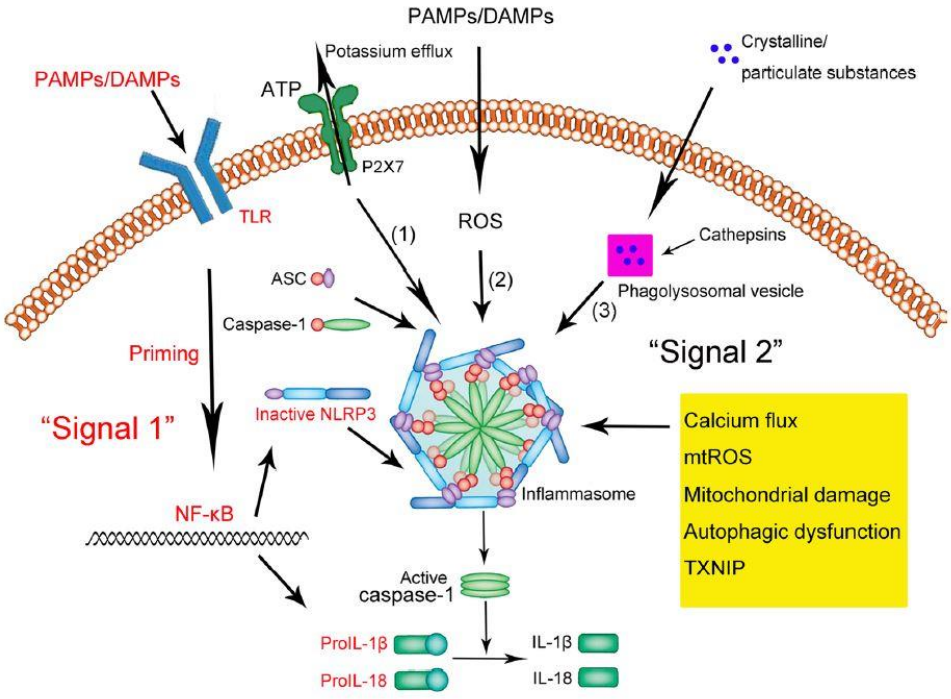

Figure 1.2. NLRP3 Inflammasome signaling pathway (Adapted from (Shao et al., 2015))

1.2.2.2 The NLRC4 (NLR family CARD containing protein 4) Inflammasome

Presence of bacterial flagellin or the Prgj rod protein (a component of the type III secretion system), in the cytosol activates the NLRC4 inflammasome. Inflammasome assembly is achieved by direct attachment of CARD domains of the caspase-1 and the NLRC4 proteins. Compared to the NLRP3 inflammasome, it was reported that ASC is not an obligatory compartment in the complex (Miao et al., 2010; Zhao et al., 2011), but similarly, active caspase-1 and IL-1β /IL-18 cytokines are produced (summarized in Figure 1.3).

Similar to the NLRP3 inflammasome, over-activation of the NLRC4 inflammasome can lead to inflammasomopathies. NLRC4-associated autoinflammatory disease (NLRC4-AID) is another life-threatening syndrome in which patients present with episodes of autoinflammation and histopathology (Romberg et al., 2017).

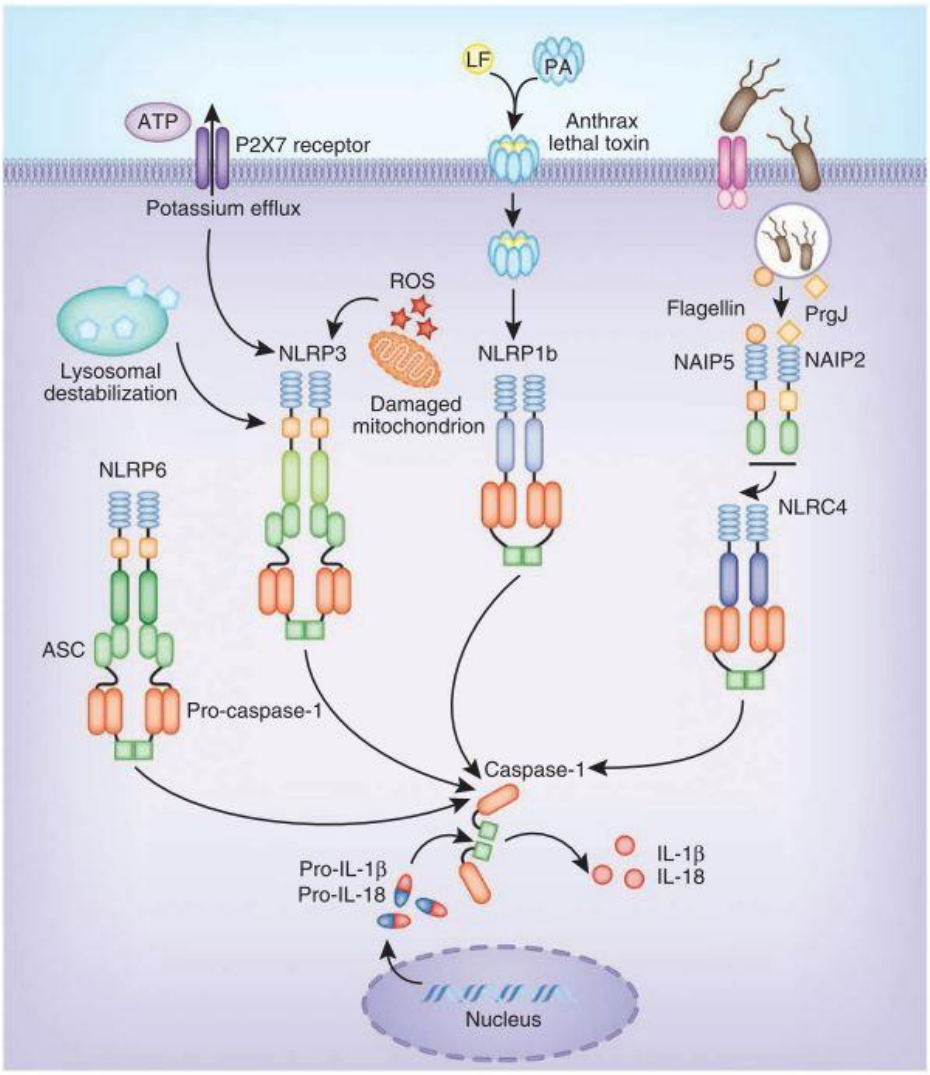

Figure 1.3. NLRP3 and NLRC4 inflammasome activation pathways (Adapted from (Rathinam et al., 2012))

1.2.2.3 The AIM2 (absent in melanoma 2) Inflammasome

Foreign or self-DNA molecules that accumulate in the cytosol during viral, bacterial, and parasitic infections or released from the nucleus as a result of DNA damage are perceived as cellular threats. ALRs promote inflammasome formation following cytosolic DNA sensing. ALR family member AIM2 protein is a cytosolic DNA sensor that forms the AIM2 Inflammasome following binding to

dsDNA. In contrast to other inflammasomes, AIM2 is composed of one HIN (or HIN200) and one PYD domain, or two HIN in its C-terminal end, and recruits adaptor protein ASC and caspase-1 for proteolytic cleave and activation of IL-1β and IL-18 (Lugrin & Martinon, 2018).

Interestingly, AIM2 preferentially binds to double-stranded DNA (dsDNA) over single-stranded DNA (Jin et al., 2012). In order to activate the AIM2 inflammasome, the double-stranded DNA analog poly(dA:dT) is frequently used. Figure 1.4 briefly summarizes the AIM2 inflammasome activation pathway.

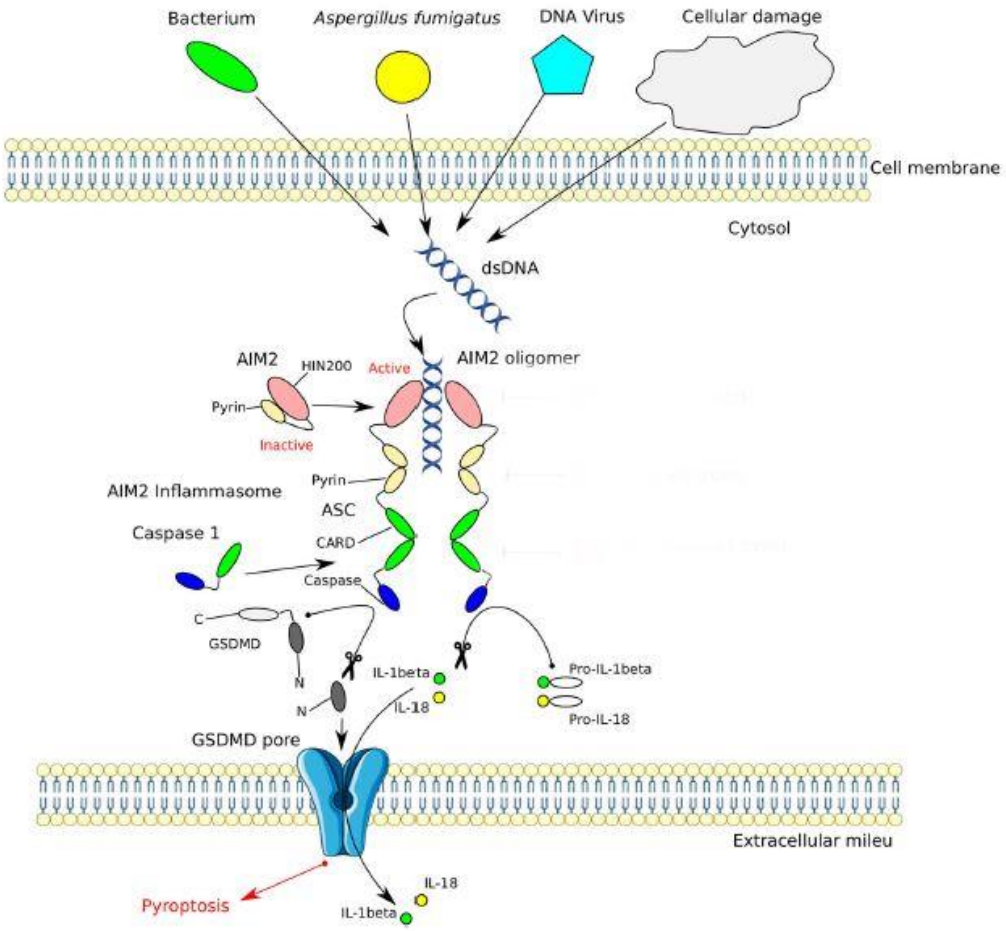

Figure 1.4 AIM2 inflammasome activation pathway (adapted from (Zheng et al., 2020).

1.3 Anti-viral Immunity

Viruses are compulsory intracellular pathogens that require host cell machinery to produce their proteins important for their replication and spreading. As the first line of defense, innate immune cells detect viral entry through PRRs leading to development of an anti-viral response.

Sensors that engage viral nucleic acids, such as RIG-I/MDA-5, trigger downstream signaling events to produce Type I IFNs (IFN-α and β), which are fundamental in establishing an anti-viral response. Type I IFN signaling leads to the transcription of several different interferon-stimulated genes (ISGs) via Janus kinase (Jak)/ signal transducer and activator of transcription (STAT) signaling pathway. ISGs encode various proteins that display immunomodulatory, antiviral and antiproliferative activities (Grandvaux et al., 2002). Following binding of type I interferons to their corresponding receptor, Jak tyrosine kinase and subsequent STAT phosphorylation, triggers interferon-stimulated gene productions including, myxovirus resistance 1 (MX1), IFN-inducible double-stranded RNA-dependent protein kinase (PKR), 2'-5'- oligoadenylate synthase (OAS) and IFN-induced transmembrane proteins (IFITMs) (Yan & Chen, 2012). Furthermore, inflammatory cytokines such as tumor necrosis factor-α (TNF-α), IFN-gamma, and IL-6 also contribute to this antiviral response (Mueller & Rouse, 2008). Numerous studies demonstrated that if type I IFN expression increases, intrinsic proteins such as TRIM5a (important for blocking viral entry), OAS-RNase L (cytosolic dsRNA sensor that interferes with viral protein translation), Mx protein GTPases (responsible for inhibition of viral replication), virus-infected cell apoptosis and cellular resistance against viral infection also increase (Haller et al., 2015; Leisching et al., 2017; Samuel, 2001; Yan & Chen, 2012; Hornung et al., 2014).

1.3.1 Interferon-stimulated Gene 15 (ISG15) as an Indicator of Anti-viral Response

Human ISG15 is a ubiquitin-like (Ubl) protein whose expression is tightly regulated by type I IFNs. Therefore, ISG15 levels critically change during viral infections. Similar to Ubls, ISG15 is capable of regulating many aspects of the immune defense. It can be conjugated to targeted proteins as a post-translational mechanism or it can be found intra- and/or extracellularly in its free form that acts as a cytokine. For example, extracellular unconjugated ISG15 can induce natural killer (NK) cell proliferation at the side of infection (Jonathan D'Cunha et al., 1996). Free-ISG15 has been detected in IFN treated patients and virally infected mice (J D'Cunha et al., 1996; Lai et al., 2009; Werneke et al., 2011)

Newly synthesized ISG15 exists in its 17 kDa precursor form, which is then converted to the 15 kDa active form by cellular proteases. Active form of the protein can be conjugated to other proteins through a process known as ISGylation, which requires three enzymes; activating-E1, conjugating-E2, and ligating-E3 (D. Zhang & Zhang, 2011).

ISG15 also impedes viral infection by interfering with host cell replication machinery used by viruses. For example, ISG15 conjugation to eukaryotic initiation factor 4E (eIF4E) blocks viral mRNA capping and RNA translation (Okumura et al., 2007). Moreover, ISG15 conjugation to Human cytomegalovirus (HCMV) pUL26 protein inhibits viral interaction with host cell NF-kB signaling and replication (Kim et al., 2016).

The free form of ISG15 also impacts cell commitment and recruitment. To illustrate, it has been shown that ISG15 stimulation of macrophages can induce M1 polarization, production of reactive oxygen species (ROS), and nitric-oxide as antiviral factors (Baldanta et al., 2017). Furthermore, if ISG15 concentration is high at the site of infection, it can act as a chemoattractant for neutrophils

(Owhashi et al., 2003). In summary, ISG15 is a critical protein establishing of an effective anti-viral response.

1.4 Innate Immune Evasion by Viruses

Having entered the body, viruses encounter various defense mechanisms that are engaged by the innate immune cells. However, viruses have evolved ways to hide from or block these mechanisms.

Some viruses directly block recognition by cytosolic sensors. For example, the herpes simplex virus 1 (HSV-1) protein US11 interacts with both RIG-I and MDA-5 to impede viral recognition (Xing et al., 2012). Porcine Deltacoronavirus (PDCoV) non-structural protein NS6 interferes with binding of RIG-I to viral dsRNA (Fang et al., 2018).

Other viruses express proteins to suppress type I IFN response. For instance, viral protein NS1 of influenza A virus directly inhibits the activation of IFN pre-mRNA, and IRF3 TF processing (Krug, 2015; Weber-Gerlach & Weber, 2016). Human cytomegalovirus (HCMV) blocks IFN-dependent antiviral activity in the host cell through viral-encoded proteins (Amsler et al., 2013). Similarly, nonstructural protein NSs belonging to phleboviruses are characterized as IFN-antagonist and are found to be effective in proteasomal degradation of cytosolic sensor RIG-I (Gori Savellini et al., 2015).

Similar to the influenza A virus, influenza B virus protein NS1 evades ISG15 mediated anti-viral response (Yuan & Krug, 2001). Vaccinia virus protein E3L similarly promotes virus replication by antagonizing ISGylation in both mice and human (Eduardo-Correia et al., 2014). SARS-CoV, MERS-CoV, and human coronavirus NL63 encode papain-like proteases (PLPs) that deubiquitylate and deISGylate target proteins (Clementz et al., 2010; Mielech et al., 2014).

1.5 SARS-CoV-2

Severe Acute Respiratory Syndrome Coronavirus 2 (SARS-CoV-2) is a positive-sense RNA virus and the causative agent of infectious Coronavirus disease 2019 (COVID-19). Similar to SARS-CoV and MERS-CoV, it belongs to the *Betacoronavirus* genus of the *Coronaviridae* family. SARS-CoV and MERS-CoV showed limited transmission among humans, SARS-CoV-2 exhibits remarkably high human-to-human transmission that has caused the ongoing pandemic. It is thought that until reaching humans, coronaviruses infect and reside in a broad range of host species such as ferrets, rabbits, cats, rats, birds, camels, and bats (Chan et al., 2015; Latif & Mukaratirwa, 2020).

Coronaviruses are divided into four genera: *Alpha*, *Beta*, *Gamma*, and *Deltacoronavirus*. While *Alpha* and *Betacoronaviruses* frequently infect mammals and humans, *Gamma* and *Deltacoronaviruses* commonly cause infections in birds and fish. As a distinctive feature of *Alpha* and *Betacoronaviruses*, the virus possesses a non-structural protein NSP-1, with no counterpart ever reported in *Gamma* and *Delta* (Mariano et al., 2020).

Similar to other *Betacoronaviruses*, SARS-CoV-2 is an enveloped, single-stranded RNA virus. Its large genome encodes four structural proteins: spike (S), envelope (E), membrane (M), and nucleocapsid (N), a series of non-structural (NSP1-16) and various accessory proteins (ORF3a, 3b, 6, 7a, 7b, 8, 9b, 9c and 10) (shown in Figure 1.5) (N. Wang et al., 2020).

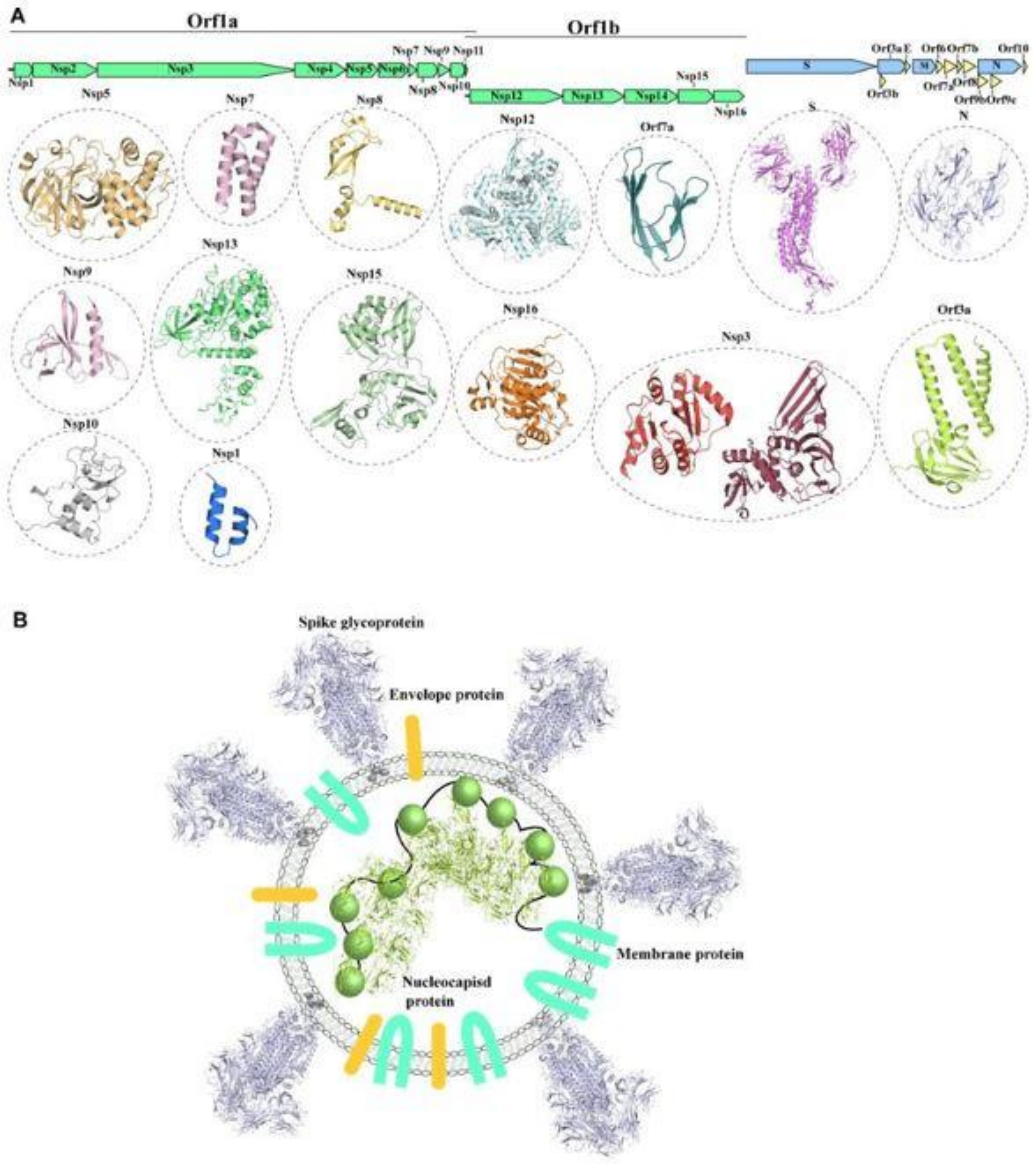

Figure 1.5 Proteins encoded by SARS-CoV-2 genome (Adopted from (Mariano et al., 2020))

Spike (S) protein helps virus to attach to host cell receptor angiotensin-converting enzyme 2 (ACE-2), which then facilitates viral entry. Furthermore, TM protease serine 2 (TMPRSS2) an enzyme that is located on the host cell membrane, stimulates viral entry by enzymatically activating the S protein. This glycoprotein binds ACE2 via its receptor-binding domain (RBD), located on the S1 subunit of spike. Following binding, S1 subunit dissociate and the S2 subunit mediates fusion

with the host cell membrane (Y. Huang et al., 2020; Letko et al., 2020). Since Spike protein is the key player during viral entry, it is also the main target of several COVID-19 vaccines. Other than S, the viral membrane protein M is important for virus assembly and egress (Mahtarin et al., 2020). SARS-CoV-2 E protein is an another critical component of viral assembly, its release, and virulence (Chai et al., 2021). It is also characterized as an ion channel protein viroporin and activator of interferon-stimulative genes (ISGs) (Lei et al., 2020). E protein has been implicated in NLRP3 inflammasome activation in the host (Kern et al., 2021). The fourth structural protein N, is responsible for the genomic packaging of the virus, mediating binding and packaging viral RNA into developing virions (Cubuk et al., 2021; Ye et al., 2021). The majority of the N protein is expressed during the early phase of infection, and it accumulates at the replication transcription complex (RTC), wherein it promotes replication and viral RNA transcription (Jack et al., 2021). N is generally the most abundant protein in infected cells so that antigenic tests to detect active virus existence depend commonly on N protein expression (Ye et al., 2021). Non-structural and accessory proteins of SARS-CoV-2 may also act as modulators of host innate defenses as described in the following Section.

1.5.1 Immunomodulatory Effects of SARS-CoV-2 Non-structural Proteins

The SARS-CoV-2 genome encodes 16 different NSPs in the long coding open reading frame 1a and 1b polyproteins (ORF1ab) which can work independently or co-interactive with each other (shown in Figure 1.5 a). Those non-structural proteins are crucial for viral replication, transcription, and production of envelope proteins, contribute to pathogenesis and interfere with host's signaling, thereby mediating immune evasion (Gordon et al., 2020; Michel et al., 2020). For example, NSP1 can negatively regulate host cell protein synthesis by blocking mRNA translation by interfering with its entry to the 40S ribosome. Also, NSP1 expression in the human cell line HEK293T interferes with IFN-I, IFN-III, and IL-8 secretion

after challenging cells with RIG-I agonists (Banerjee et al., 2020; Thoms et al., 2020). It has been found that SARS-CoV-2 specific NSP6 antagonizes phosphorylation of IRF3 and subsequent production of type I IFNs after stimulating RIG-I signaling in NSP6 expressing cells (Xia et al., 2020). A different non-structural protein NSP13 was found to downregulate RIG-I mediated IFN-β response if protein was ectopically expressed in HEK293T cells (Yuen et al., 2020). Other than these, NSP12 and NSP13 function in formation of replication complex through assembly of RNA-dependent RNA polymerase (RdRp) and helicase, respectively. While NSP10, 13, 14, and 16 are important for viral mRNA capping, NSP10, 14, and 15 work together to proofread the nascent genome (Romano et al., 2020).

1.5.2 Immunomodulatory Effects of SARS-CoV-2 Accessory Proteins

In addition to structural and non-structural proteins, nine accessory proteins from the viral genome were defined. Unlike NSP proteins, accessory proteins are not required for viral assembly and replication, but contribute to pathogenesis of SARS-CoV-2 (Rohaim et al., 2021). Specifically, ORF3a, ORF6, ORF7b, ORF8, and ORF10 were implicated in enhanced pathogenesis and transmissibility (Redondo et al., 2021).

ORF3a is a 275 amino acid long accessory protein encoded by a gene located between S and E structural proteins in the viral genome. It is the largest accessory protein defined in SARS-CoV-2 and it’s characterized as a viroporin protein when expressed in infected cells. Viroporins function as an ion channel protein to enable viral release. Hence, through viroporin activity, maximum virulence and virus replication can be achieved. The accessory protein ORF3a is also facilitates NLRP3 inflammasome activation, overproduction of IL-1β and other inflammatory cytokines, all in all leading to exacerbated inflammation in the host (Azad & Khan, 2021).

From SARS-CoV and SARS-CoV-2 studies, ORF3b and ORF6 accessory proteins were defined as antagonists for type I IFNs (Kopecky-Bromberg et al., 2007; Xia et al., 2020). Both short and long variants of ORF3b have been associated with interferon antagonism and more severe COVID-19 illness (Lam et al., 2020). Furthermore, another study from University of Tokyo has discovered that when ORF3b was expressed ectopically in the human lung cell line A549, cells exhibited significantly lower *IFNB1* expression after Sendai virus infection, and eventually impaired type I IFN response (Konno et al., 2020). In another study, ORF6 was found to be one of the highest cytotoxicity causing viral proteins together with ORF7a and NSP6 after expressing individual SARS-CoV-2 protein in human cells. The researchers also concluded that ORF6 impact subcellular localization of viral RNA, ribosome and proteasome complexes, and MHC class I antigen processing pathways (Lee et al., 2021).

The role of ORF8 accessory protein in SARS-CoV-2 infection and lung pathology remains elusive. A research group from China showed that ORF8 is the least homology sharing protein among SARS-CoV and SARS-CoV-2 (Y. Zhang et al., 2020). The same Chinese researchers also demonstrated that viral protein ORF8 disrupts antigen presentation by directly interacting with MHC I molecules on the cell surface and target them for lysosomal degradation. In addition, ORF8a and ORF8b were previously classified as viroporin in SARS-CoV, but not in SARS-CoV-2 due to the deleterious mutation that inactivates the formation of tandem ORF8ab (Neches et al., 2021). In contrast, SARS-CoV-2 ORF8 was found to be aggregated in lung cells and has been implicated as a modulator of antiviral immune response (Geng et al., 2021).

To date, not all SARS-CoV-2 NSPs and ORFs have been investigated thoroughly. Understanding the mechanism behind how/which SARS-CoV-2 viral protein mediates immune evasion needs more attention.

1.6 Aim of the Study

COVID-19, acute respiratory disease, has been associated with lung-pathology resulting hyper-inflammation (C. Huang et al., 2020; Song et al., 2020). Following recognition of viral nucleic acids through various PRRs, the immune system responds with type I IFNs production as a first line of defense. In addition, inflammasome activation is triggered in response to DAMPs and contribute to hyper-inflammation. In this context, herein, we aimed to investigate the immunomodulatory role played by some of the structural, non-structural and accessory SARS-CoV-2 proteins in terms of their ability to antagonize/enhance type I IFN signaling and inflammasome activation in THP1-Dual IRF/NF-kB reporter cells.

To this end, first, we produced lentiviral vectors to stably encode SARS-CoV-2 specific structural, non-structural, and accessory proteins in the cells. Then, viral transduction and antibiotic selection was performed. 5 different cell lines, expressing the NSP9, NSP10, ORF3a, ORF8 and Nucleocapsid proteins of SARS-CoV-2 were generated, and compared against GFP expressing MOCK and wild-type controls.

To examine the immunomodulatory effects of the proteins, IRF reporter function of the cells were used to investigate IFN antagonism following stimulation of cells with 5'ppp dsRNA, poly (I:C) and R848 to mimic viral infection. Individual cell lines were also treated with IFN-β to induce ISG15 production. Subsequently, cells were intracellularly stained to analyze ISG15 levels in relation to SARS-CoV-2 protein expression via flow cytometry. To understand how SARS-CoV-2 viral proteins affected inflammasome activation, we stimulated cells with one of the NLRP3, NLRC4, AIM2 or the non-canonical inflammasome ligands. Cell supernatants were then assessed for IL-1β production as a marker of active inflammasome. To evaluate whether inflammasome activation accompanies cell death, cell viability was assessed using LDH release or through staining of cells with SytoxOrange or Propidium Iodide in order to visualize cell death with a

fluorescent microscope, and to quantify percent viability via flow cytometry, respectively.

CHAPTER 2

MATERIALS & METHODS

2.1 Materials

2.1.1 Plasmids and Related Reagents

SARS-CoV-2 structural, non-structural, and accessory protein encoding plasmids were a generous gift from Krogan Lab (CA, USA, vector maps are shown in the Appendix A). For plasmid isolation, NucleoSpin Plasmid MiniPrep kit (Macherey-Nagel, Germany) was used. All the plasmids were verified with restriction enzyme digestion for their purities and yields by using *Bam*HI-HF (New England Biolabs, USA) and *Eco*RI-HF (New England Biolabs, USA) enzymes and 10X CutSmart buffer (New England Biolabs, USA), then loaded onto 1% agarose gel (Appendix A). 1 kb Plus DNA Ladder from NEB (cat. #N3200S) was used to determine exact size of the plasmids.

2.1.2 Bacterial Strain and Culture Media

In order to expend SARS-CoV-2 plasmids, NEB Stable strain *E.coli* competent (New England Biolabs, USA) transformation was performed. Luria Broth agar or Luria Broth medium containing ampicillin was used to culture bacteria. Media preparation is detailed in Appendix B.

2.1.3 Cell Lines

THP1-Dual, human acute monocytic leukemia cell line with reporter function for NF-kB and interferon regulatory factor (IRF) pathways was procured from Invivogen (USA). The study of IRF pathway can be achieved by measurement of secreted luciferase in the cells. HEK 293FT cell line used in the lentivirus production were kindly provided by Prof. Batu Erman from Boğaziçi University.

2.1.4 Cell Culture Media, Solutions and Buffers

Growth medium RPMI 1640 with L-glutamine was supplemented with heat-inactivated Fetal Bovine Serum (FBS), MEM non-essential amino acids, sodium pyruvate, HEPES buffer, Penicillin/Streptomycin, and other culture related solutions such as Phosphate buffered saline (PBS) and cell culture grade water were purchased from Biological Industries (Israel). Along with Normocin (cat. #ant.nr), Zeocin (cat. #ant-zn) and Blasticidine (cat. #ant-bl) antibiotics were used in the culture medium of THP1-Dual cells. After lentiviral transduction, puromycin antibiotic from Invivogen (USA) was added into the culture medium. Serum reduced transfection medium Opti-MEM was obtained from Thermo Fisher Scientific (USA). Recipes for complete culture media are listed in Appendix C.

2.1.5 Chemicals and Reagents

Lipofectamine 2000 reagent used for the transfection of various inflammasome, and viral ligands was purchased from Thermo Fisher Scientific (USA). To quantify IRF reporter function of THP1-Dual cells, luciferase detection reagent QUANTI-Luc (cat. #rep-qlc2) was procured from Invivogen (USA). Triton-X-100 (10%) which was used as a positive control for LDH assay was purchased from Cayman Chemical Company (cat. #601171). Lactate dehydrogenase (LDH) cytotoxicity

detection kit was from Roche (Switzerland). Sytox^{TM}Orange to visualize dead cells were ordered from Invitrogen (USA, cat. #S11368).

2.1.6 Antibodies, Dyes and Related Reagents

2.1.6.1 For ELISA and Intracellular Staining

Human Il-1β specific monoclonal unlabeled capture antibody, biotinylated detection antibody, and alkaline phosphatase conjugated streptavidin (Strep-ALP) used in the cytokine ELISA assay were purchased from Mabtech (Sweden). As the substrate for Strep-ALP, p-nitrophenyl phosphatase disodium salt pNPP (VWR Life Sciences, cat. #4264-839) and diethanolamine substrate buffer from Thermo Fisher Scientific (cat. # 34064) were used. 96-well plates specifically used in this assay were purchased from SPL Life Sciences (Korea). Buffers for ELISA are listed in Appendix C.

For intracellular staining, 5ul of Anti-hISG15/UCRP-PE fluorophore conjugated antibody from R&D Systems (cat. #IC8044P, concentration: 0.125 ug/ml) was used together with Permeabilization medium B after cells were fixed with Fixation Medium A (Immunostep, Spain).

2.1.6.2 For Western Blotting

Primary and secondary IgG detection antibodies are listed in TABLE 2.1. All antibodies were diluted in 5% Bovine Serum Albumin in PBS-Tween20 (0.1%) (Appendix D). Dilution factors are indicated in Table 2.1.

Table 2.1. List of antibodies used for Western Blot analysis

Name	**Company**	**Cat no.**	**Dilution factors in 5%BSA in PBS-T**
Mouse Anti-Streptag-II	ELK Biotechnology	#EM1155	1:2000
Anti-mouse IgG-HRP conjugated Ab	R&D systems	#HAF007	1:5000
SARS-CoV-2 Nucleocapsid Ab Mouse IG2B	Prosci	35-579	1:5000
Mouse β-actin (8H10D10)	Cell Signaling technology	3700	1:1500

2.1.7 Western Blotting Reagents

To separate proteins, gels were prepared according to manufacturer's protocol of TGX FastCast Acrylamide Kit 10% (Bio-rad, USA, cat. #1610173) and nitrocellulose membrane from the same brand was used to transfer proteins. As a chemiluminescent substrate for the detection antibody, ECL Prime Western Detection Reagent (Amersham, cat. #RPN2232L/AC) was used. Various buffers used in Western Blotting are listed in Appendix D.

2.1.8 Inflammasome Inducers

The PAMPs and DAMPs to activate targeted inflammasomes are listed in Table 2.2. Phorbol 12-myristate 13-acetate (PMA) was used for priming and differentiating THP1 monocytes into macrophages.

Table 2.2. Pattern recognition receptor ligands used in inflammasome activation

Ligands	Description	Working Concentration	Brand	Catalog #	Targeted pathway
Alum crystals*	Potassium and aluminum hydroxide salts	200 µg/ml	Invivogen (USA)	tlrl-alk	NLRP3 Inflammasome
Flagellin*	Bacterial flagellin component	1 µg/ml	Invivogen (USA)	tlrl-stfla	NLRC4 Inflammasome
LPS* from *E. coli*	Gram (-) bacterial outer membrane component	1 µg/ml	Sigma-Aldrich	L2630-10MG	Non-canonical Inflammasome
nigericin	Microbial toxin	2 µM	Invivogen (USA)	tlrl-nig	NLRP3 Inflammasome
Poly (dA:dT)*	dsDNA analog	5 µg/ml	Invivogen (USA)	tlrl-patn-1	AIM2 Inflammasome
PMA	phorbol 12-myristate 13-acetate	50 µg/ml	Invivogen (USA)	tlrl-pma	NF-kB

* Lipofectamine2000 (0.3 µl/well in 96-well plate) was complexed with the indicated ligands for cytosolic delivery of ligands.

2.1.9 Ligands used as Viral Infection Mimetics

To stimulate intracellular viral ligand sensing pathways, synthetic dsRNA analogs 5'ppp-dsRNA and poly I:C were transfected with Lipofectamine2000. TLR7/TLR8 agonist R848 (Resiquimod) was used as such.

Table 2.3. Pattern recognition receptor ligands used as viral infection mimetics

Ligands	Description	Working Concentration	Brand	Catalog #	Targeted Pathway
R848 ssRNA	Synthetic Resiquimod compound	5 µg/ml	Invivogen (USA)	tlrl-r848	TLR7/ TLR8
5'ppp-dsRNA*	dsRNA analog	1 µg/ml	Invivogen (USA)	tlrl-3prna	RIG-I
Poly (I:C)-dsRNA (HMW)*	dsRNA analog	1 µg/ml	Invivogen (USA)	tlrl-pic-5	MDA-5, RIG-I

* Lipofectamine2000 (0.3 µl/well in 96-well plate) was complexed with the indicated ligands for cytosolic delivery of ligands.

2.2 Methods

2.2.1 Plasmid Transformation, Isolation and Verification

Competent cells were thawed on ice (100 µl/ tube) and 5 µl of relevant plasmids were added into tubes. The tubes were slowly mixed, left on ice for 30 minutes, then heated to 42ºC 60 seconds and subsequently incubated on ice for 2 minutes. After this heat shock, 1 mL of regular LB medium was added to each tube and incubated 80 minutes at 30ºC without shaking. Afterwards, tubes were centrifuged at 2000 g for 10 minutes. Supernatants were discarded, pellets were dissolved with 500 µl regular LB medium and 100 µl of competent solution was spread onto the surface of a selective antibiotic ampicillin containing agar plate. Plates were incubated for about 18-20 hours at 30º until single colony formation was observed.

The following day, selected colonies were inoculated into LB liquid medium containing ampicillin. After overnight incubation, culture medium was centrifuged, supernatant was discarded, and plasmids were isolated according to manufacturer's protocol of the Macherey-Nagel plasmid isolation kit. 1 µg of desired circular plasmids were double digested by restriction enzymes *BamHI* and *EcoRI,* and using 1X CutSmart buffer (NEB, cat#B6004). To provide proper endonuclease digestion, plasmid-enzyme-buffer mixtures were prepared in eppendorf tubes and tubes were placed at a 37ºC incubator for 30 minutes. Next, linearized DNAs and their purities were assessed through agarose gel electrophoresis (AGE; 1%) at 100V for 1 hour.

2.2.2 Cell Culture

2.2.2.1 Maintenance of THP1-Dual Cell Line

THP1-Dual™ reporter cell line (Invivogen, USA) is a monocytic leukemia cell line, and the cells were derived from wild type THP-1 cells. THP1 monocytes are frequently used in inflammasome studies since they express high levels of NLRP3, adaptor protein ASC, pro-caspase 1 and pro-IL-1β after priming with phorbol 12-myristate 13-acetate (PMA) or any other Toll-Like Receptor (TLR) ligand. Nevertheless, maturation of pro-IL-1β and pro-caspase 1 complexes depend upon secondary stimulation with various inflammasome inducers. THP1 Dual cells were genetically modified to enable monitoring of NF-kB and IRF signaling pathways through measurement of secreted embryonic alkaline phosphatase (SEAP) and Lucia Luciferase activity, respectively upon initiation of signal transduction. These reporter functions are maintained by two selective antibiotics: Zeocin™ and blasticidin. Cells were maintained in 10% FBS supplemented RPMI 1640 medium at a confluency of 5-7 x 10^5 cells/ml and cell passaging was done between 2-3 days in order to obviate a cell density of above 2x 10^6 cells/ml. Cells were discarded before 20^{th} passage.

2.2.2.2 Stable Cell Line Generation

2.2.2.2.1 Lentiviral Vector Production

For production of lentiviruses that cannot replicate but facilitate integration of SARS-CoV-2 specific proteins into host genome, plasmids psPAX2 and pCMV-VSV-G were utilized for packaging and envelope protein expression, respectively. 1.59 µg psPAX2 and 0.88 µg pCMV-VSV-G plasmids together with 2 µg of a specific transfer plasmid DNA that encodes a SARS-CoV-2-specific protein per well were transfected to 75-80% confluent HEK 293FT cells in 6-well plates (Sarstedt, Germany). First, plasmids were diluted to the final volume of 250 µl Opti-MEM medium. Subsequently, 10 µl of Lipofectamine2000 and 250 µl Opti-MEM media were mixed and incubated for 5 minutes. Afterwards, the two mixtures were combined and incubated for 25 minutes at RT for complexation to take place. After this step, combined transfection mixture was added onto HEK293FT cells. To assess transfection efficiency, eGFP that has the same *pLVX* backbone with other SARS-CoV-2 plasmids was also used for viral vector production. Following 18 hours of incubation, GFP expression were assessed by flow cytometry, transfection medium and reagents were replenished with fresh harvest medium (listed in Appendix C.). Harvest medium containing the lentiviruses were collected every 24 hours for three consecutive days. Collected media was centrifuged at 500 g for 10 minutes, filtered through a 0.45 µm filter and then stored at -80^{o}C until THP1-Dual cell transduction. The lentiviral vector production protocols were from our laboratory's previous study (PhD Thesis of İsmail Cem Yılmaz, 2020).

2.2.2.2.2 Lentiviral Transduction of Dual Reporter THP1 Monocytes

3 x 10^5 THP1-Dual cells in 1 ml were seeded on 6-well plates with the same culture medium described in Appendix C excepts for the addition of selective antibiotics

and Normocin. Lentivirus containing medium was thawed on ice, mixed with 10 µg/ml polybrene (Merck, Germany) to increase transduction efficacy, and added onto THP1-Dual cells. 6-well plate was then spinoculated at 1000g for 1 hour at 32°C. Afterwards, wells were mixed by pipetting and incubated for 24 hours at 37°C. Following this incubation period, medium was replenished with 2 ml of fresh culture medium supplemented with Pen/Strep and 1.25 µg/ml puromycin. Plates were incubated until a cell density of 1x 10^6 cells/ml was achieved. When targeted confluency was attained, cells were diluted, seeded onto 96-well plates (Sarstedt, Germany) at a density of 0.5 cells/well and monitored with phase-contrast microscopy. At the end of nearly 50 days, single-cell colony formation was achieved. The aim of this step was to select a cell population that only expressed the targeted SARS-CoV-2 protein. In addition, lentiviruses that bear eGFP were also transduced and used as a MOCK control in all experiments.

2.2.2.2.3 Confirmation of Stable Protein Expression

Mammalian protein extraction reagent M-PER™ (Thermo Fisher Scientific, USA) supplemented with 1X Mini EDTA free protease inhibitor (Sigma-Aldrich, Germany) was used to prepare cell lysates. To verify that lentiviral transduced THP1-Dual monocytes were expressing the desired proteins, 4x10^6 cells were transferred into 1.5 ml eppendorf tubes, and centrifuged at 300 g for 10 minutes. Resultant pellets were mixed with 100 µl of M-PER™ -1X protease inhibitor mix, vigorously vortexed and incubated for 25 minutes at RT. Then, eppendorfs were centrifuged at 15.000 g, at +4°C for about 15 minutes. At the end, supernatants containing soluble proteins were collected, transferred to new tubes, and stored at -80°C for later use.

2.2.3 Western Blotting

Equal volumes (5 µl, 10 µl or 20 µl) of cell lysates were combined with reducing 6X Laemmli Buffer (Appendix D), incubated at 95ºC for 5 minutes, and then cooled on ice before loading into wells of an SDS-PAGE gel. Gel casting was done according to the manufacturer's protocol of TGX Stain-Free FastCast Acrylamide Kit, 10% (Bio-Rad, USA). In order to mark size separation, PageRular Prestained Protein Ladder 10-180 kDa (Thermo Fisher Scientific, cat. #26616) or PageRular Plus Prestained Protein Ladder 10-250 kDa (Thermo Fisher Scientific, cat. #26629) was used. After loading of wells, gel was run at 120V for 1 hour on a BioRad Miniprotean Tetra Vertical Electrophoresis Cell (USA). Following completion of SDS-PAGE, proteins were transferred onto nitrocellulose membranes by using cold transfer buffer (Appendix D) and a semi-dry gel transfer method. For this, a constant 0.25 ampere was used instead of a constant volt for 1 hour. Membranes were blocked with 5% skimmed milk in PBS-T for 1 hour at room temperature. Since all the SARS-CoV-2 structural, non-structural, and accessory proteins in this study have two Streptag in their mammalian expression vector, as a primary antibody, mouse Anti-Strep-tag-II from ELK Biotechnologies (cat. #EM1155) were used for 1 hour at room temperature or overnight incubation at +4ºC. Following wash steps for 5 minutes 3 times with PBS-T, secondary antibody was added. Secondary and other probing antibodies are listed in Table 2.1. Similarly, the membrane was incubated with the secondary antibody for 1 hour at RT or overnight at +4ºC. To develop membranes, Amersham™ ECL™ Prime Western Blotting Detection Reagents (Cytiva, cat. #RPN2232) were mixed at equal volumes and layered onto the membrane. For visualization of protein bands and ladder, membrane images were taken and analyzed using a Bio-Rad (USA) ChemiDoc imaging system.

2.2.4 Stimulation Experiments

THP1-Dual cells that were transduced with lentiviruses to ensure expression of a different SARS-CoV-2 protein were layered on a TC-treated flat-bottom 96-well plate (Sarstedt, Germany) at a density of 100,000 cells/well in 10% FBS supplemented culture medium without selective antibiotics. Each generated stable cell line was layered in duplicates. PMA was added at a final concentration of 50 ng/ml in a final volume of 200 µl culture medium. Cells were incubated for 16-18 hours (overnight) at 37^{o}C in a 5% CO_2 incubator. Then, cells were checked for attachment to bottom of wells by microscopy. Plates were centrifuged at 200 g for 5 minutes, then washed with pre-heated 1X DPBS to eliminate PMA from the culture medium. Next, inflammasome activators and viral ligands were prepared, complexed with Lipofectamine2000 if necessary and added at a final volume of 200 µl/well. 24 hours later, plates were removed from the incubator. To eliminate residual cells and debris, plates were centrifuged, and supernatants were collected into a fresh 96-well plate. Collected culture supernatants were stored at -20^{o}C until their next use in IL-1β cytokine ELISA or for quantification of secreted Lucia Luciferase and LDH assays.

2.2.5 IL-1β Cytokine Enzyme-linked Immunosorbent Assay (ELISA)

For quantification of IL-1β secretion into culture medium in response to inflammasome activation, cytokine ELISA assay was performed. Human anti-IL-1β capture antibody (Mabtech) was 1:250 diluted in 1X DPBS. 50 µl/well diluted capture antibody was dispersed into wells and incubated overnight at +4^{o}C. After overnight coating, plates were warmed to room temperature on a rocker, and then flicked to remove the capture antibody. In order to prevent unspecific binding, wells were loaded with 200 µl of blocking buffer (Appendix C.). After 2 hours of RT incubation, plates were flicked again, washed with ELISA Wash Buffer (Appendix C.) for 5 minutes and flicked. This step was repeated 3 times. Next,

following drying of wells, 50 µl of collected cell culture supernatants, and 50 µl of recombinant human-IL-1β standards were distributed into separate wells. Recombinant proteins were prepared, serially diluted in duplicates for 11 times starting at an initial concentration of 20 ng/ml. The last wells of the standard row were used as a blank, containing 50 µl of 1X DPBS alone. The blank was used to subtract background signal from absorbance. Plates were incubated for 2 hours at RT on a rocker. At the end of 2 hours, washing and air-drying steps were conducted as described above. Biotinylated detection antibody was 1:500 diluted in T-cell Buffer (Appendix C.), distributed to wells and incubated at +4^{o}C overnight. Parallel to these, Strep-ALP was similarly diluted 1:1000 in T-cell buffer and incubated at +4^{o}C overnight. The next day, plates were incubated at room temperature and washed and dried as described before. Then, 50 µl/well Strep-ALP solution was added and incubated for 1 hour at RT. Following washing and drying, pNPP substrate solution was dispersed into wells. Plates were incubated at room temperature in dark. To measure optical density (OD), Multiskan^{TM} FC Microplate Photometer Plate Reader was used at 405 nm wavelength and OD recordings were taken every 15 minutes. When recombinant protein and sample OD_{405} values reached saturation (approximately within 2 hours), measurements were stopped. Cytokine concentration was then assessed using a 4-parameter standard curve and the recorded OD values.

2.2.6 Detection of Type I IFN Production

2.2.6.1 Determination of type I IFN Expression in THP1 Dual Reporter Cells

For quantitative measurement of type I IFN production, luminescence signal of secreted Lucia Luciferase activity was used. Culture supernatants from stimulation experiments were mixed with the QUANTI-Luc solution. To prepare the QUANTI-Luc solution, 1 pouch of powder reagent was mixed with 25 ml of sterile water in

an amber bottle and kept protected from light. 20 µl of cell supernatants were layered onto 96-well opaque white plates. Just before reading, 50 µl of dissolved QUANTI-Luc solution was added onto supernatants and gently tapped. For measurements, SpectraMax iD3 (Molecular Devices, USA) plate reader and 0.1 second integration time were used.

2.2.6.2 Intracellular Interferon Stimulated Gene 15 (ISG15) Staining of Lentiviral Transduced THP1-Dual Cells

THP1 cells were layered at a density of 500,000 cells/well onto TC-treated 6-well plates in duplicates. Untreated and recombinant human IFN-β treated (Merck Serono, cat. #171031; 50 ng/ml) samples were used as a negative and a positive control, respectively. After overnight incubation at 37ºC under 5% CO_2, cells were transferred to new eppendorf tubes by pipetting. Eppendorfs were centrifuged at 300 g for 10 minutes at room temperature, and then 100 µl of Fixation Medium A (Immunostep, Spain) was added dropwise onto cell pellets while vortexing. After 15 minutes of RT incubation, 1 ml of FACS Buffer (Appendix C.) was added onto fixed pellets and cells were washed as such twice. Next, pellets were resuspended in 100 µl of Permeabilization Medium B containing 5 µl of hISG15/UCRP-Phycoerythrin (PE) conjugated antibody. Eppendorfs were left for 30 minutes incubation at RT in the dark. Finally, tubes were washed with FACS buffer as mentioned above and the final pellet was resuspended in 300 µl of FACS buffer. Stained cells were then analyzed on a Novocyte 2060R flow cytometer (ACEA Biosciences, USA). A minimum of 15,000 events were acquired. Since Phycoerythrin and GFP channels are overlapping, all lentiviral transduced cells (except MOCK) and WT cells were compared with each other but not with mock treated cells.

2.2.7 Cytotoxicity Detection assays

2.2.7.1 Lactate Dehydrogenase (LDH) Assay

For cytotoxicity assay, Roche's LDH Kit was used as recommended by the manufacturer. Briefly, previously collected, and frozen cell culture supernatants were thawed, and mixed 1:1 ratio with detection solution (70 µl+ 70 µl). For high cytotoxicity control, supernatants from cells cultured with Triton-X-100 and 10% FBS supplemented RPMI medium were used as a positive and negative controls, respectively. After incubation at dark for 30 minutes, two optical density values at 490 and 600 nm was measured.

2.2.7.1.1 Percent Cytotoxicity Calculation

For all samples, 600 nm readings were subtracted from 490 nm values. Percentage of cytotoxicity was calculated based on the following formula:

[(experimental value-low control) / (high control-low control)] *100

2.2.7.2 SytoxOrange Staining

To image dead cells, lentivirus transduced and stimulated THP cells exposed to the membrane impermeable DNA binding dye SytoxOrange. This dye stains only dead cells and is excluded by live cells. Briefly, 24 h after stimulation and harvest of supernatants, THP cells were resuspended in 200 µl of pre-heated 1X DPBS and centrifuged at 200 g for 5 minutes. SytoxOrange™ dye was then added at a final concentration of 5µM in 50 µl of 1X-DPBS. Plates were incubated at 37^{o}C for 15 minutes at dark. Imaging was performed on FLoid™ Cell Imaging Station using the red channel.

2.2.7.3 Propidium Iodide (PI) Staining

250,000 stimulated THP1 cells were stained with 2 µl of Propidium Iodide (PI) solution from BioLegend (cat. #421301, concentration: 0.5 mg/ml) in 400 µl of 1X DPBS containing eppendorfs. Tubes were incubated at +4^{o}C for 15 minutes and live-dead cell populations were analyzed on a Novocyte 2060R flow cytometer (ACEA Biosciences, USA).

2.2.8 Statistical Analysis

Statistical analysis and individual plots were established by using GraphPad Prism 9 software. Ordinary one-way ANOVA and Tukey's tests were used together for statistical analysis of IL-1β production, type I IFN quantification and calculation of cytotoxicity experiments. *, **, ***, and **** represent $p<0.05$, $p<0.01$, $p<0.001$ and $p<0.0001$, respectively. Data are presented as means ± SEM.

CHAPTER 3

RESULTS & DISCUSSION

Coronaviruses are single-stranded RNA viruses that infect many different animals such as camels, bats, and humans. Coronavirus infection in humans causes severe respiratory diseases like the ones that were seen in 2002 and 2012 by severe acute respiratory syndrome coronavirus (SARS-CoV) and middle east respiratory syndrome coronavirus (MERS-CoV) (Hu et al., 2021). At the end of 2019, a novel coronavirus, designated as SARS-CoV-2 has emerged in China, Wuhan and spread all around the world, causing the coronavirus disease 2019 (COVID-19) pandemic. The outbreak of COVID-19 has not been eradicated yet, and millions of people are still under threat of developing COVID-19, some of which culminate in death. Following infection, the disease starts with flu-like symptoms that can progress to pneumonia, respiratory/gastrointestinal hyper-inflammation, lung failure, renal problems, and even death (Harrison et al., 2020). Pathogenesis of the virus in the lung and respiratory tract is associated with over-production of cytokines (named as cytokines storm (CS)) such as IL-1β, MCP-1, IP-10, IL-4, and IFN-γ by macrophages in the lung (Asrani & Hassan, 2021). Overproduction of these inflammatory cytokines causes immune cell recruitment and infiltration, lymphocyte exhaustion, endothelial cell injury, all of which collectively contribute to lymphopenia and multiple organ failures (Tang et al., 2020). While contribution of structural proteins of SARS-CoV-2, such as the Spike has been extensively studied in host cell entry, non-structural and accessory proteins also play important roles in viral immune evasion. Herein, we aimed to investigate the impact of SARS-CoV-2 accessory/non-structural and structural proteins in modulating inflammasome activation and type I interferon signaling response of host cells. For this, we first stably expressed the SARS-CoV-2 viral proteins in human monocytic NF-κB/IRF reporter THP1-Dual cells. Then, by using the reporter function of these

cells, type I IFN responses were measured as such or following stimulation with RNA sensor ligands such as 5'ppp dsRNA, poly (I:C), and R484. Furthermore, expression of type I interferon-stimulated gene product ISG15, was assessed by intracellular staining following IFN-β treatment of the cells. The effect of SARS-CoV-2 accessory/structural/non-structural protein expression on inflammasome activation was also determined following stimulation with NLRP3-, NLRC4-, AIM2-, or non-canonical inflammasome- activators and assessment of IL-1β production and extent of cell death.

3.1 Validation and Purity Determination of SARS-CoV-2 Accessory, Structural and Non-structural Protein Expression Plasmids

SARS-CoV-2 accessory, structural and non-structural protein expressing plasmids were donated by Krogan Lab (CA). All protein encoding genes were codon-optimized and cloned into mammalian expression vectors with a 2x Strep-tag II affinity tag (Gordon et al., 2020). For validation and purity determination of the plasmids, endonuclease restriction enzyme digestions were performed, and then analyzed through agarose gel electrophoresis (AGE). Expected base pairs of digested fragments are indicated in Table 3.1 and gel images of representative restriction enzyme digestion experiments are presented in Figure 3.1 and Figure 3.2.

All digested fragments derived from endonuclease digestion of corresponding plasmids, (except linearized ORF8), were within their expected fragment lengths and their purities were within acceptable limits. Since 1 µg cut ORF8 plasmid did not generate a visible digestion fragment, (see Figure 3.1), 2 and 4 µg of ORF8 plasmid was digested and loaded onto a 1% agarose gel (Figure 3.2). This time, the expected band and purity of the plasmid was also deemed to be appropriate.

Table 3.1 Expected base-pair results of after restriction digestion performed plasmids.

	Nsp9	**Nsp10**	**ORF3a**	**ORF8**	**Nucleocapsid**	**eGFP**
BamHI-EcoRI	8793 bp	8793 bp	8793 bp	8793 bp	8793 bp	8793 bp
EcoRI-BamHI	462 bp	540 bp	945 bp	483 bp	1377 bp	849 bp

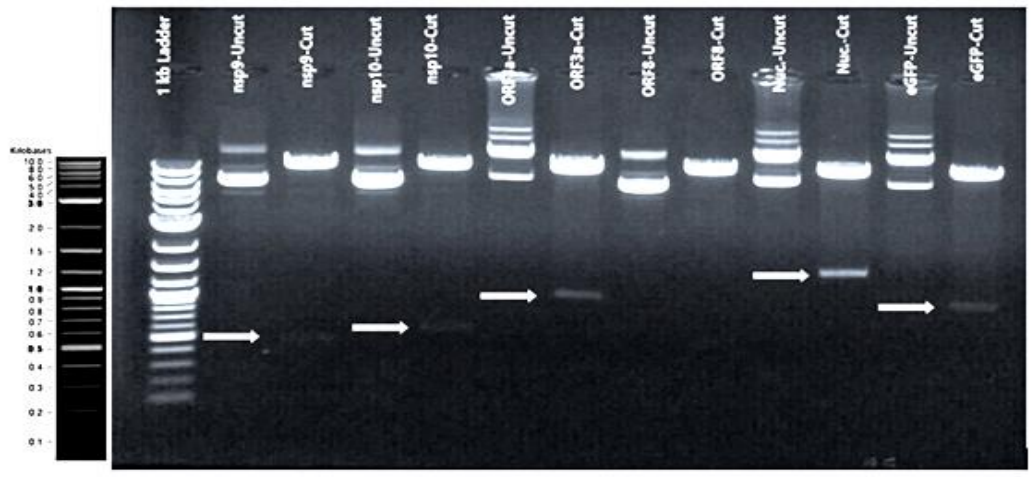

Figure 3.1 Verification of SARS-CoV-2 specific protein expressing plasmids by restriction endonuclease digestion. All plasmids, including the control eGFP plasmid were digested with *EcoRI* and *BamHI* and analyzed by agarose gel electrophoresis against the DNA ladder of 1 kb.

Lane 1: 1 kb DNA Ladder, Lane 2: NSP9 plasmid (Uncut), Lane 3: NSP9 plasmid (Cut), Lane 4: NSP10 plasmid (Uncut), Lane 5: NSP10 plasmid (Cut), Lane 6: ORF3a plasmid (Uncut), Lane 7: ORF3a plasmid (Cut), Lane 8: ORF8 plasmid (Uncut), Lane 9: ORF8 plasmid (Cut), Lane 10: Nucleocapsid plasmid (Uncut), Lane 11: Nucleocapsid plasmid (Cut), Lane 12: eGFP plasmid (Uncut), Lane 13: eGFP plasmid (Cut).

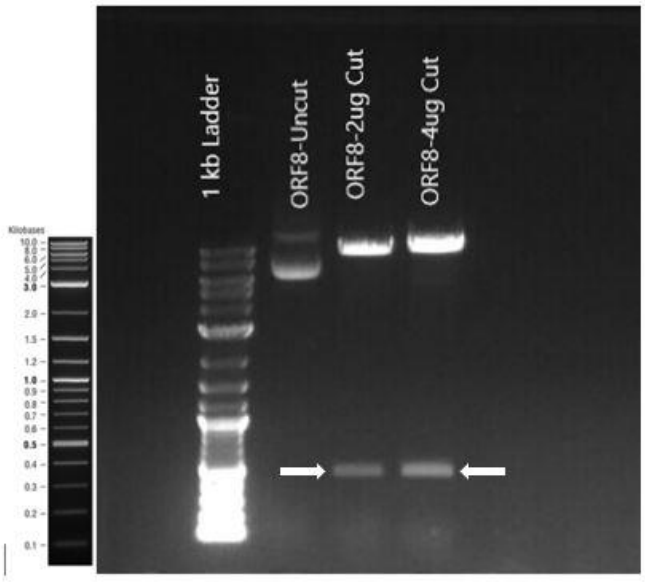

Figure 3.2 Verification of SARS-CoV-2 ORF8 expressing plasmid by restriction endonuclease digestion. 2 or 4 µg of ORF8 expression plasmid was digested with *EcoRI* and *BamHI* and analyzed by agarose gel electrophoresis against the DNA ladder of 1 kb.

Lane 1: 1 kb DNA Ladder, Lane 2: ORF8 plasmid (Uncut), Lane 3: ORF8 plasmid (2 µg Cut), Lane 4: ORF8 plasmid (4 µg Cut)

3.2 Construction and Verification of stable SARS-CoV-2 Structural, Non-structural, and Accessory Protein-expressing THP1-Dual Cell Lines

Contrary to short term protein expression with transient gene transfection approaches, stable cell lines can be generated using lentiviral vectors for long term protein expression (Levine et al., 2017; Ribeil et al., 2017). Particularly, to generate stable expression in mammalian cell lines, 3rd generation lentiviral vectors are widely used (Tandon et al., 2018). Like other viruses, lentiviruses use host cellular machinery to package and augment their genetic material. Through membrane fusion, the loaded transgene is delivered into cells (Elegheert et al., 2018). This

method is very convenient and safe, considering that these viruses are replication-incompetent. Following expansion and purification of SARS-CoV-2 protein plasmids, we first generated stable NSP9 (12.4 kDa), NSP10 (14.8 kDa), and ORF8 (13.8 kDa) expressing THP1-Dual cell lines by the lentiviral packaging and transduction system as described in Section 2.2.2.2.1 (Gordon et al., 2020). After viral transduction, cells were expanded under antibiotic selection for approximately one month period. Then, cell lysates were prepared and used for Western Blotting using an Anti-Strep-tag-II detection antibody. Figure 3.3 demonstrates that eGFP (32.7 kDa), NSP9, and NSP10 protein bands were detected at their expected MW, indicating that successful stable expression was achieved in THP1-Dual cells. On the other hand, ORF8 expression was detected at low levels in the cell line (Figure 3.3. Lane 5 and Lane 9).

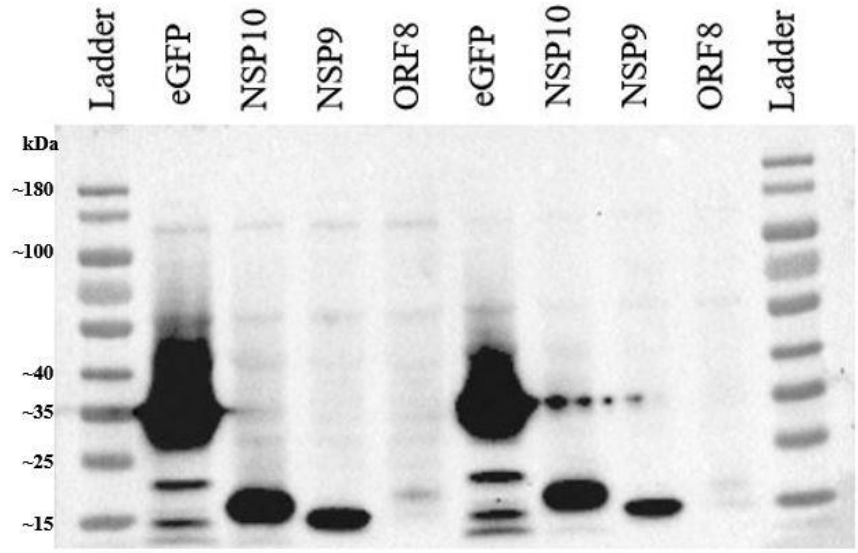

Figure 3.3 Protein expression in cells lentivirally transduced to stable express eGFP, Nsp10, Nsp9, or ORF8 proteins. Lysates were prepared at least one month after expansion under antibiotic selection. Protein bands were visualized by immunoblotting using the Anti-Step-tag-II antibody.

Lane 1: 180 kDa Protein Ladder, Lane 2: 10 µl cell lysate of eGFP, Lane 3: 10 µl cell lysate of Nsp10, Lane 4: 10 µl cell lysate of Nsp9, Lane 5: 10 µl cell lysate of

ORF8, Lane 6: 5 µl cell lysate of eGFP, Lane 7: 5 µl cell lysate of Nsp10, Lane 8: 5 µl cell lysate of Nsp9, Lane 9: 5 µl cell lysate of ORF8, Lane 10: 180 kDa Protein Ladder.

Since ORF8 expression was very low, to enrich high expressors, single-cell colony formation was followed for another 40 days. Eight expanded clones were chosen and scanned for ORF8 protein expression (Figure 3.4). To determine which clone expressed the highest amount of ORF8, immunoblots were subjected to densitometric analysis (Figure 3.5).

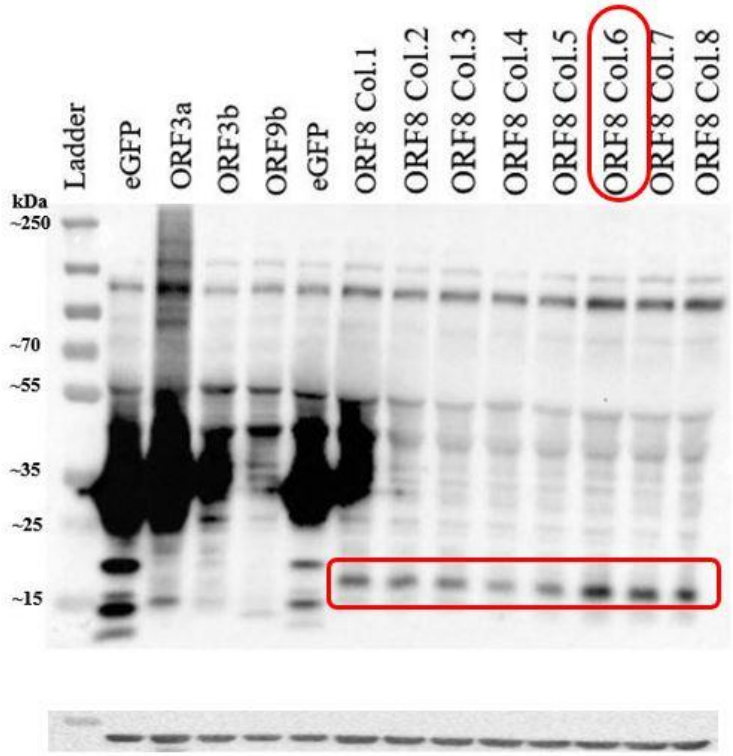

Figure 3.4 Strep-Tagged protein expression profiles of SARS-CoV-2 viral protein-expressing cells and accessory protein ORF8 expressing 8 different clones following probing with Anti-Strep-tag-II antibody.

Lane 1: 250 kDa Protein Ladder, Lane 2: eGFP lysate (20 µ), Lane 3: ORF3a (10 µl), Lane 4: ORF3b (10 µl, not detected), Lane 5: ORF9b (10 µl, not detected), Lane 6: eGFP(10 µl), Lane 7: ORF8 clone 1 (20 µl), Lane 8: ORF8 Clone 2 (20

µl), Lane 9: ORF8 clone 3 (20 µl), Lane 10: ORF8 clone 4 (20 µl), Lane 11: ORF8 clone 5 (20 µl), Lane 12: ORF8 clone 6 (20 µl), Lane 13: ORF8 clone 7 (20 µl), Lane 14: ORF8 clone 8 (20 µl).

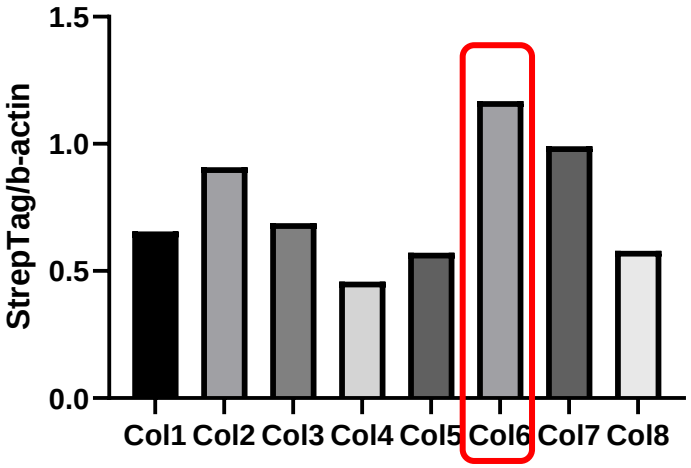

Figure 3.5 Densitometric analysis of Colony 6 Anti-Streptag band signals over housekeeping gene β-actin.

According to the densitometric analysis, the highest ORF8 protein expression was observed in Colony 6. Next, Colony 6/ ORF8 expressing THP1-Dual monocytes were expanded and cryopreserved for later use. Generation of stable ORF8 expressing cell line was important for us because, it has been shown that ORF8 protein can interact with other SARS-CoV-2 proteins and this interaction causes a notable decrease in the type I IFN response of host cells (Valcarcel et al., 2021; Zhang et al., 2020). Moreover, the protein itself can also inhibit interferon production in the cell and causes impaired nuclear translocation of IRF3 which is a critical transcription factor for type I IFN downstream signaling (Jefferies, 2019; Rashid et al., 2021).

A similar lentiviral transduction/detection strategy was also used to generate cells stably expressing ORF3a (31.1 kDa), ORF3b (6.5 kDa), ORF9b (10.8 kDa), Nucleocapsid (45.6 kDa), and Envelope proteins (8.4 kDa) (Figure 3.6 and Figure 3.7) (Gordon et al., 2020). Nucleocapsid expression was also analyzed with Anti-

SARS-CoV-2 Nucleocapsid antibody in another Western Blot (Figure 3.8) to verify expression.

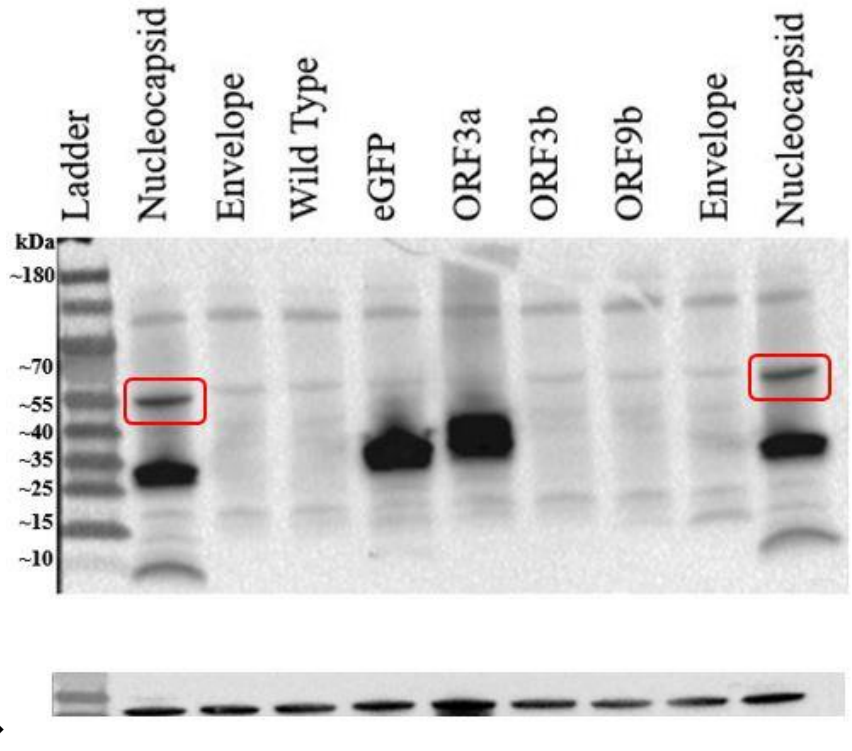

Figure 3.6 Protein expression analysis of lentivirally transduced THP1-Dual cells to stable express Nucleocapsid, Envelope, eGFP, ORF3a, ORF3b, and ORF9b proteins. Bands visualized by Anti-Strep-tag-II antibody.

Lane 1: 180 kDa Protein Ladder, Lane 2: Nucleocapsid, Lane 3: Envelope, Lane 4: WT THP1 Dual cell lysate, Lane 5: eGFP, Lane 6: ORF3a, Lane 7: ORF3b, Lane 8: ORF9b, Lane 9: Envelope, Lane 10: Nucleocapsid (all the wells contain 10 µl of cell lysates).

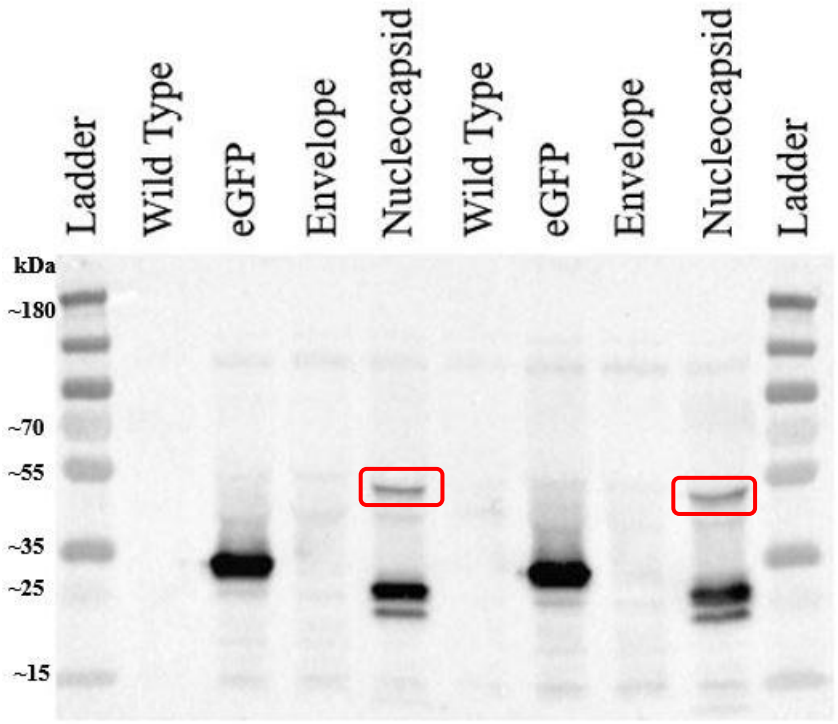

Figure 3.7 Immunoblotting analysis of stable SARS-CoV-2 structural protein-expressing THP1-Dual cells. Membrane was probed with Anti-Strep-tag-II antibody.

Lane 1: 180 kDa Protein Ladder, Lane 2: WT THP1 Dual, Lane 3: eGFP, Lane 4: Envelope, Lane 5: Nucleocapsid (all the wells 10 µl of cell lysate), Lane 6: WT THP1 Dual, Lane 7: eGFP, Lane 8: Envelope, Lane 9: Nucleocapsid (all the wells contain 5 µl of cell lysate), Lane 10: 180 kDa Protein Ladder .

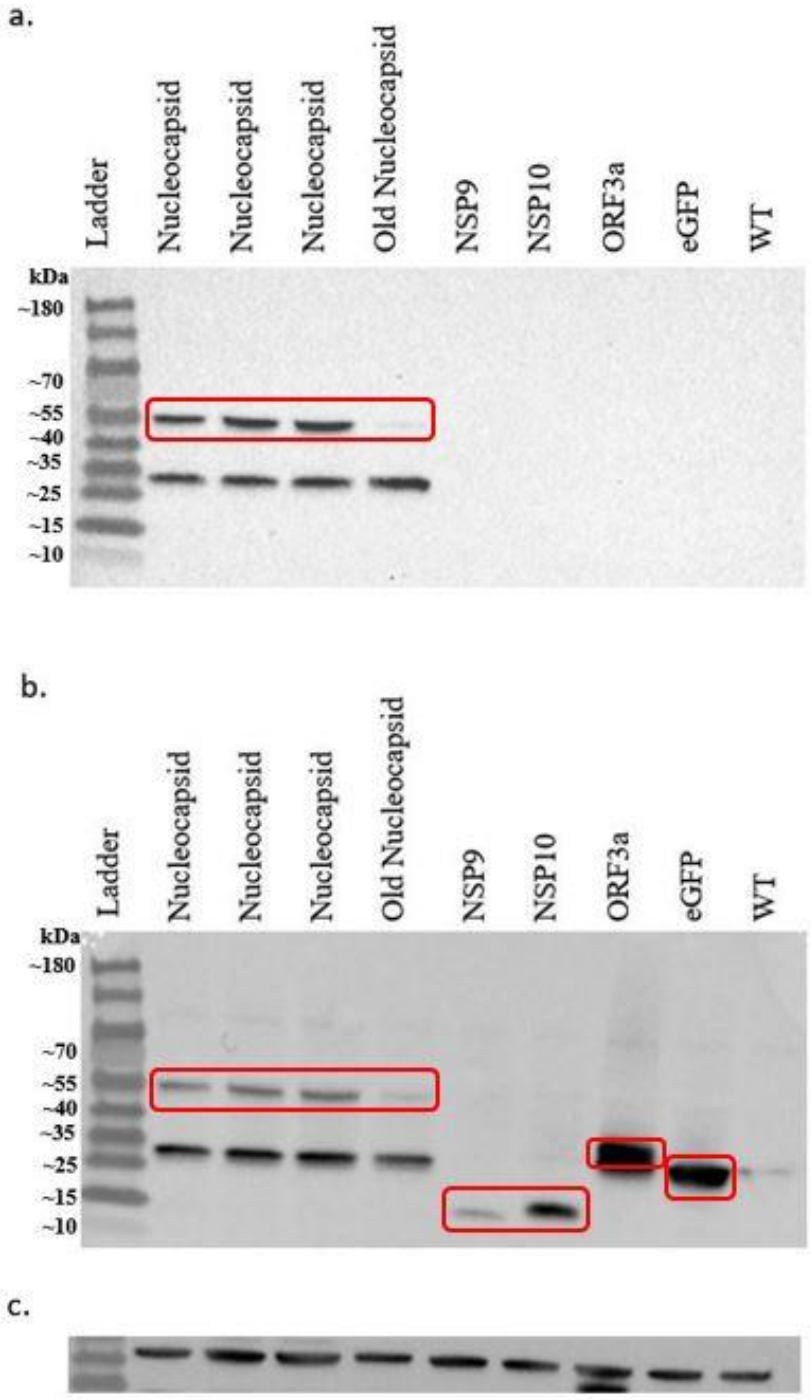

Figure 3.8 Immunoblotting analysis of SARS-CoV-2 structural protein-expressing THP1-Dual cells. Immunoblots were either probed with (a) Anti-SARS-CoV-2 Nucleocapsid antibody, (b) Anti-Strep-tag-II Antibody, Or (c) Anti-β-actin Antibody for the housekeeping gene.

In summary, among the non-structural, accessory, and structural proteins of SARS-CoV-2 used for stable cell line generation, 5 stable cell lines were generated (as indicated in Table 3.2). These cell lines were then compared to the authentic THP1-Dual monocytes or their GFP transduced mock controls in their ability to respond to PRR ligands associated with viral RNA sensing.

Table 3.2 Established and unestablished THP1-Dual cell lines.

NSP1	**NSP3**	**NSP9**	**NSP10**	**NSP13**	**NSP14**	**NSP15**	**ORF3a**
-	-	+	+	-	-	-	+
ORF3b	**ORF6**	**ORF7a**	**ORF7b**	**ORF8**	**ORF9b**	**N**	**E**
-	-	-	-	+	-	+	-

3.3 Effects of SARS-CoV-2 Structural, Non-structural, or Accessory Proteins in the Modulation of Cellular Responses to Stimulation with PRR Ligands Associated with Viral RNA Sensing

3.3.1 Investigation of Type I IFN Antagonistic Effects of SARS-CoV-2 Proteins in THP1-Dual Macrophages

3.3.1.1 Type I IFN Response in SARS-CoV-2 Protein-expressing THP1-Dual Cell Lines Stimulated with PRR Ligands Associated with Viral RNA Sensing

Type I IFNs are major cytokines that are produced upon viral infection. The early production of IFN-α or/and IFN-β is crucial for the activation of innate and adaptive immunity, controlling antiviral response, and viral replication (Lee & Ashkar, 2018). To evade and hide from this defense mechanism, viruses evolved mechanisms to antagonize IFN response of the host cell. Similar to SARS-CoV, SARS-CoV-2 has structural, nonstructural, and accessory proteins such as nsp1,

nsp3, nsp7, nsp15, ORF3b, ORF6, and Nucleocapsid that were previously described as interferon antagonists (Xia et al., 2020). Moreover, one of the early studies about SARS-CoV-2 from China found that nsp1, nsp3, nsp12, nsp13, nsp14, ORF3, ORF6, E, and M proteins were able to inhibit the promoter activity of IFN-β (Lei et al., 2020). On a separate note, lentiviral gene transduction itself is known to activate the type I IFN response (Brown et al., 2007; Follenzi et al., 2007). Therefore, in addition to comparing the response of the stable cell lines with wild-type cells, MOCK controls lentivirally transduced with GFP were also included.

To compare the effects of SARS-CoV-2 proteins modulating cellular responses to PRR ligands associated with viral RNA sensing, we monitored type I IFN response of the cell lines by using their IRF reporter functions. Following stimulation with the indicated PRR ligands, supernatants were mixed with the QUANTI-Luc reagent to analyze secreted luciferase enzyme into the culture medium.

Quantitative results of enzyme activity of cells showed that accessory proteins ORF3a, ORF8, nonstructural protein nsp9, and structural protein Nucleocapsid expression in THP1 macrophages had an antagonistic effect when cells were stimulated with various RNA analogs (Figure 3.9). When 5'ppp dsRNA (RIG-I agonist) was used, almost 3-fold decline in type I IFN production was observed in ORF8 expressing cells compared to WT and MOCK (Figure 3.9.a, $p < 0.001$). Similarly, ORF3a expressing macrophages stimulated with the same ligand, there was a significant decrease in type I IFN response (Figure 3.9.a, $p < 0.05$). Following cytosolic delivery of the dsRNA analog poly (I:C) (RIG-ı/MDA5 ligand), nsp9, ORF8, and N expression downmodulated type I IFN production compared to WT cells (Figure 3.8 b, $p<0.05$ and $p<0.01$). Moreover, ORF3a had ~2-fold reduction compared to WT and MOCK controls (Figure 3.9 b, $p<0.0001$). When single-stranded RNA analog R848 was used (TLR7/8 agonist), ~4-fold and ~2-fold decreases were observed in ORF3a or ORF8 expressing cells, respectively (Figure 3.9 c, $p<0.001$, $p<0.0001$). Vehicle control (only Lipofectamine 2000) QUANTI-Luc assay results are indicated in Appendix E.1.

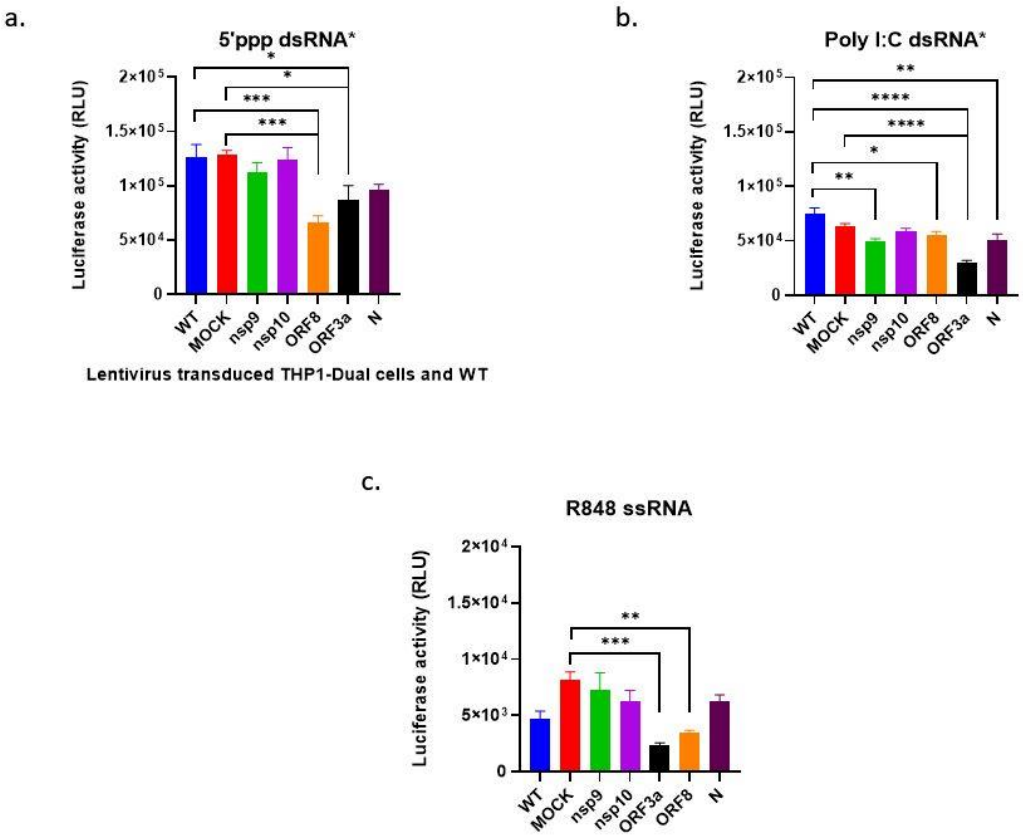

Figure 3.9 Secreted luciferase enzyme activity results of Type I IFN reporter function from WT, MOCK, and SARS-CoV-2 viral protein-expressing macrophages. 100,000 cells/ well were treated with PMA overnight and subsequently stimulated with PRR ligands associated with RNA sensing. Type I IFN production in response to stimulation with (a) intracellular 5'ppp dsRNA; (b) intracellular poly (I:C); (c) R848. Bar graphs show mean ± SEM of n=4-8 independent experiments and statistically analyzed by Tukey's multiple comparison test (*p<0.05, **p<0.01, ***p<0.001, ****p<0.0001).

3.3.1.2 ISG15 production in SARS-CoV-2 protein-expressing THP1-Dual Cell Lines as a Response to IFN-β

During host defense to avert viral infection, type I IFN signaling induces the expression of multiple genes that are broadly referred to as interferon-stimulated

genes (ISGs)(Malterer et al., 2014). Among several mechanistic features sharing ISGs, the 15 kDa interferon-inducible protein ISG15 is one of the most robust and rapidly induced gene products that is a member of the ubiquitin family. ISG15 can exist as a free protein (intra- or extracellularly) or found conjugated to other proteins, a phenomenon known as ISGylation (Narasimhan et al., 2005). Free ISG15 and ISGylation proteins is strongly induced by type I IFNs, and they both play a critical role in antiviral defense. Various mice studies concluded that ISG15 lacking mice exhibit enhanced susceptibility to different viruses such as murine gamma herpesvirus 68, Sindbis virus, herpes simplex virus 1 (HSV-1), Chikungunya virus, and vaccinia virus (Lenschow et al., 2016; Guerra et al., 2008; Werneke et al., 2011). In contrast, human studies from ISG15-deficient patients suggest susceptibility only to hepatitis C virus (HCV) but not to other virus infections. Interestingly, ISG15-deficient patients have a propensity to develop mycobacterial diseases (Bogunovic et al., 2012; Speer et al., 2016; X. Zhang et al., 2015).

To verify whether SARS-CoV-2 proteins antagonize type I IFN related signaling, intracellular ISG15 levels were monitored following overnight stimulation with recombinant IFN-β and then intracellular staining. All cell lines, except for the ORF3a cells, showed nearly 30-fold increased ISG15 production after treatment with IFN-β compared to their untreated counterparts (Figure 3.10 and 3.11). ORF3a expressing cells showed nearly 6.6-fold lower ISG15 positive cells compared to other cell groups (Figure 3.11 d, and g). Our results indicate that amoung the SARS-CoV-2 viral proteins, only ORF3a protein had a direct antagonistic effect on Type I interferon-stimulated ISG15 production.

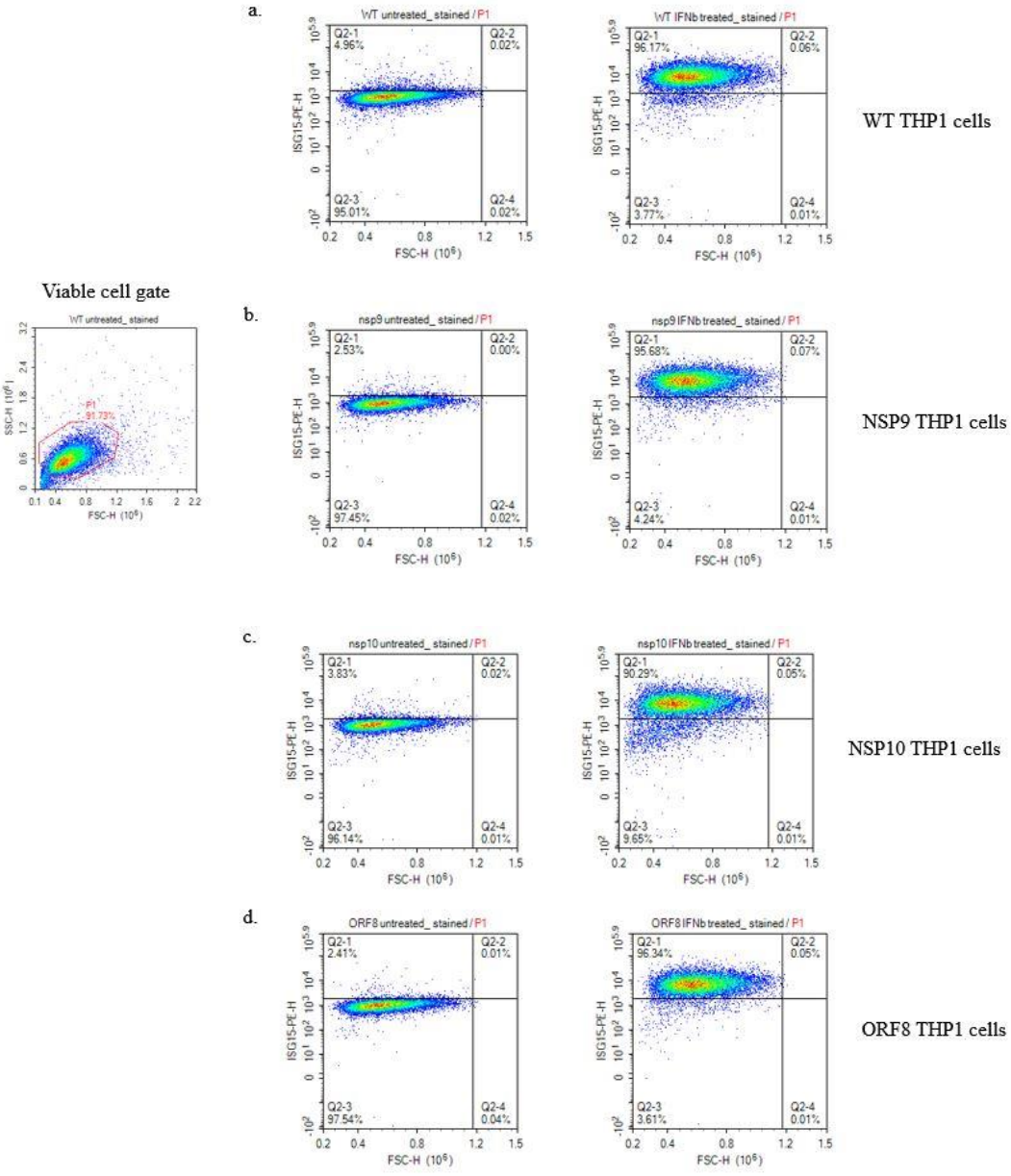
a.
WT untreated_ stained / P1
Q2-1 4.96%
Q2-2 0.02%
Q2-3 95.01%
Q2-4 0.02%
WT IFNb treated_ stained / P1
Q2-1 96.17%
Q2-2 0.06%
Q2-3 3.77%
Q2-4 0.01%
WT THP1 cells
Viable cell gate
WT untreated_ stained
P1 91.73%
b.
nsp9 untreated_ stained / P1
Q2-1 2.53%
Q2-2 0.00%
Q2-3 97.45%
Q2-4 0.02%
nsp9 IFNb treated_ stained / P1
Q2-1 95.68%
Q2-2 0.07%
Q2-3 4.24%
Q2-4 0.01%
NSP9 THP1 cells
c.
nsp10 untreated_ stained / P1
Q2-1 3.83%
Q2-2 0.02%
Q2-3 96.14%
Q2-4 0.01%
nsp10 IFNb treated_ stained / P1
Q2-1 90.29%
Q2-2 0.05%
Q2-3 9.65%
Q2-4 0.01%
NSP10 THP1 cells
d.
ORF8 untreated_ stained / P1
Q2-1 2.41%
Q2-2 0.01%
Q2-3 97.54%
Q2-4 0.04%
ORF8 IFNb treated_ stained / P1
Q2-1 96.34%
Q2-2 0.05%
Q2-3 3.61%
Q2-4 0.01%
ORF8 THP1 cells
ISG15-PE-H
FSC-H (10^6)
SSC-H (10^6)

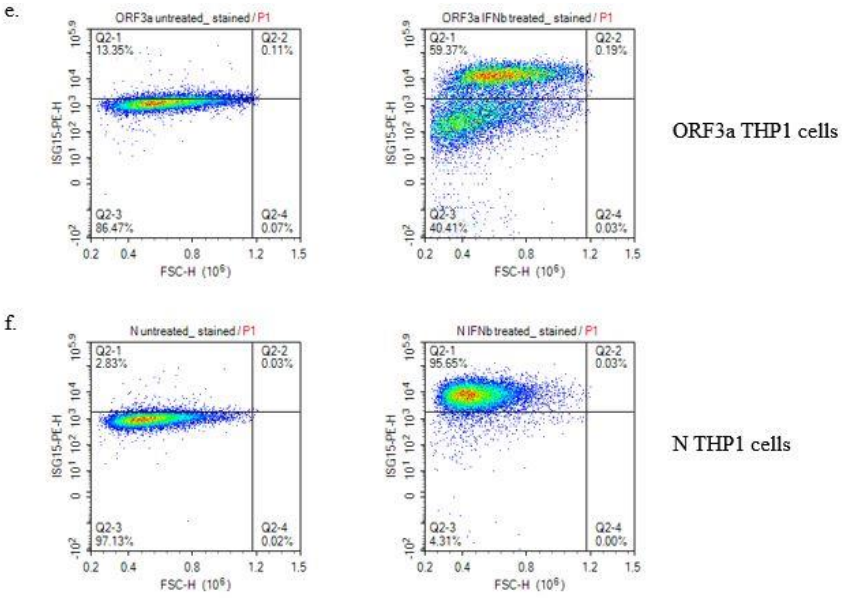

Figure 3.10 Flow cytometric analysis of intracellular ISG15 staining in WT versus SARS-CoV-2 viral protein-expressing macrophages. (a) untreated and IFN-β treated Wild-type cells; (b) Untreated/ IFN-β treated NSP9; (c)NSP10; (d) ORF8; (e) ORF3a; (f)N ISG15 positive populations and their percentages are indicated on individual density plots.

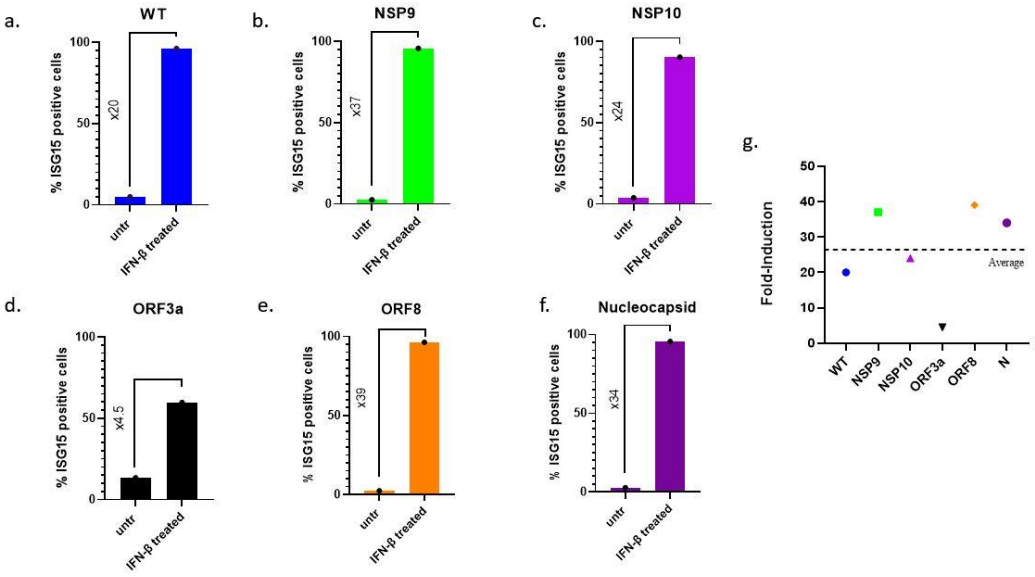

Figure 3.11 Bar Graphs representing % ISG15 positive cells (a, b, c, d, e, f). Comparison of cell lines in terms of Fold induction in ISG-15 production (untreated over IFN-β treated ISG-15 positive cell percentages) (g).

3.4 Effects of SARS-CoV-2 Structural, Non-structural, or Accessory Proteins on Inflammasome Activation

3.4.1 IL-1β Cytokine Release in THP1-Dual Macrophages Expressing SARS-CoV-2 Viral Proteins in Response to Inflammasome Activators

After the SARS-CoV-2 pandemic has emerged in 2020, several research groups have studied the virus's structural, non-structural, and accessory proteins to gain insight to mechanism that cause excessive inflammation in the host. In this context, we continued to examine the impact of SARS-CoV-2 viral proteins expression on host cell inflammasome activation using different signaling pathways: non-canonical, AIM2, NLRP3, and NLRC4 inflammasomes. It has been proposed that SARS-CoV-2 encodes ion-channel proteins (named as viroporins) such as Envelope, ORF8, and ORF3a, which may play a role in disrupting intracellular ion

concentrations to activate the NLRP3 inflammasome in the host (Shah, 2020). Moreover, in 2021 a study from China concluded that the Nucleocapsid protein from the virus can directly interact with the NLRP3 protein and promote inflammasome activation (Pan et al., 2021).

Based on the above information, we quantitated IL-1β inflammatory cytokine release into the culture medium in response to various inflammasome ligands in SARS-CoV-2 protein expressing cells. When cell lines were stimulated with intracellular LPS (non-canonical inflammasome activator) and dsDNA analog poly (dA:dT; AIM2 inflammasome activator), there was no significant difference in IL-1β production (Figure 3.12 b, c). In contrast, when Nigericin or Aluminum crystals were used for the activation of the NLRP3 inflammasome, ORF3a expressing cells showed ~5- and ~10- fold higher IL-1β secretion into the culture medium compared to the control groups, respectively (Figure 3.12 d, e). Although ORF8 expressing cell line responded to Nigericin ~2-fold higher than the control groups, the difference was not significant (Figure 3.12 e). When NLRC4 inflammasome was activated in response to cytosolic flagellin delivery, only the ORF3a expressing cells were found to increase IL-1β production (~2.5-fold) in comparison to control groups (Figure 3.12 f). As expected, the negative control ligand K3 CpG ODN and untreated groups did not induce IL-1β (Figures 3.12 g and a, respectively). The vehicle control results are presented in Appendix E.2.

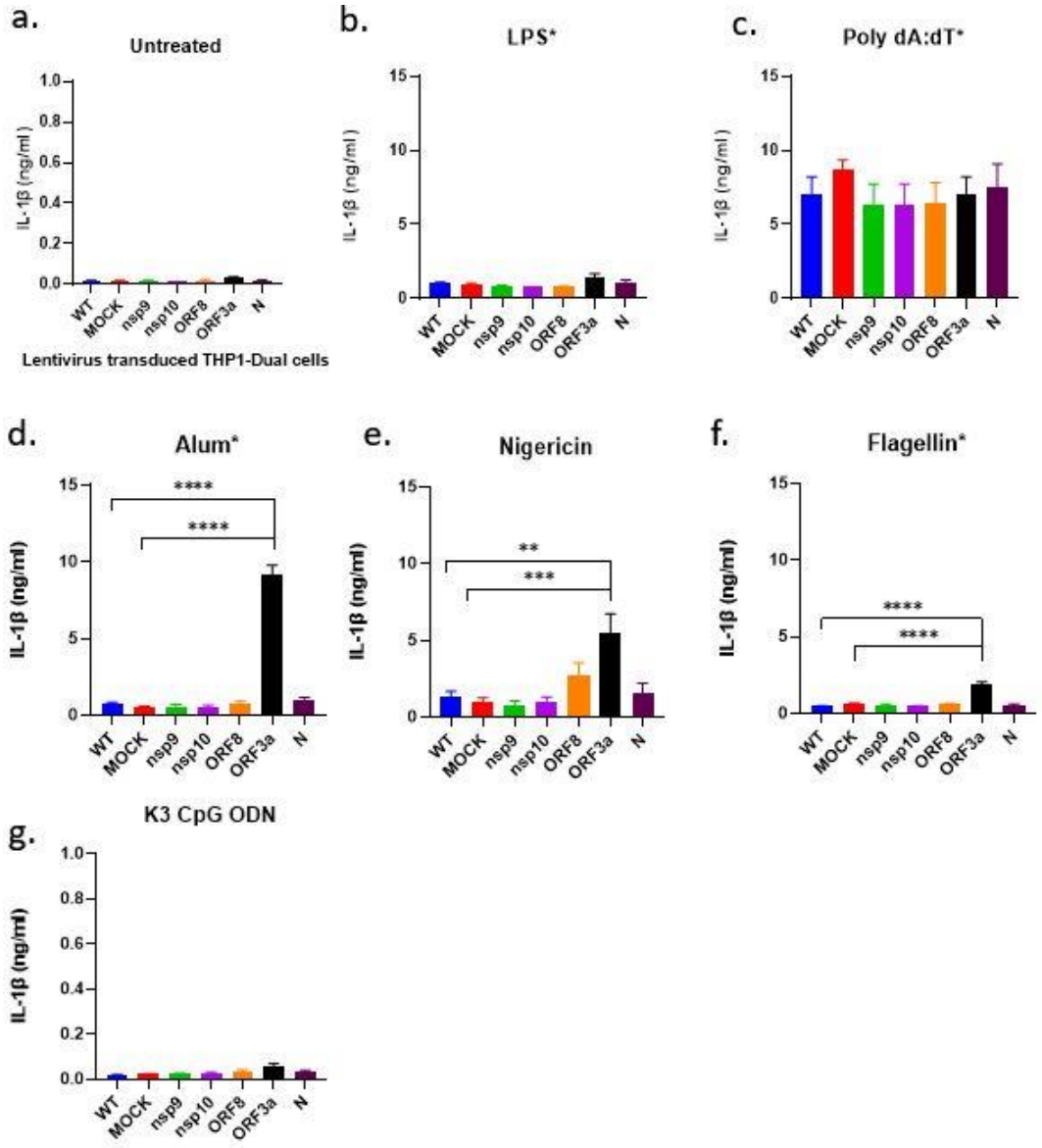

Figure 3.12 IL-1β cytokine production in response to various inflammasome activators from THP1-Dual macrophages expressing SARS-CoV-2 proteins. 100.000/ well cells were primed with 50 ng/ml PMA followed by stimulation with various inflammasome activators. (a) untreated; (b) intracellular LPS for non-canonical inflammasomal pathway; (c) intracellular poly (dA:dT) for AIM2 inflammasome; (d, e) intracellular alum, and nigericin treatment for NLRP3 inflammasome; (f) intracellular flagellin for NLRC4 inflammasome activation (g) K3 CpG ODN treatment as a negative ligand control. Data represent mean ± SEM

of n=3-8 of multiple experiments and statistically analyzed by Tukey's multiple comparison test (*p<0.05, **p<0.01, ***p<0.001, ****p<0.0001).

3.4.2 Assessment of Pyroptosis Related Cell Death in SARS-CoV-2 Viral Protein-expressing THP1-Dual Macrophages in Response to Inflammasome Activation

3.4.2.1 Measurement of Cellular Cytotoxicity in SARS-CoV-2 Viral Protein-expressing THP1-Dual Macrophages

Inflammasome activation leads to pyroptosis, a form of cell death in which inflammatory cytokine IL-1β and other cellular inflammatory contents leak to the extracellular environment. In the previous section, we validated that ORF3a had a significant impact on NLRP3 and NLRC4 inflammasomes. To understand whether SARS-CoV-2 proteins also impact pyroptosis, we first measured lactate dehydrogenase (LDH) release as an indicator of pyroptosis. LDH is a cytosolic enzyme that is released to the outside when cellular membrane integrity is disrupted, and colorimetric measurement of the enzyme activity gives an indication of cell lysis and pyroptosis.

All cell types shown less than ~20% cytotoxicity in the absence of any stimulation (Figure 3.13 a). When AIM2 or non-canonical inflammasome pathways were activated (except for the N expressing cells), cytotoxicity percentages were found to be consistent with IL-1β cytokine production (Figure 3.13 b and c). Moreover, Nigericin-treated cells displayed higher cytotoxicity compared to their untreated controls (Figure 3.13 e). Furthermore, alum-treated ORF3a expressing macrophages exhibited significantly higher cytotoxicity compared to WT and MOCK cells (3.13 d) and the data was compatible with IL-1β results. In flagellin-treated groups, ORF3a expressing cells displayed higher cytotoxicity that was significantly different from MOCK (Figure 3.13 f). Although intracellular flagellin was ~2-fold more cytotoxic to ORF3a cells compared to WT, this difference was

nonsignificant probably owing to the low sample size (n=4). Cytotoxicity results for the NLRC4 inflammasome activated groups were found to be in line with their IL-1β secretion patterns. When non-canonical, or Alum-mediated NLRP3 or/and NLRC4 inflammasome assembly was triggered in Nucleocapsid expressing cells, cytotoxicity was found to be lower than WT or other stable cell lines (Figure 3.13 b, d, f). This may be related to a finding showing that SARS-CoV-2 viral protein nucleocapsid can inhibit host cell pyroptosis by blocking Gasdermin D following pro-caspase-1 cleavage, hence averting pyroptosis and IL-1β release after inflammasome assembly (Ma et al., 2021). Finally, again K3 CpG ODN was used as a negative control and as expected, cytotoxicity levels were similar to untreated controls (Figure 3.13 g).

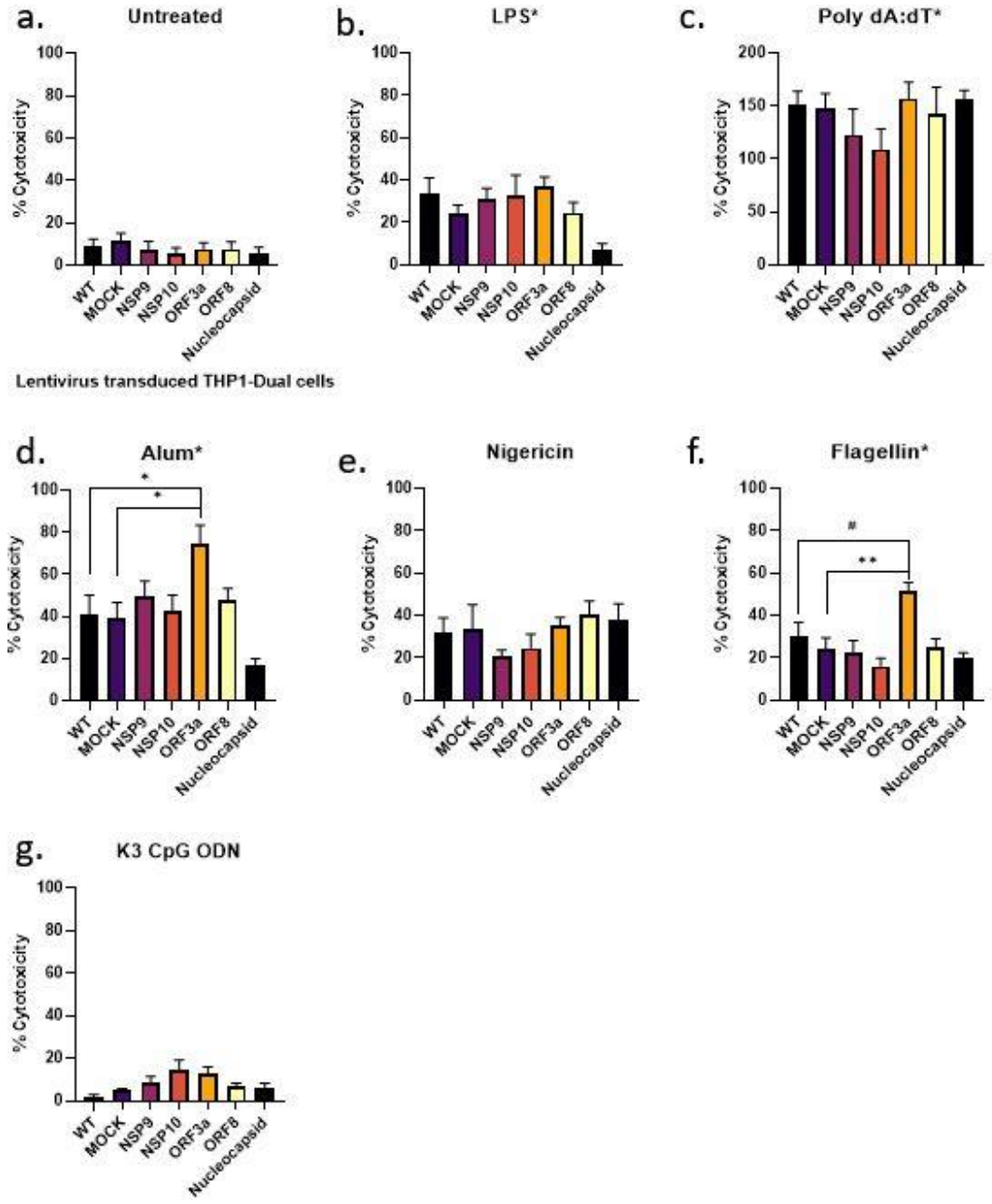

Figure 3.13 Effects of SARS-CoV-2 structural, non-structural, or accessory proteins on inflammasome activation induced cell death. (a) untreated; (b) intracellular LPS for non-canonical inflammasomal pathway; (c) intracellular poly (dA:dT) for AIM2 inflammasome; (d, e) intracellular alum, and nigericin treatment for NLRP3 inflammasome; (f) intracellular flagellin for NLRC4 inflammasomal pathway and (g) K3 CpG ODN treatment as a negative ligand control. Data

represent mean ± SEM of n=4-8 discrete experiments and statistically analyzed by Tukey's multiple comparison test (*p<0.05, **p<0.01, ***p<0.001, ****p<0.0001, # < 0.05).

3.4.2.2 Imaging of Inflammasome Activation-induced Cell Death in SARS-CoV-2 Structural, Non-structural, or Accessory Protein Expressing Cells

For further validation of cell death resulting from inflammasome activation, we performed SytoxOrange nucleic acid staining and subsequent fluorescent microscopy imaging. SytoxOrange is a membrane impermeable dye that can bind to nucleic acids only when the cell membrane is compromised, and the cell has deteriorated or died. Cells were stained after inflammasome activation with fluorescent SytoxOrange dye to investigate how inflammasome assembly affected different cell lines.

Fluorescence microscopy images of SytoxOrange stained lentiviral transduced or Wild-type control THP1 macrophages without any treatment are given in Figure 3.14. In the absence of any stimulation, ORF3a expressing cells were found to be induce accelerated cell death, suggesting a role in inducing one of the cell death pathways (Figure 3.14). Data presented in Section 3.4.2.1 pertaining to untreated ORF3a cells was not in support of increased LDH release and hence, pyroptosis. Therefore, these results may suggest that ORF3a protein itself may trigger a non-lytic cell death mechanism, such as apoptosis. When cells were stimulated with various inflammasome ligands as described before, viral proteins were found to be equally effective in inducing cell death upon non-canonical and AIM2 inflammasome activation, which are consistent with as the results presented IL-1β and percent cytotoxicity calculations (Figure 3.15 and 3.16). When cells were treated with Aluminum crystals to activate the NLRP3 inflammasomal signaling pathway, the greatest cell death was detected in ORF3a expressing macrophages. Since ORF3a expressing cells had almost 10-fold higher IL-1β secretion and

displayed highest cytotoxicity percentage, SytoxOrange staining pattern was also consistent with a role for ORF3a in enhancing NLRP3-mediated inflammasome activation (Figure 3.17). Treatment with the potassium ionophore Nigericin resulted in similar levels of SytoxOrange staining in different cell types although ORF3a expressing cells generated a stronger red signal when compared to WT and other lentiviral transduced groups (Figure 3.18). Interestingly, consistent with the cytotoxicity results, NSP9 expression was found to be effective in hindering cell death when cells were treated with nigericin (Figure 3.18). Recent studies showed that this RNA-binding viral protein is essential for viral replication/transcription, and it interferes with host cell membrane trafficking during infection (Banerjee et al., 2020; Littler et al., 2020). On a separate note, nigericin is a negatively charges molecule that binds to H+ ions in the extracellular space, passes across the plasma membrane in its protonated from (nigericin-H) to release H+ on to intracellular side. It then binds to and transport K+ as nigericin-K on the outside of the cell (Pressman, 1976). It is possible that NSP9 binds to deprotonated nigericin and inhibits potassium efflux through the membrane, resulting in decreased IL-1β secretion and cell death.

With respect to flagellin-induced NLRC4 inflammasome activation, consistent with previous results, ORF3a expressing cells demonstrated higher levels of SytoxOrange staining (Figure 3.19). Positive control Triton X-100 treated SytoxOrange staining images are also presented in Figure 3.20, demonstrating that the assay correctly identified dead cells.

Finally, for further evaluation and quantification of cell death, we performed Propidium Iodide (PI) staining following stimulation with inflammasome activators as described before. Similar to SytoxOrange, PI is a red-fluorescent DNA stain that only permease dead cells. Thus, PI negativity on flow cytometry indicates the percentage of live cells. Quantitative analysis of PI staining of cells was consistent with SytoxOrange staining patterns (Figure 3.21). Nucleocapsid expressing THP1-Dual macrophages showed reduced live-cell percentage when treated with intracellular Flagellin and LPS (Figure3.21 b and h), suggesting that SARS-CoV-2

Nucleocapsid may induce a pyroptosis-independent cell death in these stimulated cells.

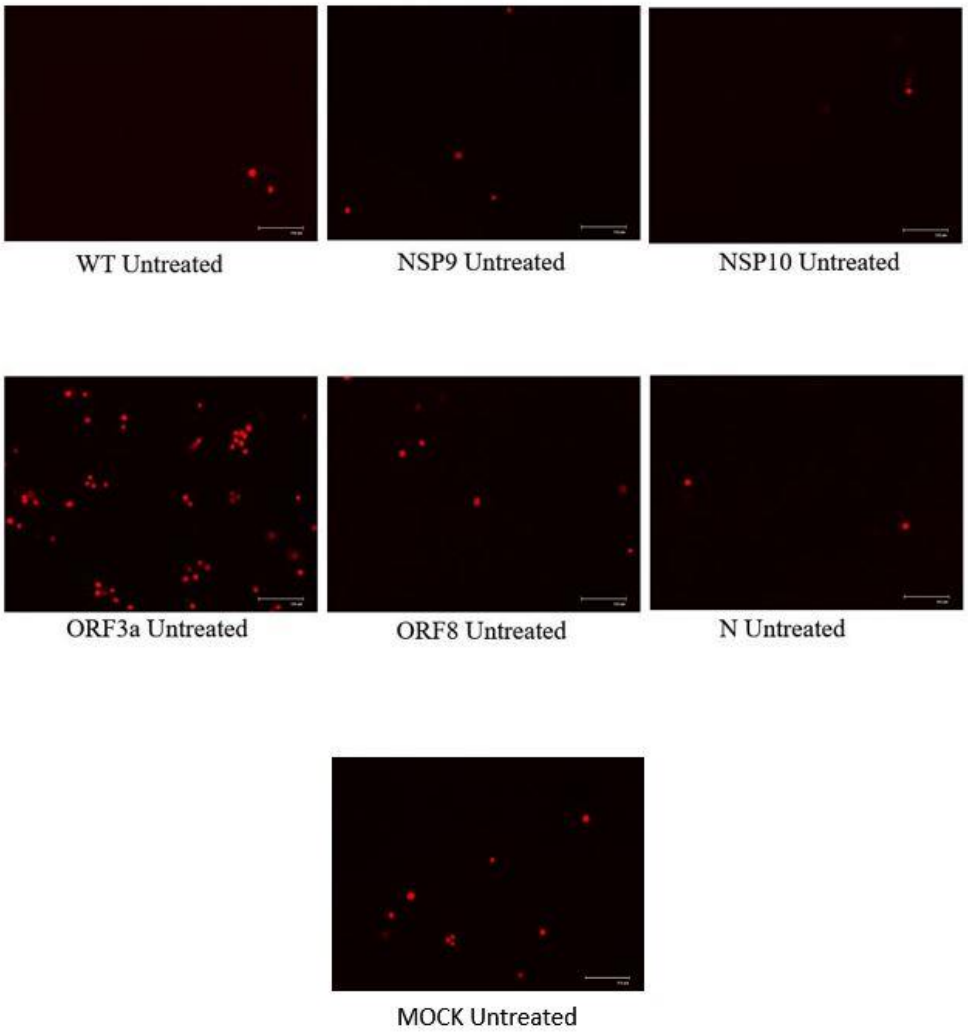

Figure 3.14 Fluorescence Microscopy images of untreated but SytoxOrange stained SARS-CoV-2 protein expressing THP1-Dual Macrophages. Top panels: WT, NSP9, NSP10; Middle panels: ORF3a, ORF8, N; Bottom panel: MOCK

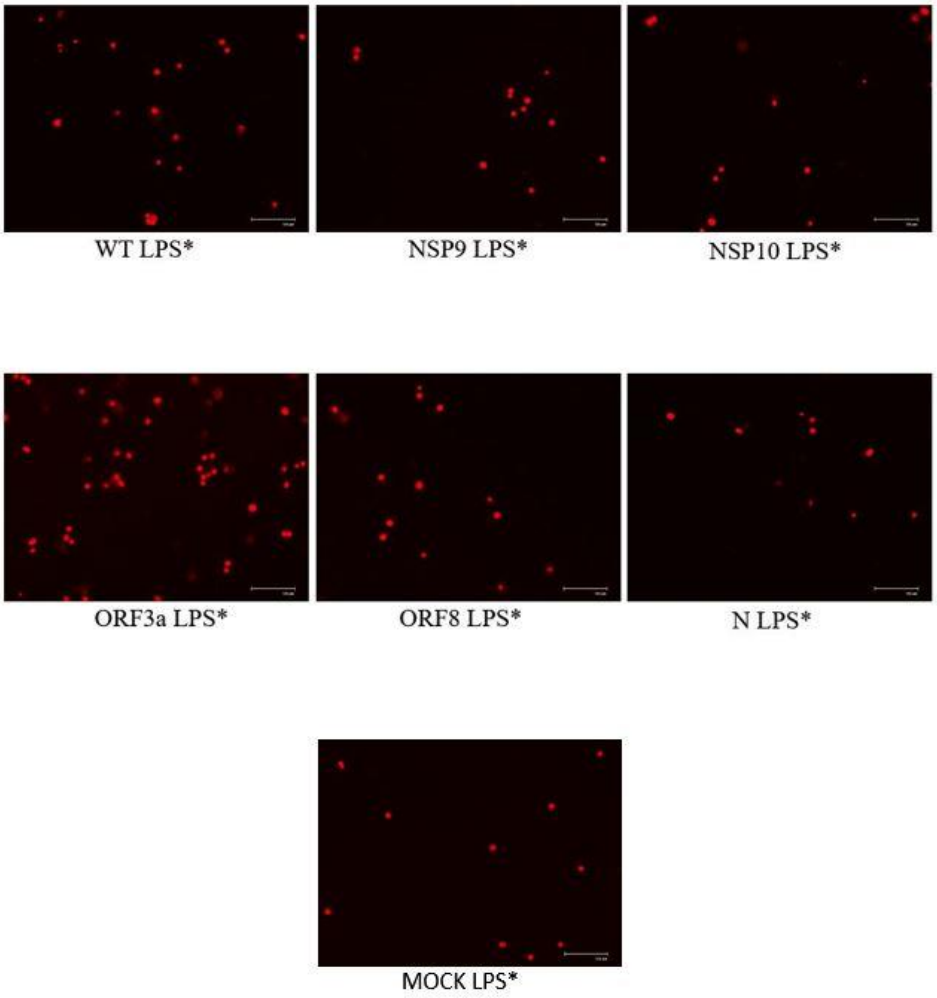

Figure 3.15 SytoxOrange staining results of non-canonical inflammasomal pathway activated SARS-CoV-2 protein expressing cells. Top panels: WT, NSP9, NSP10; Middle panels: ORF3a, ORF8, N; Bottom panel: MOCK.

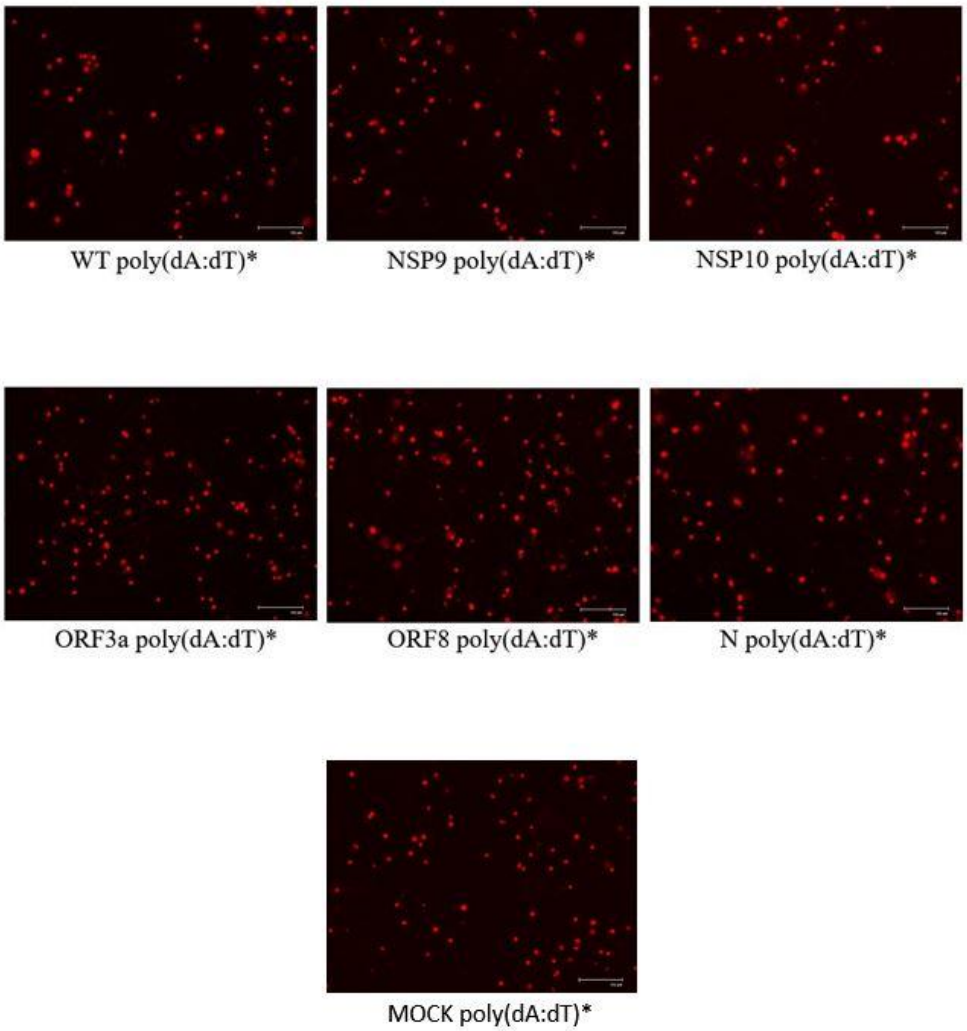

Figure 3.16 SytoxOrange staining results of AIM2 inflammasome pathway activated SARS-CoV-2 protein expressing cells. Top panels: WT, NSP9, NSP10; Middle panels: ORF3a, ORF8, N; Bottom panel: MOCK.

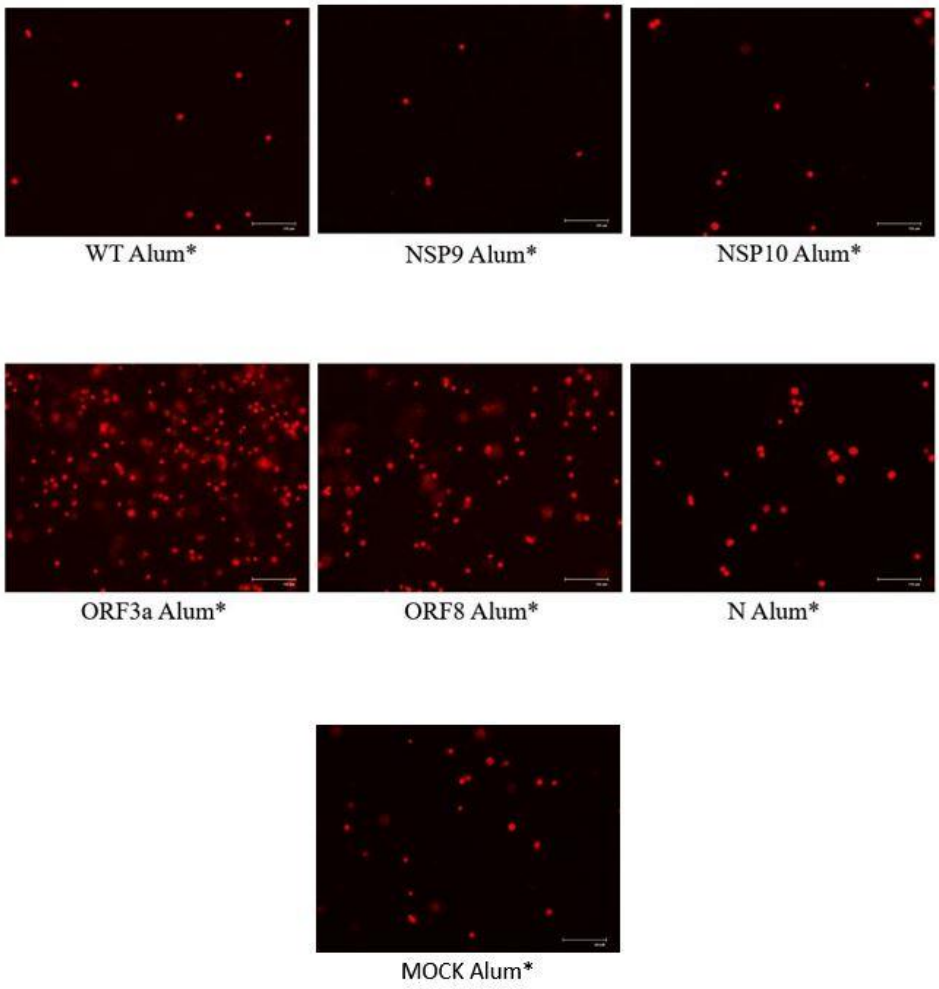

Figure 3.17 SytoxOrange staining results of Aluminum crystals mediated NLRP3 inflammasome signaling pathway activated SARS-CoV-2 protein expressing cell lines. Top panels: WT, NSP9, NSP10; Middle panels: ORF3a, ORF8, N; Bottom panel: MOCK.

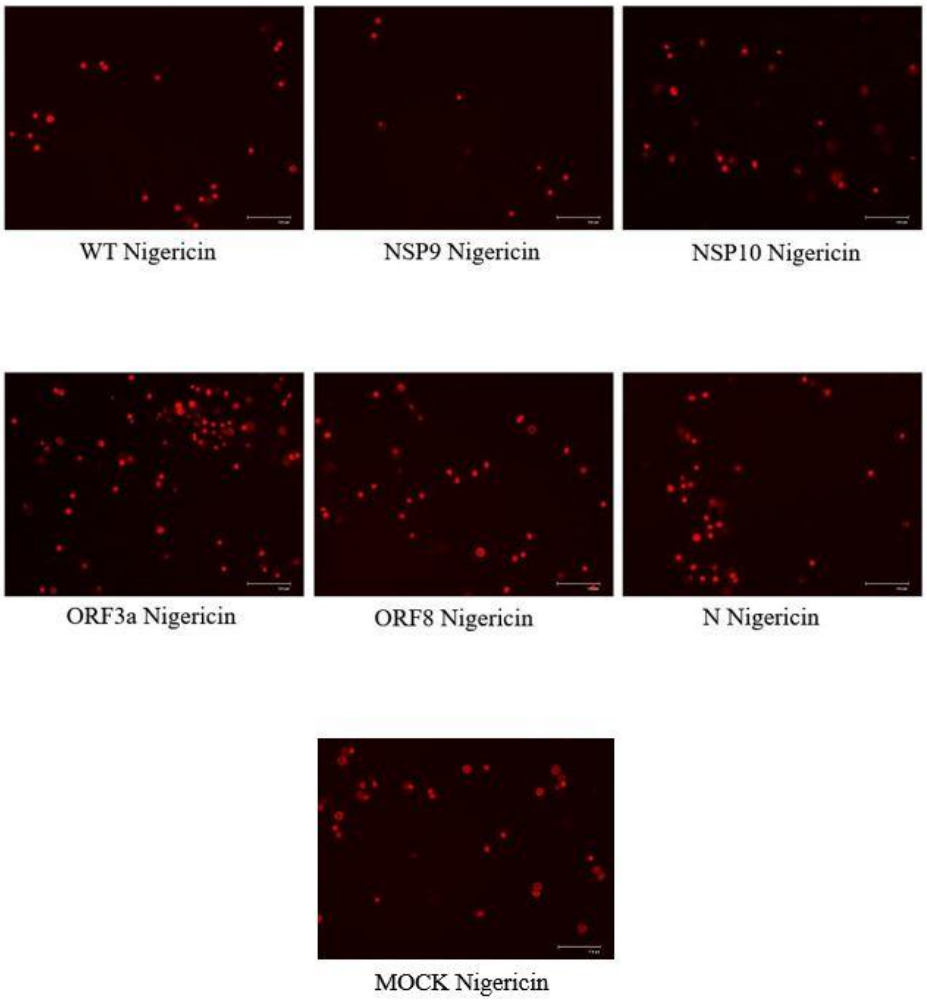

Figure 3.18 SytoxOrange staining results of Nigericin-mediated NLRP3 inflammasome pathway activated SARS-CoV-2 protein expressing THP1-Dual macrophages. Top panels: WT, NSP9, NSP10; Middle panels: ORF3a, ORF8, N; Bottom panel: MOCK

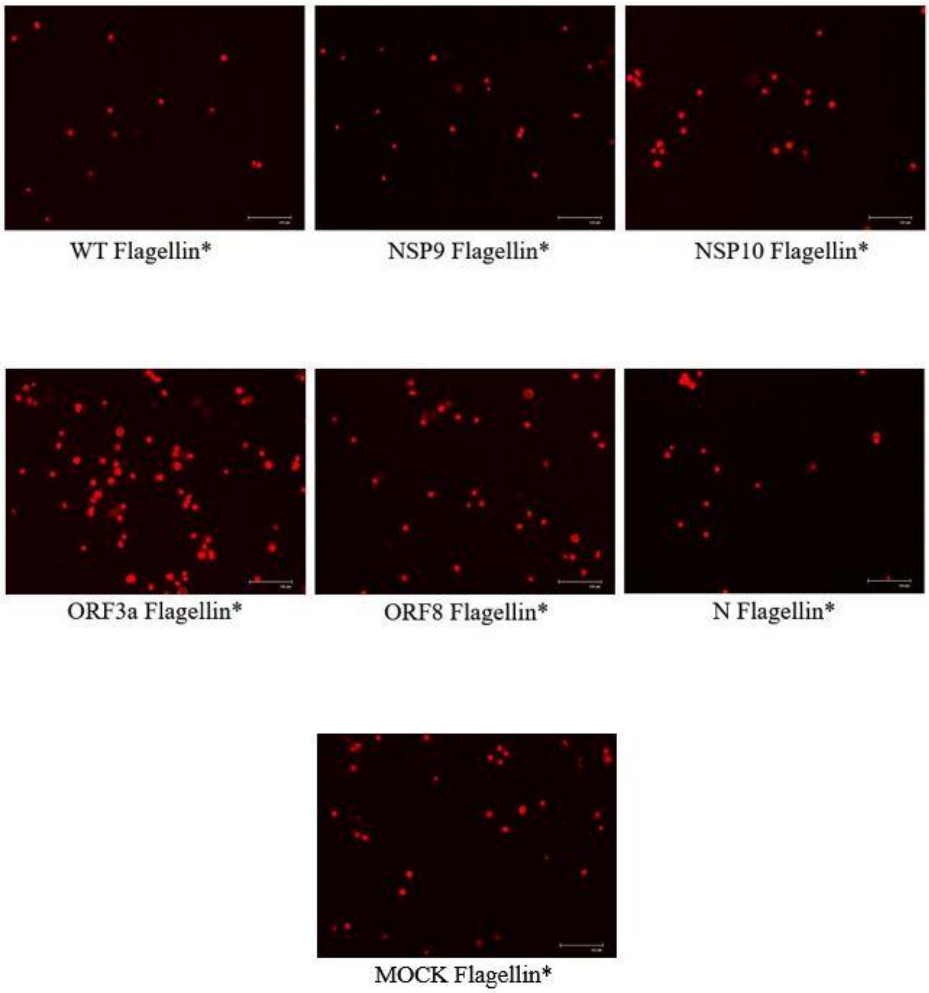

Figure 3.19 SytoxOrange staining results of NLRC4 inflammasome signaling pathway activated SARS-CoV-2 protein expressing cell lines. Top panels: WT, NSP9, NSP10; Middle panels: ORF3a, ORF8, N; Bottom panel: MOCK.

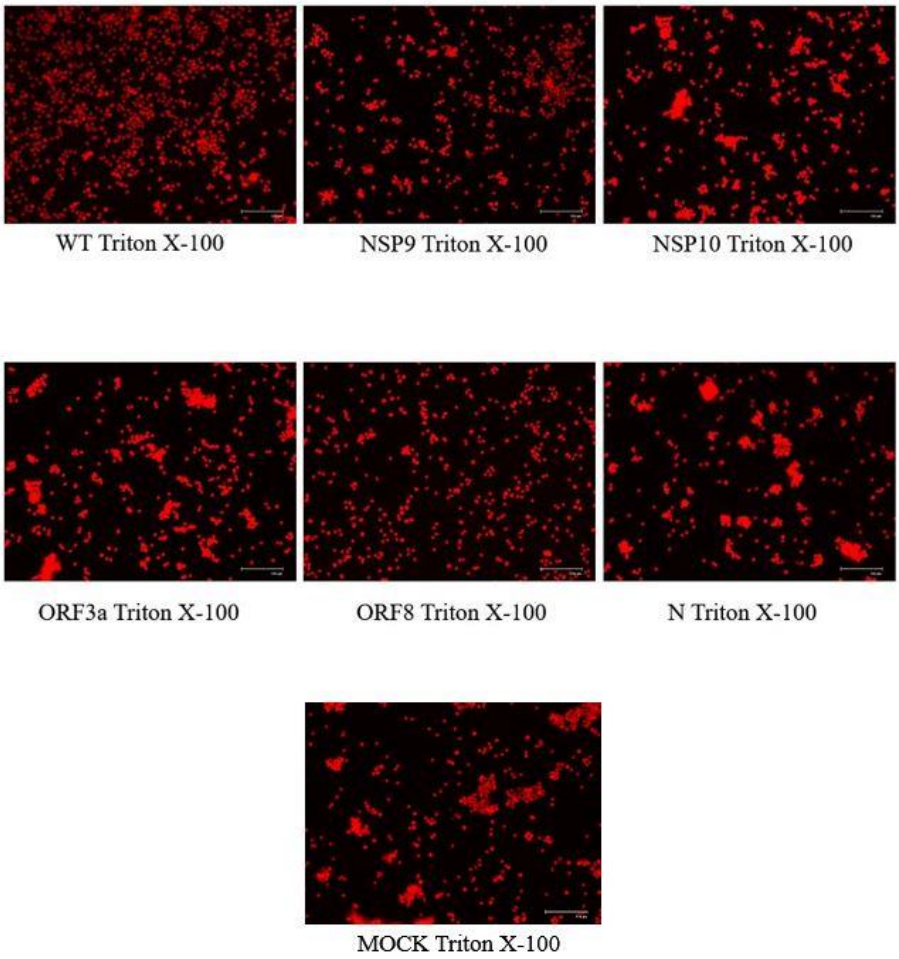

Figure 3.20 SytoxOrange staining results of positive control Triton X-100 treated SARS-CoV-2 protein expressing cell lines. Top panels: WT, NSP9, NSP10; Middle panels: ORF3a, ORF8, N; Bottom panel: MOCK.

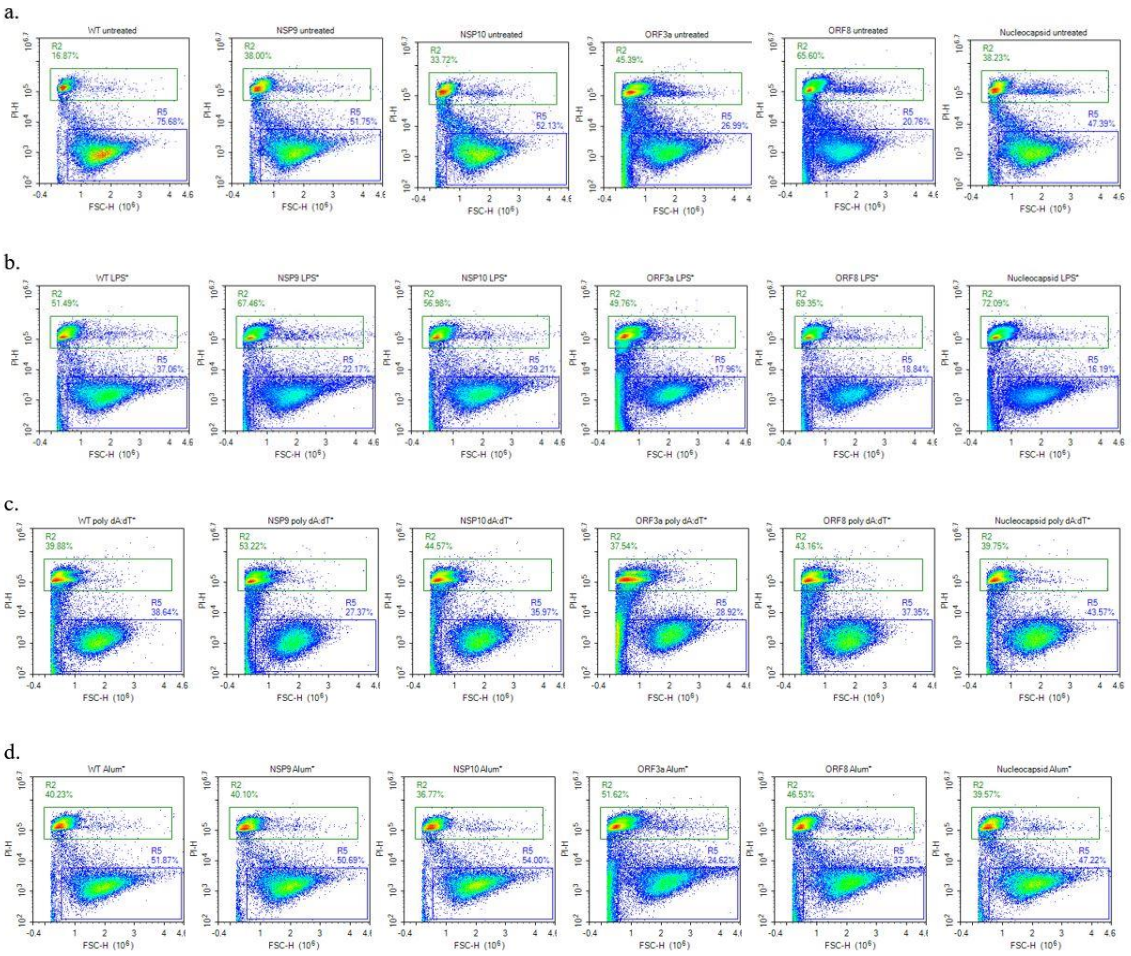
a.
WT untreated
R2 16.87%
R5 75.68%
NSP9 untreated
R2 38.00%
R5 51.75%
NSP10 untreated
R2 33.72%
R5 52.13%
ORF3a untreated
R2 45.39%
R5 26.99%
ORF8 untreated
R2 65.60%
R5 20.76%
Nucleocapsid untreated
R2 38.23%
R5 47.39%
b.
WT LPS*
R2 51.49%
R5 37.06%
NSP9 LPS*
R2 67.46%
R5 22.17%
NSP10 LPS*
R2 56.98%
R5 29.21%
ORF3a LPS*
R2 49.76%
R5 17.96%
ORF8 LPS*
R2 69.35%
R5 18.84%
Nucleocapsid LPS*
R2 72.09%
R5 16.19%
c.
WT poly dA:dT*
R2 39.88%
R5 38.64%
NSP9 poly dA:dT*
R2 53.22%
R5 27.37%
NSP10 dA:dT*
R2 44.57%
R5 35.97%
ORF3a poly dA:dT*
R2 37.54%
R5 28.92%
ORF8 poly dA:dT*
R2 43.16%
R5 37.35%
Nucleocapsid poly dA:dT*
R2 39.75%
R5 43.57%
d.
WT Alum*
R2 40.23%
R5 51.87%
NSP9 Alum*
R2 40.10%
R5 50.69%
NSP10 Alum*
R2 36.77%
R5 54.00%
ORF3a Alum*
R2 51.62%
R5 24.62%
ORF8 Alum*
R2 46.53%
R5 37.35%
Nucleocapsid Alum*
R2 39.57%
R5 47.22%
PI-H
FSC-H (10^6)

e.

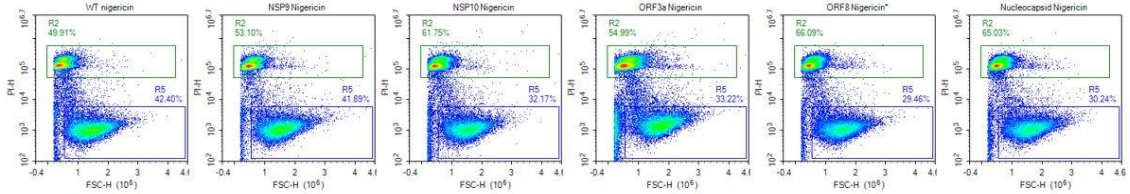
WT nigericin
R2 49.91%
R5 42.40%
NSP9 Nigericin
R2 53.10%
R5 41.89%
NSP10 Nigericin
R2 61.75%
R5 32.17%
ORF3a Nigericin
R2 54.99%
R5 33.22%
ORF8 Nigericin*
R2 66.09%
R5 29.46%
Nucleocapsid Nigericin
R2 65.03%
R5 30.24%
Pl-H
FSC-H (10^6)

f.

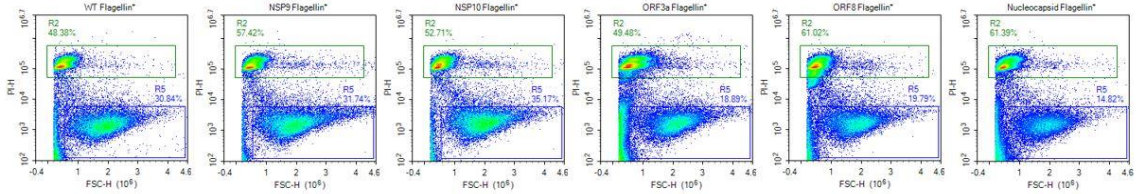
WT Flagellin*
R2 48.38%
R5 30.84%
NSP9 Flagellin*
R2 57.42%
R5 31.74%
NSP10 Flagellin*
R2 52.71%
R5 35.17%
ORF3a Flagellin*
R2 49.48%
R5 18.89%
ORF8 Flagellin*
R2 61.02%
R5 19.79%
Nucleocapsid Flagellin*
R2 61.39%
R5 14.82%
Pl-H
FSC-H (10^6)

g.

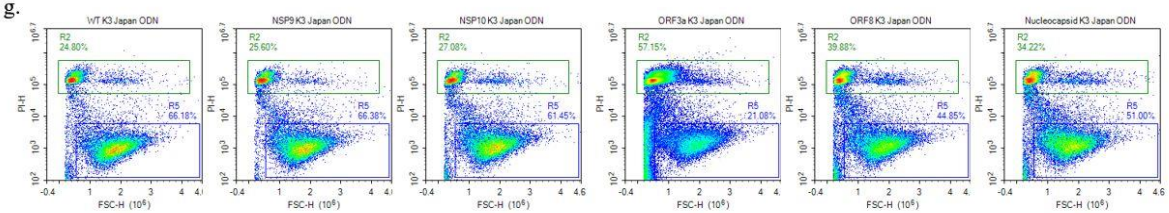
WT K3 Japan ODN
R2 24.80%
R5 66.18%
NSP9 K3 Japan ODN
R2 25.60%
R5 66.38%
NSP10 K3 Japan ODN
R2 27.08%
R5 61.45%
ORF3a K3 Japan ODN
R2 57.15%
R5 21.08%
ORF8 K3 Japan ODN
R2 39.88%
R5 44.85%
Nucleocapsid K3 Japan ODN
R2 34.22%
R5 51.00%
Pl-H
FSC-H (10^6)

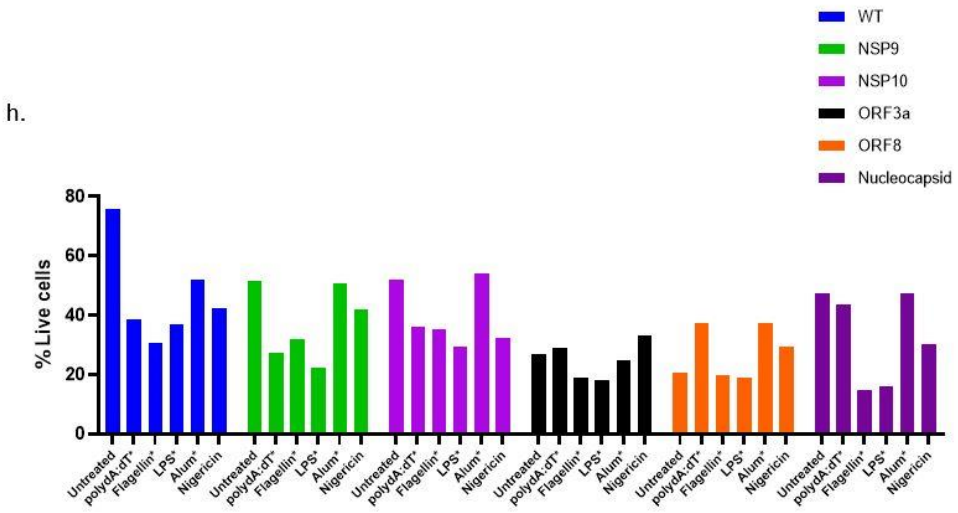

Figure 3.21 Flow cytometric analysis of Propidium Iodide-stained cells for quantification of live-cell percentages following inflammasome stimulation with inflammasome activators. 250,000 cells/well were PMA-primed, and then stimulated with previously indicated inflammasome activators. After 24 hours, cells were stained with PI for 15 minutes and acquired on a Novocyte 2060R flow cytometer. 20,000 events/ sample were acquired. PI staining density plots of (a) untreated; (b) LPS*; (c) poly (dA:dT)*; (d) Alum*; (e) Nigericin; (f) flagellin*; (g) K3 CpG ODN treated groups' and (h) Live cell percentages of different cell types in response to stimulation with inflammasome activators.

CHAPTER 4

CONCLUSION

SARS-CoV-2-induced infectious disease COVID-19 has become a global health concern since the end of 2019. Clinical symptoms of the disease can progress to pneumonia and even can lead to death (Zhu et al., 2020). The virus encodes four structural proteins, various nonstructural and accessory proteins to enter/replicate in host cells and modulate the host immune response to enable the virus to multiply and spread. Dysregulated host innate immune response has been implicated to lead to an exaggerated inflammatory response, including the over-production of pro-inflammatory cytokines such as IL-1β, IL-6, and TNF-α, leading to immune pathology (C. Huang et al., 2020). This enveloped virus induces an antiviral response from a broad range of immune cells such as macrophages and neutrophils, which also produce those pro-inflammatory cytokines after sensing the virus via specialized sensors, for example, RIG-I, and MDA-5. On the other hand, the major innate antiviral response, type I IFNs, is diminished or delayed in COVID-19 patients, promoting the critical disease state (Galani et al., 2021). Over-production of IL-1β which is also one of the major markers of inflammasome activation was exaggerated responses in severe COVID-19 patients. In this respect, this thesis intended to investigate the impact of SARS-CoV-2 structural, nonstructural, and accessory proteins' on type I IFN antagonism, interferon-gene product ISG15 expression, inflammasome activation, and cell death.

To this end, first, we tried to stably express SARS-CoV-2 structural, non-structural and accessory proteins in IRF and NF-kB reporter cell line THP1-Dual monocytes via a 3rd generation lentiviral expression and transduction system (Section 3.2). After antibiotic selection, structural protein Nucleocapsid, non-structural protein 9

(NSP9), NSP10, open reading frame 3a (ORF3a), ORF8 expressing, or as a lentiviral transduction control GFP expressing MOCK cell lines were generated. ORF6, ORF9b, Envelope, and many other viral proteins (as indicated in Table 3.1.2) were also tried but were not successful. We concluded that some of these proteins E.g., ORF9b and ORF3b have very low molecular weights (10.8 kDa and 7.3 kDa, respectively) which might have contributes to our inability to detect them by SDS-PAGE/western, we abandoned the use of these cell lines for this study (Gordon et al., 2020). Furthermore, during the antibiotic selection of the cell lines, nsp1, nsp3, and ORF7a expressing monocytes could not be expanded but died. We hypothesized that these proteins could have been too toxic to the cells (Hasan & Yan, 2016).

Next, by using the reporter function of cell lines, type I IFN production was assessed following stimulation after with several RNA analogs that mimic viral infection (Section 3.3.1.1). It has been shown that SARS-CoV-2 ORF8 accessory proteins antagonize type I IFN response in a cell-type specific manner (J. Y. Li et al., 2020; Yuen et al., 2020). In addition to this, other studies found that ORF8 can affect type I IFN production in autocrine signaling but does not affect the induction of antiviral ISG family genes, especially not ISG15 (Geng et al., 2021; J. Y. Li et al., 2020). As expected, when RIG-I agonist 5'ppp dsRNA, RIG-I/MDA-5 agonist dsRNA poly (I:C), and TLR7/8 agonist ssRNA R848 was used, ORF8 expression in the cell line significantly antagonized type I IFN production. Specifically, ORF8 expression downmodulated IFN production 3- and 2-fold in response to RIG-I and TLR7/8 agonists, respectively. However, ORF8 expression had no effect on ISG15 expression when cells were stimulated with IFN-β, consistent with previous literature fundings. ORF3a protein was found to be significantly effective in decreasing IFN production when the cell line was stimulated with RIG-I, RIG-I/MDA-5, and TLR7/8 agonists. In addition to type I IFN production, ORF3a SARS-CoV-2 protein was assessed as the only protein that downmodulated ISG15 expression. Evidence suggests that, ORF3a interfere with and significantly downmodulates type I IFN signaling and IRF-responsive genes such as ISG56,

ISG15, and STAT2 (R. Wang et al., 2021). In conclusion, our findings in the multiple experiments related to type I IFN production and intracellular staining of ISG15 support these findings. Therefore, ORF3a and ORF8 proteins can be characterized as type I IFN antagonists.

In parallel experiments, in order to investigate SARS-CoV-2 structural, non-structural, and accessory proteins' effect on inflammasome activation, IL-1β cytokine ELISA, and lactate dehydrogenase (LDH) enzyme release assays were performed. To assess cell death, cell lines were also stained with SytoxOrange or PI and subsequently analyzed. First, cells were primed and then stimulated/transfected with nigericin, alum, flagellin, LPS, and poly (dA:dT) stimulants for the activation of NLRP3, NLRP3, NLRC4, non-canonical and AIM2 inflammasomes, respectively.

SARS-CoV-2 accessory protein ORF3a was previously found to have 95% amino acid similarity with SARS-CoV in which the protein was characterized as NLRP3 inflammasome activator by inducing K^+ efflux as a viroporin (Xu et al., 2020; Yap et al., 2020). We also determined that ORF3a expressing cell line displayed significantly higher (5 to 10-fold) IL-1β production after the cells were exposed NLRP3 inflammasome activators, and the protein was found to significantly enhance pyroptosis, indicating our results also concluded that SARS-CoV-2 protein ORF3a can be named as an NLRP3 activator or a viroporin. In addition, SARS-CoV-2 ORF3a protein was found to be significantly effective in NLRC4 inflammasome activation, although IL-1β production was not as elevated as NLRP3-mediated IL-1β results. This could suggest that NLRC4 and NLRP3 inflammasomes are both activated during the SARS-CoV-2 infections, synergistically contributing to hyper-inflammation.

Experiments carried out with the NSP9 non-structural protein expressing cells revealed type I IFN production was downmodulated only when the cell line was treated with intracellular poly(I:C) and when compared to wild-type but not mock transfected cells. As described in Section 3.3.1.1, type I IFN readouts should be

compared with MOCK to take into account the type I IFN activation potential of the lentiviral transduction and therefore, data based on just one type of ligand and comparison to WT control is not enough to conclude that NSP9 protein acts as an interferon antagonist. On the other hand, NSP9 non-structural protein was observed to inhibit nigericin-mediated cell death (both pyroptosis-dependent and -independent). We concluded that NSP9 non-structural protein may indeed impede host cell membrane trafficking, consistent with previous literature findings as mentioned in Section 3.4.2.2.

Last but not the least, Nucleocapsid structural protein-expressing cell line showed type I IFN modulation only in response to intracellular poly(I:C) treatment, and similar to NSP9, only when results were compared to WT, but not to mock. Thus, our study did not support a role for the Nucleocapsid protein as an interferon antagonist. Furthermore, we detected that Nucleocapsid expression in the cell line abrogated pyroptosis after Alum-mediated NLRP3, non-canonical, or flagellin-mediated NLRC4 inflammasome activation. In literature, evidence suggests a role by Nucleocapsid protein in blocking Gasdermin D function, thus membrane pore formation (Ma et al., 2021). We also detected that N structural protein induces pyroptosis-independent cell death following activation of non-canonical and NLRC4 inflammasomes. Therefore, we concluded that Nucleocapsid expression impacts pore formation in the cell line, but this needs further investigation. There is a suggestion that SARS-CoV-2 N protein promotes inflammasome activation but IL-1β does not correlate with disease severity, instead IL-18, another product of inflammasome activation, should be investigated together with Gasdermin D (Del Valle et al., 2020).

In future experiments, we intent to further study the contribution of Nucleocapsid in activation/inhibition of the NLRP3 inflammasome. To do so, we aimed to mutate the N terminal Gasdermin D via phosphorylating the 6^{th} threonine residue in the Nucleocapsid expressing cell line. In addition to inflammatory cytokines and LDH, we intend to check the role of different caspases such as caspase-3 or caspase-7 to target different cell death mechanisms. Moreover, other than

expressing SARS-CoV-2 proteins one by one in the cell line, co-expression of nonstructural and accessory proteins, revealing their synergetic effects are planned to be investigated.

REFERENCES

Amsler, L., Verweij, M. C., & Defilippis, V. R. (2013). The tiers and dimensions of evasion of the type i interferon response by human cytomegalovirus. *Journal of Molecular Biology*, *425*(24), 4857–4871. https://doi.org/10.1016/j.jmb.2013.08.023

Asrani, P., & Hassan, M. I. (2021). SARS-CoV-2 mediated lung inflammatory responses in host: targeting the cytokine storm for therapeutic interventions. *Molecular and Cellular Biochemistry*, *476*(2), 675–687. https://doi.org/10.1007/s11010-020-03935-z

Azad, G. K., & Khan, P. K. (2021). Variations in Orf3a protein of SARS-CoV-2 alter its structure and function. *Biochemistry and Biophysics Reports*, *26*, 100933. https://doi.org/10.1016/j.bbrep.2021.100933

Baldanta, S., Fernández-Escobar, M., Acín-Perez, R., Albert, M., Camafeita, E., Jorge, I., Vázquez, J., Enríquez, J. A., & Guerra, S. (2017). ISG15 governs mitochondrial function in macrophages following vaccinia virus infection. *PLoS Pathogens*, *13*(10), 1–30. https://doi.org/10.1371/journal.ppat.1006651

Banerjee, A. K., Blanco, M. R., Bruce, E. A., Honson, D. D., Chen, L. M., Chow, A., Bhat, P., Ollikainen, N., Quinodoz, S. A., Loney, C., Thai, J., Miller, Z. D., Lin, A. E., Schmidt, M. M., Stewart, D. G., Goldfarb, D., De Lorenzo, G., Rihn, S. J., Voorhees, R. M., … Guttman, M. (2020). SARS-CoV-2 Disrupts Splicing, Translation, and Protein Trafficking to Suppress Host Defenses. *Cell*, *183*(5), 1325-1339.e21. https://doi.org/10.1016/j.cell.2020.10.004

Bogunovic, D., Byun, M., Durfee, L. A., Abhyankar, A., Sanal, O., Mansouri, D., Salem, S., Radovanovic, I., Grant, A. V., Adimi, P., Mansouri, N., Okada, S., Bryant, V. L., Kong, X. F., Kreins, A., Velez, M. M., Boisson, B., Khalilzadeh, S., Ozcelik, U., … Casanova, J. L. (2012). Mycobacterial disease and impaired IFN-γ immunity in humans with inherited ISG15 deficiency.

Science, *337*(6102), 1684–1688. https://doi.org/10.1126/science.1224026

Brisse, M., & Ly, H. (2019). Comparative structure and function analysis of the RIG-I-like receptors: RIG-I and MDA5. *Frontiers in Immunology*, *10*(JULY), 1–27. https://doi.org/10.3389/fimmu.2019.01586

Brown, B. D., Sitia, G., Annoni, A., Hauben, E., Sergi, L. S., Zingale, A., Roncarolo, M. G., Guidotti, L. G., & Naldini, L. (2007). In vivo administration of lentiviral vectors triggers a type I interferon response that restricts hepatocyte gene transfer and promotes vector clearance. *Blood*, *109*(7), 2797–2805. https://doi.org/10.1182/blood-2006-10-049312

Chai, J., Cai, Y., Pang, C., Wang, L., McSweeney, S., Shanklin, J., & Liu, Q. (2021). Structural basis for SARS-CoV-2 envelope protein recognition of human cell junction protein PALS1. *Nature Communications*, *12*(1), 1–6. https://doi.org/10.1038/s41467-021-23533-x

Chakrabarti, A., Banerjee, S., Franchi, L., Loo, Y. M., Gale, M., Núñez, G., & Silverman, R. H. (2015). RNase L activates the NLRP3 inflammasome during viral infections. *Cell Host and Microbe*, *17*(4), 466–477. https://doi.org/10.1016/j.chom.2015.02.010

Chan, J. F. W., To, K. K. W., Chen, H., & Yuen, K. Y. (2015). Cross-species transmission and emergence of novel viruses from birds. *Current Opinion in Virology*, *10*(January), 63–69. https://doi.org/10.1016/j.coviro.2015.01.006

Chen, I. Y., Moriyama, M., Chang, M. F., & Ichinohe, T. (2019). Severe acute respiratory syndrome coronavirus viroporin 3a activates the NLRP3 inflammasome. *Frontiers in Microbiology*, *10*(JAN), 1–9. https://doi.org/10.3389/fmicb.2019.00050

Chen, X., He, W. T., Hu, L., Li, J., Fang, Y., Wang, X., Xu, X., Wang, Z., Huang, K., & Han, J. (2016). Pyroptosis is driven by non-selective gasdermin-D pore and its morphology is different from MLKL channel-mediated necroptosis. *Cell Research*, *26*(9), 1007–1020. https://doi.org/10.1038/cr.2016.100

Clementz, M. A., Chen, Z., Banach, B. S., Wang, Y., Sun, L., Ratia, K., Baez-Santos, Y. M., Wang, J., Takayama, J., Ghosh, A. K., Li, K., Mesecar, A. D., & Baker, S. C. (2010). Deubiquitinating and Interferon Antagonism Activities of Coronavirus Papain-Like Proteases. *Journal of Virology*, *84*(9), 4619–4629. https://doi.org/10.1128/jvi.02406-09

Cubuk, J., Alston, J. J., Incicco, J. J., Singh, S., Stuchell-Brereton, M. D., Ward, M. D., Zimmerman, M. I., Vithani, N., Griffith, D., Wagoner, J. A., Bowman, G. R., Hall, K. B., Soranno, A., & Holehouse, A. S. (2021). The SARS-CoV-2 nucleocapsid protein is dynamic, disordered, and phase separates with RNA. *Nature Communications*, *12*(1), 1–17. https://doi.org/10.1038/s41467-021-21953-3

D'Cunha, J, Ramanujam, S., Wagner, R. J., Witt, P. L., Knight, E., & Borden, E. C. (1996). In vitro and in vivo secretion of human ISG15, an IFN-induced immunomodulatory cytokine. *Journal of Immunology (Baltimore, Md. : 1950)*, *157*(9), 4100–4108. http://www.ncbi.nlm.nih.gov/pubmed/8892645

D'Cunha, Jonathan, Knight, E., Haas, A. L., Truitt, R. L., & Borden, E. C. (1996). Immunoregulatory properties of ISG15, an interferon-induced cytokine. *Proceedings of the National Academy of Sciences of the United States of America*, *93*(1), 211–215. https://doi.org/10.1073/pnas.93.1.211

da Costa, L. S., Outlioua, A., Anginot, A., Akarid, K., & Arnoult, D. (2019). RNA viruses promote activation of the NLRP3 inflammasome through cytopathogenic effect-induced potassium efflux. *Cell Death and Disease*, *10*(5). https://doi.org/10.1038/s41419-019-1579-0

Del Valle, D. M., Kim-Schulze, S., Huang, H. H., Beckmann, N. D., Nirenberg, S., Wang, B., Lavin, Y., Swartz, T. H., Madduri, D., Stock, A., Marron, T. U., Xie, H., Patel, M., Tuballes, K., Van Oekelen, O., Rahman, A., Kovatch, P., Aberg, J. A., Schadt, E., … Gnjatic, S. (2020). An inflammatory cytokine signature predicts COVID-19 severity and survival. *Nature Medicine*, *26*(10),

1636–1643. https://doi.org/10.1038/s41591-020-1051-9

Eduardo-Correia, B., Martinez-Romero, C., Garcia-Sastre, A., & Guerra, S. (2014). ISG15 Is Counteracted by Vaccinia Virus E3 Protein and Controls the Proinflammatory Response against Viral Infection. *Journal of Virology*, *88*(4), 2312–2318. https://doi.org/10.1128/jvi.03293-13

Fang, P., Fang, L., Ren, J., Hong, Y., Liu, X., Zhao, Y., Wang, D., Peng, G., & Xiao, S. (2018). Porcine Deltacoronavirus Accessory Protein NS6 Antagonizes Interferon Beta Production by Interfering with the Binding of RIG-I/MDA5 to Double-Stranded RNA. *Journal of Virology*, *92*(15). https://doi.org/10.1128/jvi.00712-18

Follenzi, A., Santambrogio, L., & Annoni, A. (2007). Immune Responses to Lentiviral Vectors. *Current Gene Therapy*, *7*(5), 306–315. https://doi.org/10.2174/156652307782151515

Galani, I. E., Rovina, N., Lampropoulou, V., Triantafyllia, V., Manioudaki, M., Pavlos, E., Koukaki, E., Fragkou, P. C., Panou, V., Rapti, V., Koltsida, O., Mentis, A., Koulouris, N., Tsiodras, S., Koutsoukou, A., & Andreakos, E. (2021). Untuned antiviral immunity in COVID-19 revealed by temporal type I/III interferon patterns and flu comparison. *Nature Immunology*, *22*(1), 32–40. https://doi.org/10.1038/s41590-020-00840-x

Gay, N. J., Symmons, M. F., Gangloff, M., & Bryant, C. E. (2014). Assembly and localization of Toll-like receptor signalling complexes. *Nature Reviews Immunology*, *14*(8), 546–558. https://doi.org/10.1038/nri3713

Geng, H., Subramanian, S., Wu, L., Bu, H. F., Wang, X., Du, C., De Plaen, I. G., & Tan, X. Di. (2021). SARS-CoV-2 ORF8 Forms Intracellular Aggregates and Inhibits IFNγ-Induced Antiviral Gene Expression in Human Lung Epithelial Cells. *Frontiers in Immunology*, *12*(June), 679482. https://doi.org/10.3389/fimmu.2021.679482

Gong, Y. N., Wang, X., Wang, J., Yang, Z., Li, S., Yang, J., Liu, L., Lei, X., &

Shao, F. (2010). Chemical probing reveals insights into the signaling mechanism of inflammasome activation. *Cell Research*, *20*(12), 1289–1305. https://doi.org/10.1038/cr.2010.135

Gordon, D. E., Jang, G. M., Bouhaddou, M., Xu, J., Obernier, K., White, K. M., O'Meara, M. J., Rezelj, V. V., Guo, J. Z., Swaney, D. L., Tummino, T. A., Hüttenhain, R., Kaake, R. M., Richards, A. L., Tutuncuoglu, B., Foussard, H., Batra, J., Haas, K., Modak, M., … Krogan, N. J. (2020). A SARS-CoV-2 protein interaction map reveals targets for drug repurposing. *Nature*, *583*(7816), 459–468. https://doi.org/10.1038/s41586-020-2286-9

Gori Savellini, G., Gandolfo, C., & Cusi, M. G. (2015). Truncation of the C-terminal region of Toscana Virus NSs protein is critical for interferon-β antagonism and protein stability. *Virology*, *486*, 255–262. https://doi.org/10.1016/j.virol.2015.09.021

Grandvaux, N., TenOever, B. R., Servant, M. J., & Hiscott, J. (2002). The interferon antiviral response: From viral invasion to evasion. *Current Opinion in Infectious Diseases*, *15*(3), 259–267. https://doi.org/10.1097/00001432-200206000-00008

Gritsenko, A., Yu, S., Martin-Sanchez, F., Diaz-del-Olmo, I., Nichols, E. M., Davis, D. M., Brough, D., & Lopez-Castejon, G. (2020). Priming Is Dispensable for NLRP3 Inflammasome Activation in Human Monocytes In Vitro. *Frontiers in Immunology*, *11*(September), 1–14. https://doi.org/10.3389/fimmu.2020.565924

Guerra, S., Cáceres, A., Knobeloch, K. P., Horak, I., & Esteban, M. (2008). Vaccinia virus E3 protein prevents the antiviral action of ISG15. *PLoS Pathogens*, *4*(7). https://doi.org/10.1371/journal.ppat.1000096

Haller, O., Staeheli, P., Schwemmle, M., & Kochs, G. (2015). Mx GTPases: Dynamin-like antiviral machines of innate immunity. *Trends in Microbiology*, *23*(3), 154–163. https://doi.org/10.1016/j.tim.2014.12.003

Harrison, A. G., Lin, T., & Wang, P. (2020). Mechanisms of SARS-CoV-2 Transmission and Pathogenesis. *Trends in Immunology*, *41*(12), 1100–1115. https://doi.org/10.1016/j.it.2020.10.004

Hasan, M., & Yan, N. (2016). Therapeutic potential of targeting TBK1 in autoimmune diseases and interferonopathies. *Pharmacological Research*, *111*, 336–342. https://doi.org/10.1016/j.phrs.2016.04.008

Hornung, V., Ellegast, J., Kim, S., Brzózka, K., Jung, A., Kato, H., Poeck, H., Akira, S., Conzelmann, K. K., Schlee, M., Endres, S., & Hartmann, G. (2006). 5′-Triphosphate RNA is the ligand for RIG-I. *Science*, *314*(5801), 994–997. https://doi.org/10.1126/science.1132505

Hornung, V., Hartmann, R., Ablasser, A., & Hopfner, K. P. (2014). OAS proteins and cGAS: Unifying concepts in sensing and responding to cytosolic nucleic acids. *Nature Reviews Immunology*, *14*(8), 521–528. https://doi.org/10.1038/nri3719

Hu, B., Guo, H., Zhou, P., & Shi, Z. L. (2021). Characteristics of SARS-CoV-2 and COVID-19. *Nature Reviews Microbiology*, *19*(3), 141–154. https://doi.org/10.1038/s41579-020-00459-7

Huang, C., Wang, Y., Li, X., Ren, L., Zhao, J., Hu, Y., Zhang, L., Fan, G., Xu, J., Gu, X., Cheng, Z., Yu, T., Xia, J., Wei, Y., Wu, W., Xie, X., Yin, W., Li, H., Liu, M., … Cao, B. (2020). Clinical features of patients infected with 2019 novel coronavirus in Wuhan, China. *The Lancet*, *395*(10223), 497–506. https://doi.org/10.1016/S0140-6736(20)30183-5

Huang, Y., Yang, C., Xu, X. feng, Xu, W., & Liu, S. wen. (2020). Structural and functional properties of SARS-CoV-2 spike protein: potential antivirus drug development for COVID-19. *Acta Pharmacologica Sinica*, *41*(9), 1141–1149. https://doi.org/10.1038/s41401-020-0485-4

Iwasaki, H., & Akashi, K. (2007). Myeloid Lineage Commitment from the Hematopoietic Stem Cell. *Immunity*, *26*(6), 726–740.

https://doi.org/10.1016/j.immuni.2007.06.004

Jack, A., Ferro, L. S., Trnka, M. J., Wehri, E., Nadgir, A., Nguyenla, X., Fox, D., Costa, K., Stanley, S., Schaletzky, J., & Yildiz, A. (2021). SARS-CoV-2 nucleocapsid protein forms condensates with viral genomic RNA. *PLoS Biology*, *19*(10), 1–30. https://doi.org/10.1371/journal.pbio.3001425

Jin, T., Perry, A., Jiang, J., Smith, P., Curry, J. A., Unterholzner, L., Jiang, Z., Horvath, G., Rathinam, V. A., Johnstone, R. W., Hornung, V., Latz, E., Bowie, A. G., Fitzgerald, K. A., & Xiao, T. S. (2012). Structures of the HIN Domain: DNA Complexes Reveal Ligand Binding and Activation Mechanisms of the AIM2 Inflammasome and IFI16 Receptor. *Immunity*, *36*(4), 561–571. https://doi.org/10.1016/j.immuni.2012.02.014

Kanneganti, T. D. (2010). Central roles of NLRs and inflammasomes in viral infection. *Nature Reviews Immunology*, *10*(10), 688–698. https://doi.org/10.1038/nri2851

Keestra-Gounder, A. M., & Tsolis, R. M. (2017). NOD1 and NOD2: Beyond Peptidoglycan Sensing. *Trends in Immunology*, *38*(10), 758–767. https://doi.org/10.1016/j.it.2017.07.004

Kern, D. M., Sorum, B., Mali, S. S., Hoel, C. M., Sridharan, S., Remis, J. P., Toso, D. B., Kotecha, A., Bautista, D. M., & Brohawn, S. G. (2021). Cryo-EM structure of SARS-CoV-2 ORF3a in lipid nanodiscs. *Nature Structural and Molecular Biology*, *28*(7), 573–582. https://doi.org/10.1038/s41594-021-00619-0

Kesavardhana, S., & Kanneganti, T. D. (2017). Mechanisms governing inflammasome activation, assembly and pyroptosis induction. *International Immunology*, *29*(5), 201–210. https://doi.org/10.1093/intimm/dxx018

Kim, Y. J., Kim, E. T., Kim, Y. E., Lee, M. K., Kwon, K. M., Kim, K. Il, Stamminger, T., & Ahn, J. H. (2016). Consecutive Inhibition of ISG15 Expression and ISGylation by Cytomegalovirus Regulators. *PLoS Pathogens*,

12(8), 1–28. https://doi.org/10.1371/journal.ppat.1005850

Konno, Y., Kimura, I., Uriu, K., Fukushi, M., Irie, T., Koyanagi, Y., Sauter, D., Gifford, R. J., Nakagawa, S., & Sato, K. (2020). SARS-CoV-2 ORF3b Is a Potent Interferon Antagonist Whose Activity Is Increased by a Naturally Occurring Elongation Variant. *Cell Reports*, *32*(12), 108185. https://doi.org/10.1016/j.celrep.2020.108185

Kopecky-Bromberg, S. A., Martínez-Sobrido, L., Frieman, M., Baric, R. A., & Palese, P. (2007). Severe Acute Respiratory Syndrome Coronavirus Open Reading Frame (ORF) 3b, ORF 6, and Nucleocapsid Proteins Function as Interferon Antagonists. *Journal of Virology*, *81*(2), 548–557. https://doi.org/10.1128/jvi.01782-06

Kovtonyuk, L. V., Fritsch, K., Feng, X., Manz, M. G., & Takizawa, H. (2016). Inflamm-aging of hematopoiesis, hematopoietic stem cells, and the bone marrow microenvironment. *Frontiers in Immunology*, *7*(NOV), 1–13. https://doi.org/10.3389/fimmu.2016.00502

Krug, R. M. (2015). Functions of the influenza A virus NS1 protein in antiviral defense. *Current Opinion in Virology*, *12*, 1–6. https://doi.org/10.1016/j.coviro.2015.01.007

Lai, C., Struckhoff, J. J., Schneider, J., Martinez-Sobrido, L., Wolff, T., García-Sastre, A., Zhang, D.-E., & Lenschow, D. J. (2009). Mice Lacking the ISG15 E1 Enzyme UbE1L Demonstrate Increased Susceptibility to both Mouse-Adapted and Non-Mouse-Adapted Influenza B Virus Infection. *Journal of Virology*, *83*(2), 1147–1151. https://doi.org/10.1128/jvi.00105-08

Lam, J. Y., Yuen, C. K., Ip, J. D., Wong, W. M., To, K. K. W., Yuen, K. Y., & Kok, K. H. (2020). Loss of orf3b in the circulating SARS-CoV-2 strains. *Emerging Microbes and Infections*, *9*(1), 2685–2696. https://doi.org/10.1080/22221751.2020.1852892

Latif, A. A., & Mukaratirwa, S. (2020). Zoonotic origins and animal hosts of

coronaviruses causing human disease pandemics: A review. *Onderstepoort Journal of Veterinary Research*, *87*(1), 1–9. https://doi.org/10.4102/OJVR.V87I1.1895

Lee, J. G., Huang, W., Lee, H., van de Leemput, J., Kane, M. A., & Han, Z. (2021). Characterization of SARS-CoV-2 proteins reveals Orf6 pathogenicity, subcellular localization, host interactions and attenuation by Selinexor. *Cell and Bioscience*, *11*(1), 1–12. https://doi.org/10.1186/s13578-021-00568-7

Lei, X., Dong, X., Ma, R., Wang, W., Xiao, X., Tian, Z., Wang, C., Wang, Y., Li, L., Ren, L., Guo, F., Zhao, Z., Zhou, Z., Xiang, Z., & Wang, J. (2020). Activation and evasion of type I interferon responses by SARS-CoV-2. *Nature Communications*, *11*(1), 1–12. https://doi.org/10.1038/s41467-020-17665-9

Leisching, G., Wiid, I., & Baker, B. (2017). The Association of OASL and Type I Interferons in the Pathogenesis and Survival of Intracellular Replicating Bacterial Species. *Frontiers in Cellular and Infection Microbiology*, *7*(MAY), 3–8. https://doi.org/10.3389/fcimb.2017.00196

Letko, M., Marzi, A., & Munster, V. (2020). Functional assessment of cell entry and receptor usage for SARS-CoV-2 and other lineage B betacoronaviruses. *Nature Microbiology*, *5*(4), 562–569. https://doi.org/10.1038/s41564-020-0688-y

Li, D., & Wu, M. (2021). Pattern recognition receptors in health and diseases. *Signal Transduction and Targeted Therapy*, *6*(1), 1–24. https://doi.org/10.1038/s41392-021-00687-0

Li, J. Y., Liao, C. H., Wang, Q., Tan, Y. J., Luo, R., Qiu, Y., & Ge, X. Y. (2020). The ORF6, ORF8 and nucleocapsid proteins of SARS-CoV-2 inhibit type I interferon signaling pathway. *Virus Research*, *286*(June), 198074. https://doi.org/10.1016/j.virusres.2020.198074

Littler, D. R., Gully, B. S., Colson, R. N., & Rossjohn, J. (2020). Crystal Structure of the SARS-CoV-2 Non-structural Protein 9, Nsp9. *IScience*, *23*(7), 101258.

https://doi.org/10.1016/j.isci.2020.101258

Louvrier, C., Assrawi, E., El Khouri, E., Melki, I., Copin, B., Bourrat, E., Lachaume, N., Cador-Rousseau, B., Duquesnoy, P., Piterboth, W., Awad, F., Jumeau, C., Legendre, M., Grateau, G., Georgin-Lavialle, S., Karabina, S. A., Amselem, S., & Giurgea, I. (2020). NLRP3-associated autoinflammatory diseases: Phenotypic and molecular characteristics of germline versus somatic mutations. *Journal of Allergy and Clinical Immunology*, *145*(4), 1254–1261. https://doi.org/10.1016/j.jaci.2019.11.035

Lugrin, J., & Martinon, F. (2018). The AIM2 inflammasome: Sensor of pathogens and cellular perturbations. *Immunological Reviews*, *281*(1), 99–114. https://doi.org/10.1111/imr.12618

Ma, J., Zhu, F., Zhao, M., Shao, F., Yu, D., Ma, J., Zhang, X., Li, W., Qian, Y., Zhang, Y., Jiang, D., Wang, S., & Xia, P. (2021). SARS-CoV-2 nucleocapsid suppresses host pyroptosis by blocking Gasdermin D cleavage. *The EMBO Journal*, *40*(18), 1–17. https://doi.org/10.15252/embj.2021108249

Mahtarin, R., Islam, S., Islam, M. J., Ullah, M. O., Ali, M. A., & Halim, M. A. (2020). Structure and dynamics of membrane protein in SARS-CoV-2. *Journal of Biomolecular Structure and Dynamics*, *0*(0), 1–14. https://doi.org/10.1080/07391102.2020.1861983

Malterer, M. B., Glass, S. J., & Newman, J. P. (2014). Interferon-stimulated genes: A complex web of host defenses. *Annual Review of Immunology*, *44*(3), 735–745. https://doi.org/10.1038/jid.2014.371

Mariano, G., Farthing, R. J., Lale-Farjat, S. L. M., & Bergeron, J. R. C. (2020). Structural Characterization of SARS-CoV-2: Where We Are, and Where We Need to Be. *Frontiers in Molecular Biosciences*, *7*(December). https://doi.org/10.3389/fmolb.2020.605236

Miao, E. A., Mao, D. P., Yudkovsky, N., Bonneau, R., Lorang, C. G., Warren, S. E., Leaf, I. A., & Aderem, A. (2010). Innate immune detection of the type III

secretion apparatus through the NLRC4 inflammasome. *Proceedings of the National Academy of Sciences of the United States of America*, *107*(7), 3076–3080. https://doi.org/10.1073/pnas.0913087107

Michel, C. J., Mayer, C., Poch, O., & Thompson, J. D. (2020). Characterization of accessory genes in coronavirus genomes. *BioRxiv*, 1–13. https://doi.org/10.1101/2020.05.26.118208

Mielech, A. M., Kilianski, A., Baez-Santos, Y. M., Mesecar, A. D., & Baker, S. C. (2014). MERS-CoV papain-like protease has deISGylating and deubiquitinating activities. *Virology*, *450–451*, 64–70. https://doi.org/10.1016/j.virol.2013.11.040

Minervina, A., Pogorelyy, M., & Mamedov, I. (2019). T-cell receptor and B-cell receptor repertoire profiling in adaptive immunity. *Transplant International*, *32*(11), 1111–1123. https://doi.org/10.1111/tri.13475

Mueller, S. N., & Rouse, B. T. (2008). Immune responses to viruses. *Clinical Immunology*, *January*, 421–431. https://doi.org/10.1016/B978-0-323-04404-2.10027-2

Narasimhan, J., Wang, M., Fu, Z., Klein, J. M., Haas, A. L., & Kim, J. J. P. (2005). Crystal structure of the interferon-induced ubiquitin-like protein ISG15. *Journal of Biological Chemistry*, *280*(29), 27356–27365. https://doi.org/10.1074/jbc.M502814200

Neches, R. Y., Kyrpides, N. C., & Ouzounis, C. A. (2021). Atypical divergence of SARS-CoV-2 Orf8 from Orf7a within the coronavirus lineage suggests potential stealthy viral strategies in immune evasion. *MBio*, *12*(1), 1–12. https://doi.org/10.1128/mBio.03014-20

Netea, M. G., Schlitzer, A., Placek, K., Joosten, L. A. B., & Schultze, J. L. (2019). Innate and Adaptive Immune Memory: an Evolutionary Continuum in the Host's Response to Pathogens. *Cell Host and Microbe*, *25*(1), 13–26. https://doi.org/10.1016/j.chom.2018.12.006

Okumura, F., Zou, W., & Zhang, D. E. (2007). ISG15 modification of the eIF4E cognate 4EHP enhances cap structure-binding activity of 4EHP. *Genes and Development*, *21*(3), 255–260. https://doi.org/10.1101/gad.1521607

Owhashi, M., Taoka, Y., Ishii, K., Nakazawa, S., Uemura, H., & Kambara, H. (2003). Identification of a ubiquitin family protein as a novel neutrophil chemotactic factor. *Biochemical and Biophysical Research Communications*, *309*(3), 533–539. https://doi.org/10.1016/j.bbrc.2003.08.038

Pan, P., Shen, M., Yu, Z., Ge, W., Chen, K., Tian, M., Xiao, F., Wang, Z., Wang, J., Jia, Y., Wang, W., Wan, P., Zhang, J., Chen, W., Lei, Z., Chen, X., Luo, Z., Zhang, Q., Xu, M., … Wu, J. (2021). SARS-CoV-2 N protein promotes NLRP3 inflammasome activation to induce hyperinflammation. *Nature Communications*, *12*(1), 1–17. https://doi.org/10.1038/s41467-021-25015-6

Pichlmair, A., Schulz, O., Tan, C.-P., Rehwinkel, J., Kato, H., Takeuchi, O., Akira, S., Way, M., Schiavo, G., & Reis e Sousa, C. (2009). Activation of MDA5 Requires Higher-Order RNA Structures Generated during Virus Infection. *Journal of Virology*, *83*(20), 10761–10769. https://doi.org/10.1128/jvi.00770-09

Pressman, B. C. (1976). BIOLOGICAL APPLICATIONS OF IONOPHORES. *Annual Review of Biochemistry*, *45:501-530*. https://doi.org/10.1146/annurev.bi.45.070176.002441

Rathinam, V. A. K., Vanaja, S. K., & Fitzgerald, K. A. (2012). Regulation of inflammasome signaling. *Nature Immunology*, *13*(4), 333–342. https://doi.org/10.1038/ni.2237

Redondo, N., Zaldívar-López, S., Garrido, J. J., & Montoya, M. (2021). SARS-CoV-2 Accessory Proteins in Viral Pathogenesis: Knowns and Unknowns. *Frontiers in Immunology*, *12*(July), 1–8. https://doi.org/10.3389/fimmu.2021.708264

Rehwinkel, J., & Gack, M. U. (2020). RIG-I-like receptors: their regulation and

roles in RNA sensing. *Nature Reviews Immunology*, *20*(9), 537–551. https://doi.org/10.1038/s41577-020-0288-3

Rohaim, M. A., El Naggar, R. F., Clayton, E., & Munir, M. (2021). Structural and functional insights into non-structural proteins of coronaviruses. *Microbial Pathogenesis*, *150*, 104641. https://doi.org/10.1016/j.micpath.2020.104641

Romano, M., Ruggiero, A., Squeglia, F., Maga, G., & Berisio, R. (2020). A Structural View of SARS-CoV-2 RNA Replication Machinery: RNA Synthesis, Proofreading and Final Capping. *Cells*, *9*(5). https://doi.org/10.3390/cells9051267

Romberg, N., Vogel, T. P., & Canna, S. W. (2017). NLRC4 inflammasomopathies. *Current Opinion in Allergy and Clinical Immunology*, *17*(6), 398–404. https://doi.org/10.1097/ACI.0000000000000396

Samuel, C. E. (2001). Antiviral actions of interferons. *Clinical Microbiology Reviews*, *14*(4), 778–809. https://doi.org/10.1128/CMR.14.4.778-809.2001

Sanders, M. G., Parsons, M. J., Howard, A. G. A., Liu, J., Fassio, S. R., Martinez, J. A., & Bouchier-Hayes, L. (2015). Single-cell imaging of inflammatory caspase dimerization reveals differential recruitment to inflammasomes. *Cell Death and Disease*, *6*(7), 1–11. https://doi.org/10.1038/cddis.2015.186

Schaefer, L. (2014). Complexity of danger: The diverse nature of damage-associated molecular patterns. *Journal of Biological Chemistry*, *289*(51), 35237–35245. https://doi.org/10.1074/jbc.R114.619304

Shah, A. (2020). Novel Coronavirus-Induced NLRP3 Inflammasome Activation: A Potential Drug Target in the Treatment of COVID-19. *Frontiers in Immunology*, *11*(May), 1–5. https://doi.org/10.3389/fimmu.2020.01021

Song, P., Li, W., Xie, J., Hou, Y., & You, C. (2020). *Cytokine storm induced by SARS-CoV-2*. *January*.

Speer, S. D., Li, Z., Buta, S., Payelle-Brogard, B., Qian, L., Vigant, F., Rubino, E.,

Gardner, T. J., Wedeking, T., Hermann, M., Duehr, J., Sanal, O., Tezcan, I., Mansouri, N., Tabarsi, P., Mansouri, D., Francois-Newton, V., Daussy, C. F., Rodriguez, M. R., … Bogunovic, D. (2016). ISG15 deficiency and increased viral resistance in humans but not mice. *Nature Communications*, *7*(May). https://doi.org/10.1038/ncomms11496

Takeuchi, O., & Akira, S. (2010). Pattern Recognition Receptors and Inflammation. *Cell*, *140*(6), 805–820. https://doi.org/10.1016/j.cell.2010.01.022

Tang, Y., Liu, J., Zhang, D., Xu, Z., Ji, J., & Wen, C. (2020). Cytokine Storm in COVID-19: The Current Evidence and Treatment Strategies. *Frontiers in Immunology*, *11*(July), 1–13. https://doi.org/10.3389/fimmu.2020.01708

Thoms, M., Buschauer, R., Ameismeier, M., Koepke, L., Denk, T., Hirschenberger, M., Kratzat, H., Hayn, M., MacKens-Kiani, T., Cheng, J., Straub, J. H., Stürzel, C. M., Fröhlich, T., Berninghausen, O., Becker, T., Kirchhoff, F., Sparrer, K. M. J., & Beckmann, R. (2020). Structural basis for translational shutdown and immune evasion by the Nsp1 protein of SARS-CoV-2. *Science*, *369*(6508), 1249–1256. https://doi.org/10.1126/SCIENCE.ABC8665

Vanaja, S. K., Rathinam, V. A. K., & Fitzgerald, K. A. (2015). Mechanisms of inflammasome activation: Recent advances and novel insights. *Trends in Cell Biology*, *25*(5), 308–315. https://doi.org/10.1016/j.tcb.2014.12.009

Wang, N., Shang, J., Jiang, S., & Du, L. (2020). Subunit Vaccines Against Emerging Pathogenic Human Coronaviruses. *Frontiers in Microbiology*, *11*(February). https://doi.org/10.3389/fmicb.2020.00298

Wang, R., Yang, X., Chang, M., Xue, Z., Wang, W., Bai, L., Zhao, S., & Liu, E. (2021). ORF3a Protein of Severe Acute Respiratory Syndrome Coronavirus 2 Inhibits Interferon-Activated Janus Kinase/Signal Transducer and Activator of Transcription Signaling via Elevating Suppressor of Cytokine Signaling 1. *Frontiers in Microbiology*, *12*(September), 1–13.

https://doi.org/10.3389/fmicb.2021.752597

Weber-Gerlach, M., & Weber, F. (2016). To Conquer the Host, Influenza Virus Is Packing It In: Interferon-Antagonistic Strategies beyond NS1. *Journal of Virology*, *90*(19), 8389–8394. https://doi.org/10.1128/jvi.00041-16

Werneke, S. W., Schilte, C., Rohatgi, A., Monte, K. J., Michault, A., Arenzana-Seisdedos, F., Vanlandingham, D. L., Higgs, S., Fontanet, A., Albert, M. L., & Lenschow, D. J. (2011). ISG15 is critical in the control of chikungunya virus infection independent of UbE1l mediated conjugation. *PLoS Pathogens*, *7*(10). https://doi.org/10.1371/journal.ppat.1002322

Wu, L., & Liu, Y. J. (2007). Development of Dendritic-Cell Lineages. *Immunity*, *26*(6), 741–750. https://doi.org/10.1016/j.immuni.2007.06.006

Xia, H., Cao, Z., Xie, X., Zhang, X., Chen, J. Y. C., Wang, H., Menachery, V. D., Rajsbaum, R., & Shi, P. Y. (2020). Evasion of Type I Interferon by SARS-CoV-2. *Cell Reports*, *33*(1), 108234. https://doi.org/10.1016/j.celrep.2020.108234

Xing, J., Wang, S., Lin, R., Mossman, K. L., & Zheng, C. (2012). Herpes Simplex Virus 1 Tegument Protein US11 Downmodulates the RLR Signaling Pathway via Direct Interaction with RIG-I and MDA-5. *Journal of Virology*, *86*(7), 3528–3540. https://doi.org/10.1128/jvi.06713-11

Xu, H., Chitre, S. A., Akinyemi, I. A., Loeb, J. C., Lednicky, J. A., McIntosh, M. T., & Bhaduri-McIntosh, S. (2020). SARS-CoV-2 viroporin triggers the NLRP3 inflammatory pathway. *BioRxiv*, 2020.10.27.357731. https://doi.org/10.1101/2020.10.27.357731

Yamasaki, K., Muto, J., Taylor, K. R., Cogen, A. L., Audish, D., Bertin, J., Grant, E. P., Coyle, A. J., Misaghi, A., Hoffman, H. M., & Gallo, R. L. (2009). NLRP3/cryopyrin is necessary for interleukin-1β (IL-1β) release in response to hyaluronan, an endogenous trigger of inflammation in response to injury. *Journal of Biological Chemistry*, *284*(19), 12762–12771.

https://doi.org/10.1074/jbc.M806084200

Yan, N., & Chen, Z. J. (2012). Intrinsic antiviral immunity. *Nature Immunology*, *13*(3), 214–222. https://doi.org/10.1038/ni.2229

Yap, J. K. Y., Moriyama, M., & Iwasaki, A. (2020). Inflammasomes and Pyroptosis as Therapeutic Targets for COVID-19. *The Journal of Immunology*, *205*(2), 307–312. https://doi.org/10.4049/jimmunol.2000513

Ye, Q., Lu, S., & Corbett, K. D. (2021). Structural Basis for SARS-CoV-2 Nucleocapsid Protein Recognition by Single-Domain Antibodies. *Frontiers in Immunology*, *12*(July), 1–9. https://doi.org/10.3389/fimmu.2021.719037

Yuan, W., & Krug, R. M. (2001). Influenza B virus NS1 protein inhibits conjugation of the interferon (IFN)-induced ubiquitin-like ISG15 protein. *EMBO Journal*, *20*(3), 362–371. https://doi.org/10.1093/emboj/20.3.362

Yuen, C. K., Lam, J. Y., Wong, W. M., Mak, L. F., Wang, X., Chu, H., Cai, J. P., Jin, D. Y., To, K. K. W., Chan, J. F. W., Yuen, K. Y., & Kok, K. H. (2020). SARS-CoV-2 nsp13, nsp14, nsp15 and orf6 function as potent interferon antagonists. *Emerging Microbes & Infections*, *9*(1), 1418–1428. https://doi.org/10.1080/22221751.2020.1780953

Zhang, D., & Zhang, D. E. (2011). Interferon-stimulated gene 15 and the protein ISGylation system. *Journal of Interferon and Cytokine Research*, *31*(1), 119–130. https://doi.org/10.1089/jir.2010.0110

Zhang, P., Liu, X., & Cao, X. (2015). Extracellular pattern recognition molecules in health and diseases. *Cellular and Molecular Immunology*, *12*(3), 255–257. https://doi.org/10.1038/cmi.2014.81

Zhang, X., Bogunovic, D., Payelle-Brogard, B., Francois-Newton, V., Speer, S. D., Yuan, C., Volpi, S., Li, Z., Sanal, O., Mansouri, D., Tezcan, I., Rice, G. I., Chen, C., Mansouri, N., Mahdaviani, S. A., Itan, Y., Boisson, B., Okada, S., Zeng, L., … Pellegrini, S. (2015). Human intracellular ISG15 prevents

interferon-α/β over-amplification and auto-inflammation. *Nature*, *517*(7532), 89–93. https://doi.org/10.1038/nature13801

Zhang, Y., Zhang, J., Chen, Y., Luo, B., Yuan, Y., Huang, F., Yang, T., Yu, F., Liu, J., Liu, B., Song, Z., Chen, J., Pan, T., Zhang, X., Li, Y., Li, R., Huang, W., Xiao, F., & Zhang, H. (2020). The ORF8 protein of SARS-CoV-2 mediates immune evasion through potently downregulating MHC-I. *BioRxiv*. https://doi.org/10.1101/2020.05.24.111823

Zhao, Y., Yang, J., Shi, J., Gong, Y. N., Lu, Q., Xu, H., Liu, L., & Shao, F. (2011). The NLRC4 inflammasome receptors for bacterial flagellin and type III secretion apparatus. *Nature*, *477*(7366), 596–602. https://doi.org/10.1038/nature10510

Zhu, N., Zhang, D., Wang, W., Li, X., Yang, B., Song, J., Zhao, X., Huang, B., Shi, W., Lu, R., Niu, P., Zhan, F., Ma, X., Wang, D., Xu, W., Wu, G., Gao, G. F., & Tan, W. (2020). A Novel Coronavirus from Patients with Pneumonia in China, 2019. *New England Journal of Medicine*, *382*(8), 727–733. https://doi.org/10.1056/nejmoa2001017

APPENDICES

A. Vector Maps, AGE Solutions & Buffers

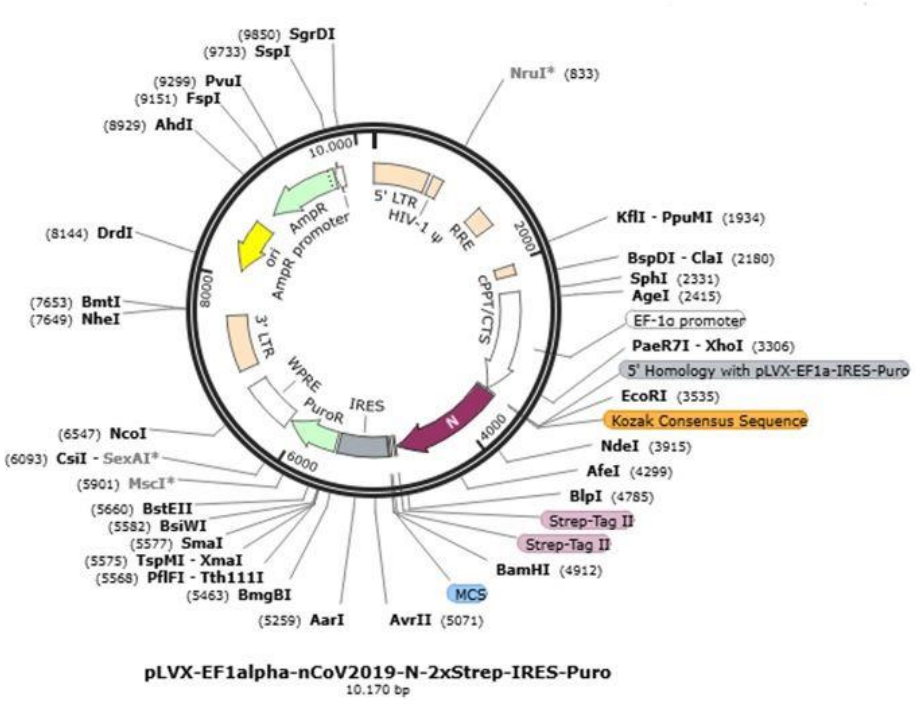

Figure A.1 The vector map of pLVX-EF1alpha-nCoV2019-N-2xStrep-IRES-Puro

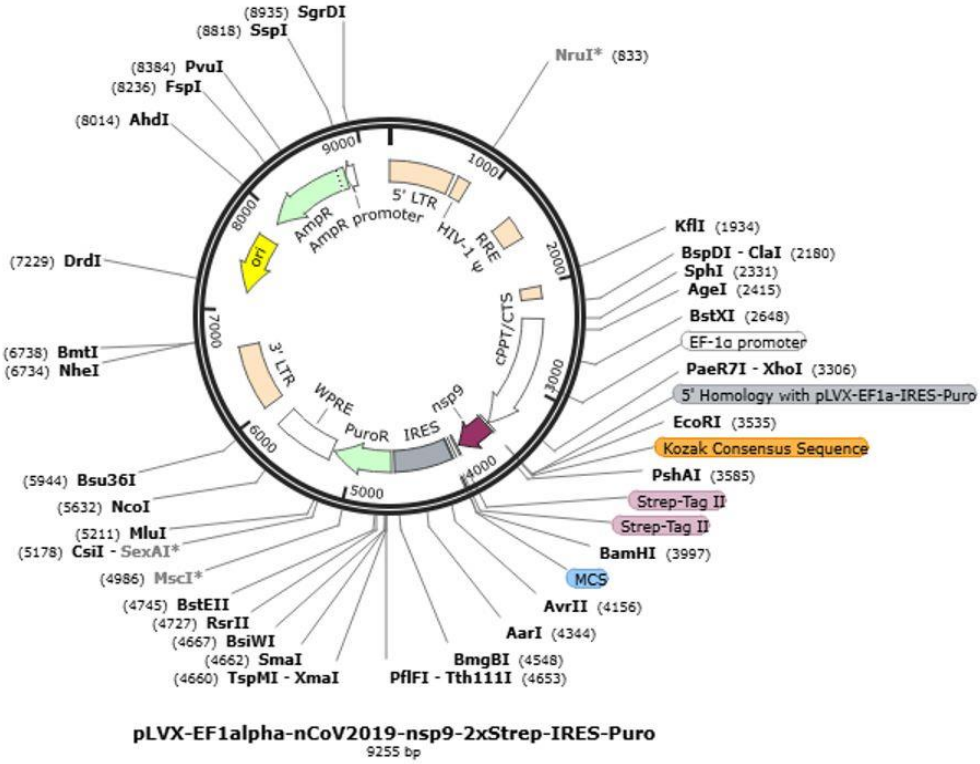

Figure A.2 The vector map of pLVX-EF1alpha-nCoV2019-nsp9-2xStrep-IRES-Puro

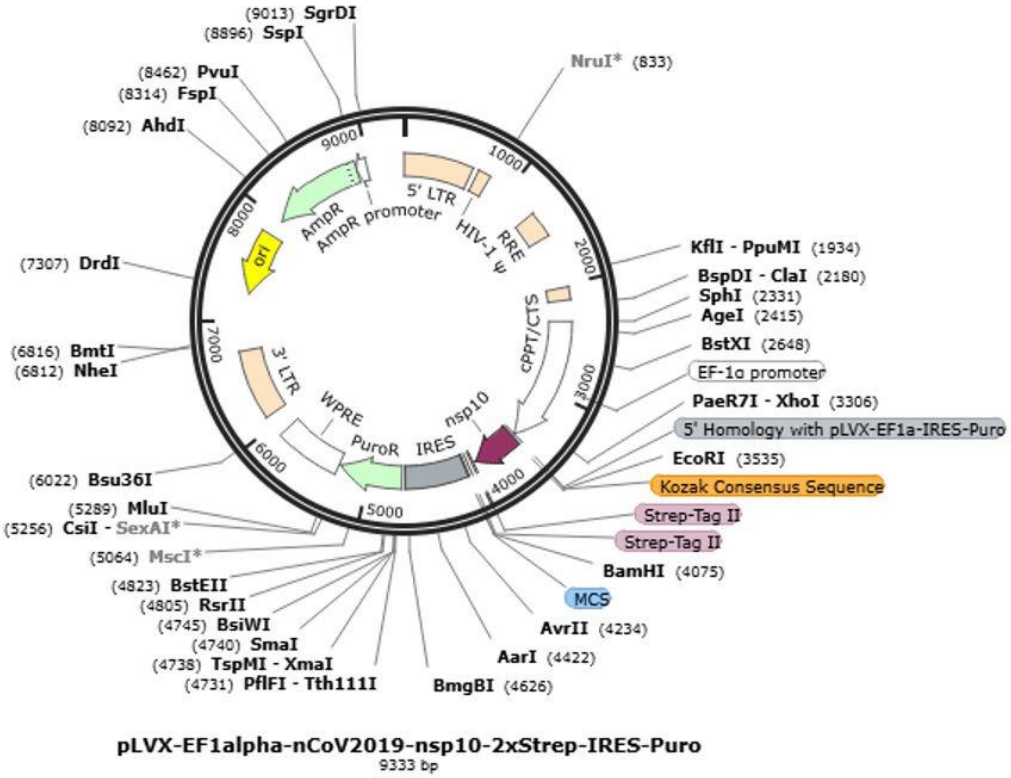

Figure A.3 The vector map of pLVX-EF1alpha-nCoV2019-nsp10-2xStrep-IRES-Puro

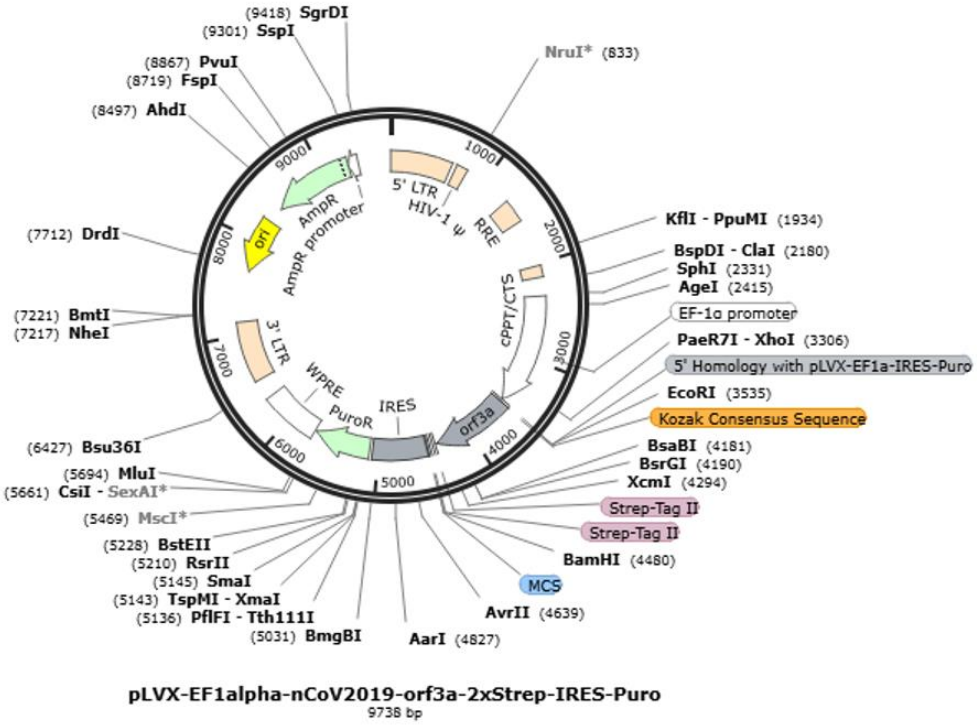

Figure A.4 The vector map of pLVX-EF1alpha-nCoV2019-orf3a-2xStrep-IRES-Puro

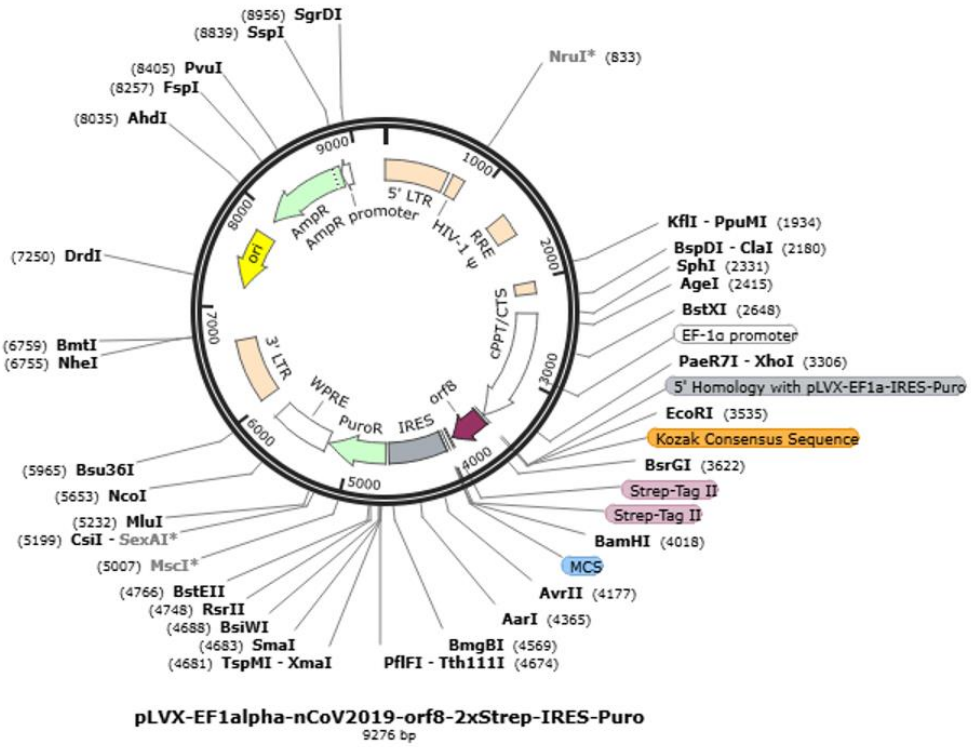

Figure A.5 The vector map of pLVX-EF1alpha-nCoV2019-orf8-2xStrep-IRES-Puro

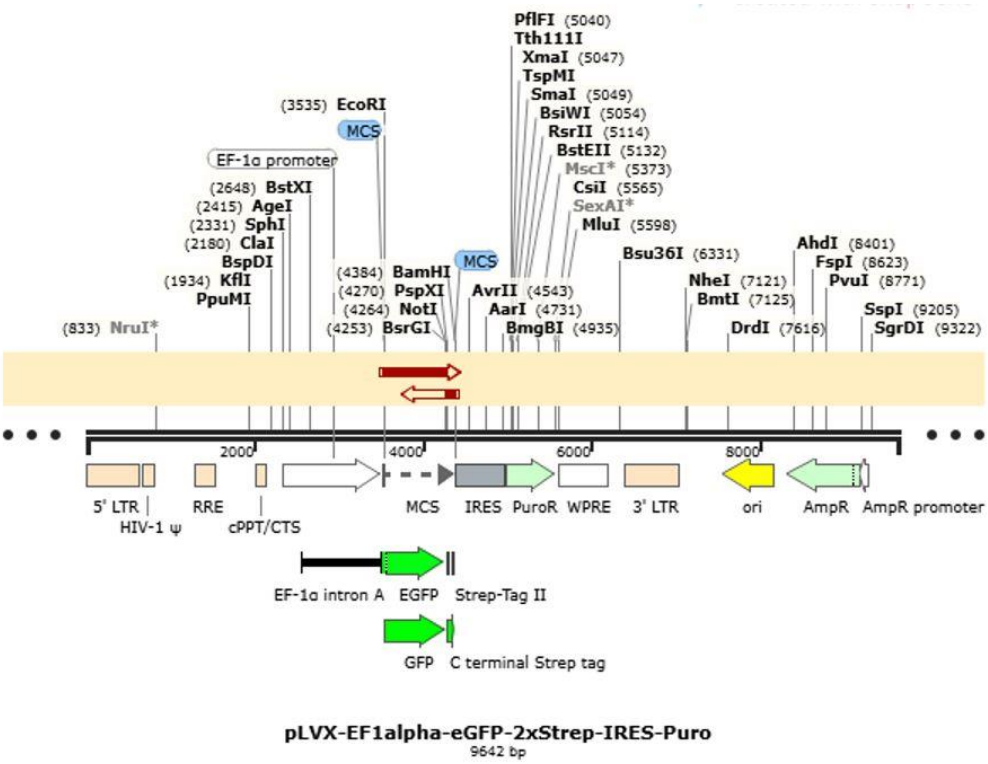

Figure A.6 The vector map of pLVX-EF1alpha-eGFP-2xStrep-IRES-Puro

1% Agarose Gel

1.5 g Agarose

150 mL 1X TAE Buffer

3 μL EtBr

10X TAE Buffer

48.4 g Tris-base

11.4 ml Glacial Acetic Acid (17.4M)

3.2 g EDTA (w/o Na)

Complete to 1L with deionized H_2O

B. Culture Media Used in Bacterial Growth

Luria Broth (LB):

10 g Tryptone

5 g NaCl

5 g Yeast Extract

1 L dH_2O

Autoclaved

LB Agar:

10 g Tryptone

5 g NaCl

5 g Yeast Extract

5 g Agar

1 L dH_2O

C. Mammalian Cell Culture Media, Buffers & Solutions

10 % FBS containing RPMI 1640 (Referred as growth medium):

50 ml FBS (heat inactivated at 55^{o}C)

5 ml Penicillin/ Streptomycin (final concentration is 50 μg/ml)

5 ml Sodium Pyruvate (final concentration is 0,11 mg/ml)

5 ml HEPES (final concentration is 10 mM)

5 ml NEAA (non- essential amino acid) (diluted to 1X from 100X concentrate stock)

500 ml RPMI 1640 cell culture medium

10% FBS containing HEK293FT Cell Culture Media

50 ml FBS (heat inactivated at 55^{o}C)

5 ml Sodium Pyruvate (final concentration is 0,11 mg/ml)

5 ml HEPES (final concentration is 10 mM)

5 ml NEAA (non- essential amino acid) (diluted to 1X from 100X concentrate stock)

500 ml DMEM (Dulbecco's Modified Eagle Medium) cell culture medium

Lentivirus Harvest Media

30% FBS

Penicillin/ Streptomycin (final concentration is 50 μg/ml)

DMEM (Dulbecco's Modified Eagle Medium)

ELISA Blocking Buffer

500 ml 1X PBS (pH 7.2)

5 g BSA (final concentration is 1%)

250 μl Tween-20

Stored at -20ºC.

ELISA Wash Buffer

2.5 ml Tween-20

500 ml 10X PBS (pH 6.8)

4.5 L dH_2O

FACS Buffer (PBS, BSA and Na-Azide)

500 ml 1X PBS

5 g BSA (final concentration is 1%)

125 mg Na-Azide (final concentration is 0,25%)

Stored at +4ºC.

ELISA T-cell Buffer

500 ml 1X PBS (pH 7.2)

25 ml FBS

250 µl Tween-20

Stored at -20ºC.

10X Phosphate Buffered Saline (PBS) (pH 6.8)

2 g KCl

2 g KH_2PO_4

8.01 g $Na2HPO_4.2H_2O$

80 g NaCl

Complete to 1 L with dH_2O

D. Western Blotting Buffers & Solutions

6X Laemmli Sample Loading Buffer

1.2 gr SDS (sodium dodecyl sulfate)

6 mg bromophenol blue

4.7 ml glycerol

1.2 ml Tris 0.5M pH 6.8

2.1 ml dH_2O

Completely dissolved.

2.5% v/v 2-Mercaptoethanol was added just before boiling

Running Buffer (10X)

30 g Tris-base

144 g Glycine

10 g SDS

in 1L of filtered dH_2O

Transfer Buffer (1X):

700 ml dH_2O

200ml absolute Methanol

100 ml 10X Transfer Buffer

Transfer Buffer (10X):

30 g Tris

144 g Glycine

pH is adjusted to 8.3 in 1 1L dH2O. Stored at room temperature.

PBS-T (1X, 1 L):

100 ml of PBS (10X)

pH is adjusted to 7.2, then complete the volume with dH_2O 1 L and add 0.1% Tween 20

Blocking Buffer

2.5 g skimmed milk (5% w/v) with 50 ml PBST

Mild Stripping Buffer

Glycine 15 g

SDS 1g

Tween20 10 ml

pH was adjusted to 2.2, then completed with dH_2O to 1L

E. Vehicle Control Versus Untreated Results' Comparison of THP1-Dual Cell Lines

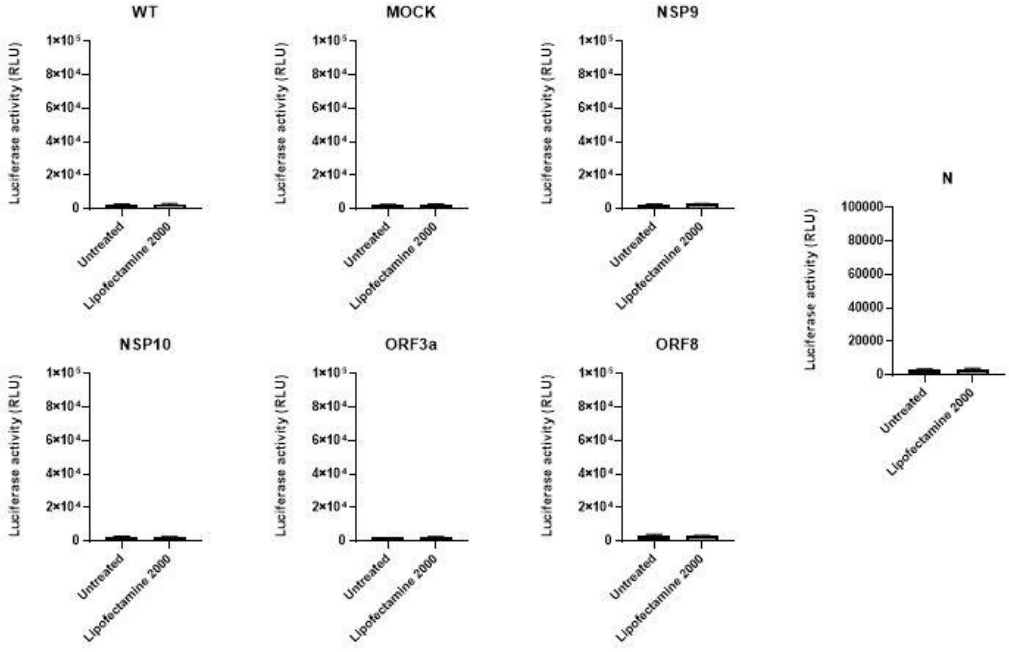

Figure E.1 Bar graph representation of quantitative enzyme activity for type I IFN results of untreated or Lipofectamine 2000 treated THP1-Dual Macrophages**.** Graphs show mean ± SEM of n=2-4 independent experiments and statistically analyzed by Tukey's multiple comparison test.

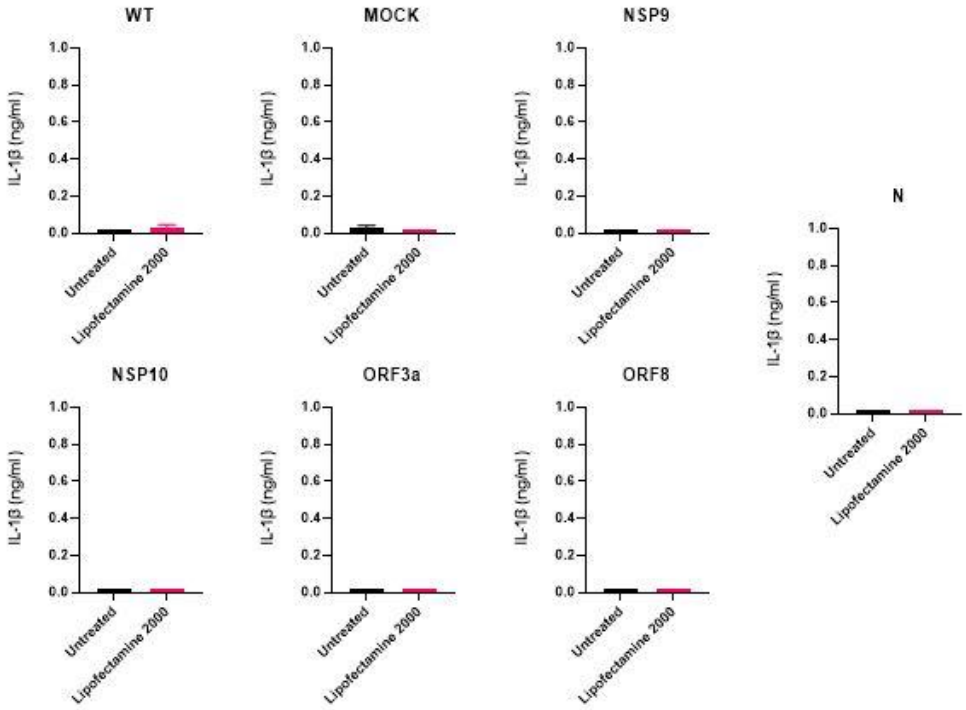

Figure E.2 Bar graph representation of IL-1β production from THP1-Dual cell lines in response to Lipofectamine 2000 versus untreated. Graphs show mean ± SEM of n=2-4 independent experiments and statistically analyzed by Tukey's multiple comparison test.